RV SONNE SO243
Cruise Report / Fahrtbericht

Guayaquil, Ecuador: 05. October 2015
Antofagasta, Chile: 22. October 2015

SO243 ASTRA-OMZ: AIR SEA INTERACTION OF TRACE ELEMENTS IN OXYGEN MINIMUM ZONES

Prof. Dr. Christa Marandino,GEOMAR
Helmholtz Centre for Ocean Research Kiel

Table of Contents

1. Cruise Summary/Zusammenfassung

The ASTRA-OMZ SO243 cruise on board the R/V Sonne took place between the 5th and 22nd October 2015 from Guayaquil, Ecuador to Antofagasta, Chile. Scientists from Germany, the U.S.A, and Norway participated, spanning chemical, biological, and physical oceanography, as well as atmospheric science. The main goal of the cruise was to determine the impact of low oxygen conditions on trace element cycling and distributions, as well as to determine how air-sea exchange of trace elements is influenced by high productivity conditions. The subsequent impact of trace element ocean-atmosphere exchange on atmospheric chemistry and climate will be determined.

A summary of the main preliminary results is below:

- a strong source of nitrous oxide (N_2O) and carbon dioxide (CO_2) was detected from surface waters in the Peruvian upwelling, particularly in the near-coastal area between 9°S and 18°S
- generally, surface N_2O during the SO-243 cruise was lower than previously observed, probably due to the reduced extent of upwelling events because of El Niño conditions
- less dimethyl sulphide (DMS) (< 2nmol L^{-1}) and isoprene (at 20-30 pmol L^{-1}) than on board previous cruises in the coastal upwelling region (8°-12°S) were detected, likely due to suppressed upwelling off of Peru because of the El Niño conditions
- a strong source for atmospheric carbonyl sulphide (OCS) was observed, as well as a strong correlation with oxygen. OCS decreased below the detection limit in oxygen depleted zones.
- a strong contrast between normal and El Niño conditions were detected for the halocarbon compounds. Both surface and deeper water was characterized by much larger concentrations of bromocarbons than of iodocarbons during ASTRA-OMZ, which stands in contrast to the previous M91 cruise during neutral conditions.
- it appears that the direct flux eddy covariance method was successful for sea-to-air flux measurements of N_2O (for the first time)
- a pronounced atmospheric inversion layer at approximately 1 km altitude was striking, which was accompanied by an accumulation of high relative humidity and moderate to fresh southerly winds below this inversion. Convective activity was limited and very few precipitation events were detected. Tropospheric ozone levels reveal distinct fluctuations within 9.5°S and 16.5°S latitude.
- the oxygen distribution measured at about 9°S showed that the upwelling in October 2015 was very weak. Low oxygen water with less than 5 µmol kg^{-1} was located only below 250 m in October 2015
- higher oxygen distribution in 2015, as well as the changes in water temperature, salinity and density indicate the influence of El Niño. We have already published our first paper related to El Niño during SO243 (Stramma et al. 2016).

Die Sonne Fahrt SO243 (ASTRA-OMZ) fand zwischen dem 5. und 22. Oktober 2015 statt und führte von Guayaquil/Ecuador nach Antofagasta/Chile. An Bord waren deutsche, amerikanische und norwegische Wissenschaftler, die sowohl Themen der biologischen, chemischen und physikalischen Ozeanographie bearbeiteten als auch atmosphärische Messungen durchführten. Der Schwerpunkt dieser Reise war es, den Einfluss von niedrigen Sauerstoffkonzentrationen im Ozean auf den Kreislauf von Spurenelementen und deren Verteilung zu untersuchen. Weiterhin galt es zu untersuchen, wie der Austausch von Spurenelementen zwischen Ozean und Atmosphäre durch die hochproduktiven Bedingungen vor Ort beeinflusst werden und welchen Einfluss dies auf die Chemie der Atmosphäre und das Klima haben kann.

Im Folgenden sind die vorläufigen Ergebnisse stickpunktartig aufgelistet:

- Das Auftriebsgebiet vor Peru wurde als Quelle für Lachgas (N_2O) und Kohlendioxid (CO_2) identifiziert, vor allem nahe der Küste zwischen 9°S und 18°S.
- Allgemein waren die N_2O Konzentrationen im Oberflächenwasser geringer als bei vorherigen Fahrten, was vermutlich auf den reduzierten Auftrieb durch die El Niño-Bedingungen zurückzuführen ist.
- Ebenfalls aufgrund des reduzierten Auftriebs wurden im Vergleich zu vorhergehenden Fahrten reduzierte Konzentrationen von Dimethylsulfid (DMS, <2 µmol L^{-1}) und Isopren (20-30 µmol L^{-1}) beobachtet.
- Die Forschungsregion war eine starke Quelle für Carbonylsulfid (OCS), welches stark mit der Sauerstoffkonzentration korrelierte. In sauerstofffreien Wassermassen sank die Konzentration von OCS unter das Detektionslimit.
- Für Halogenverbindungen wurde ein starker Unterschied zwischen normalen und El Niño-Bedingungen beobachtet. Sowohl im Oberflächen- als auch das Tiefenwasser wurden signifikant höhere Konzentrationen an bromierten und iodierten Kohlenstoffverbindungen gefunden. Dies steht in starkem Kontrast zu früheren Messungen während M91.
- Es wurden zum ersten Mal erfolgreich Direktflussmessungen von N_2O mit der Eddy-Kovarianz-Methode durchgeführt.
- Auffällig war eine ausgeprägte atmosphärische Inversionsschicht in etwa 1 km Höhe, die von erhöhter Luftfeuchtigkeit und mäßigem bis frischem Südwind begleitet wurde. Es wurde nur in beschränktem Maße Konvektion beobachtet und es gab auch nur wenig Niederschlag. Die Ozonwerte in der Troposphäre zeigten deutliche Schwankungen zwischen 9.5°S und 16.5°S.
- Auch die gemessenen Sauerstoffwerte zeigen, dass der Auftrieb im Oktober 2015 nur sehr schwach war. Sauerstoffwerte unter 5 µmol L-1 wurden nur in Wassermassen unterhalb von 250 m beobachtet.
- Sowohl die hohen Sauerstoffkonzentrationen in 2015 als auch veränderten Wassertemperaturen, Salzgehalt und Dichte deuten auf den Einfluss von El Niño hin. Über die beobachteten Bedingungen mit Bezug auf El Niño wurde schon die erste Arbeit veröffentlicht (Stramma et al. 2016).

2. Participants

1. Christa Marandino	Chief Scientist	GEOMAR
2. Damian Grundle	Co-Chief Scientist	GEOMAR
3. Tobias Steinhoff	Co-PI, Carbon cycle	GEOMAR
4. Damian Arevalo	Scientist C, N cycles	GEOMAR
5. Dennis Booge	PhD Trace gases	GEOMAR
6. Astrid Bracher	Scientist Biological oceanography	AWI
7. Tom Browning	Scientist Biogeochemistry	GEOMAR
8. Hanna Campen	Student helper Oxygen	GEOMAR
9. Anne Cruz	Scientist Nitrogen cycle	UMass
10. Sonja Endres	Scientist Biological oceanography	GEOMAR
11. Alina Fiehn	PhD Atmospheric physics	GEOMAR
12. Tim Fischer	Scientist Physical oceanography	GEOMAR
13. Martha Gledhill	Scientist Biogeochemistry	GEOMAR
14. Helmke Hepach	Scientist Halogenated gases	GEOMAR
15. Kirstin Krüger	Scientist Atmospheric physics	UIO
16. Fred Lemoigne	Scientist Biological oceanography	GEOMAR
17. Sinikka Lennartz	PhD Halogen and S gases	GEOMAR
18. Rudolph Link	Technician CTD	GEOMAR
19. Martina Lohmann	Technician Nutrients and oxygen	GEOMAR
20. Mike Lomas	Scientist Biological oceanography	Bigelow
21. Mario Müller	Engineer OTIS/CTD	GEOMAR
22. Gert Petrick	Scientist Halogenated gases	GEOMAR
23. Andreas Pinck	Engineer OTIS/CTD	GEOMAR
24. Birgit Quack	Scientist Halogenated gases	GEOMAR
25. Insa Rapp	PhD Trace metals	GEOMAR
26. Jon Roa	Techn. Biological oceanography	GEOMAR
27. Rüdiger Röttgers	Scientist Biological oceanography	HZG
28. Christian Schlosser	Scientist Trace metals	GEOMAR
29. Cathleen Schlundt	Scientist Trace gases	GEOMAR
30. Karen Stange	Techn. Chemical oceanography	GEOMAR
31. Tim Stöven	Scientist Oceanic tracers	GEOMAR
32. Lothar Stramma	Scientist Physical oceanography	GEOMAR
33. Sun Mingshuan	PhD Nitrogen cycle	GEOMAR
34. Toste Tanhua	Scientist Oceanic tracers	GEOMAR
35. Xiao Ma	PhD Nitrogen Cycle	GEOMAR
36. Birthe Zäncker	PhD Biological oceanography	GEOMAR
37. Alex Zavarsky	PhD Eddy covariance	GEOMAR
38. Wilson C. Bernabe	Observer Peru	IMARPE
39. Geovanny Z. Castillo	Observer Ecuador	Ecuadorian Navy

Figure 2.1. Participants of ASTRA-OMZ SO243.

3. Narrative of the cruise

The R/V SONNE left the port of Guayaquil in the morning of 05th October 2015. Around 15:00 local time we left coastal waters and the water pump for underway sampling of surface waters was started. While the ship was heading northwest to our first set of stations, the underway measurements for continuous monitoring of the surface water for N_2O, CO_2, O_2, OCS, total dissolved gases, sea surface temperature, salinity, and chlorophyll began. Most groups on board began discrete sampling in a 3 hourly rhythm from the underway pumping system. This included samples for nutrients, gases (dissolved O_2, CO_2, N_2O, DMS, halocarbons, isoprene, etc.) and biological parameters. In addition to the water samples, atmospheric samples and radio-/ozonsonde deployments took place with similar timing. During the transit to the first station the eddy covariance (direct flux) measurements of DMS, N_2O and CO_2 were started at the front of the ship.

On the evening of the 06th October we reached the first station in open ocean waters at 1° N, 85.5°W. This was the beginning of a three station repeat ADCP transit. Here we completed two CTD casts (a shallow one of about 100 m and a deeper one of 1000 m), lowered the RAMSES (a light measurement device), and performed microstructure measurements (small scale turbulence in the upper 200 m of the water column). This was a test station; we had to serve the water needs of many gas and biological sampling groups and stretch a new Kevlar wire to be used for trace metal water sampling with Go-Flo bottles. The protocols for CTD casts, depths, and sampling order were finalized and three different types of biological and chemical incubation experiments were started.

After a 10 hour transect southwards along 85.5°W we reached the second station. Here we added the Zodiac for microlayer samples and a continuously sampling profile pump for continuous O_2 and trace gas depth profiles (to 150 m) to the deployment rotation. Furthermore, the trace metal group started sampling the water column using their Go-Flow bottles attached to the new Kevlar wire. Moving further south, after another 12 hour transect,

we came to station 3, where we performed our normal station work and added the first of three particle pump tests. The pumps were attached to the CTD wire at three different depths and pumped for about two hours in order to collect particles on the inserted filters for later analysis. Unfortunately, this test was not successful. We finished station 3 in the afternoon of 07th October and began our transect to the coast.

On our way to the coast, we performed a hunt for a mode water eddy. Eddies are rotating mesoscale structures in the ocean that contain different water properties than their surroundings. Recently, eddies have been identified as low oxygen natural laboratories, in which we can investigate how the biogeochemistry is different from the surrounding waters (Karstensen et al. 2008). In the morning of the 10th October we arrived at the approximate location of the predicted eddy and did a first CTD cast. Heading to the center of the eddy, we made a CTD cast approximately every 5 nm in order to find the core. The core was located at approximately 10°S, 82°W, but the eddy was, unfortunately, a normal anticyclonic eddy. We resumed with our transect to the coast with the extensive station work at three stations off the Peruvian coast (one on the boundary of the eddy, one in shelf water outside the eddy, and one at the coast). Near the coast we found signs of upwelling (enhanced values for CO_2 and N_2O and decreased temperature). But the upwelling signal was less pronounced than expected, which may have been caused by the El Niño conditions we encountered during the cruise.

Our cruise track led us further south along the coast, always staying in upwelled water masses, until station 9 where the first water mass tracer deployment took place. Here the Ocean tracer injection system (OTIS) was deployed. The OTIS is designed to be towed behind the ship at a set density surface. However, this time we wanted a tracer release very close to the bottom, so the OTIS was equipped with “legs” and “feet” so that we could deploy the OTIS on the bottom of the ocean and release the tracer there. The reason for the close-to-bottom release is that we wanted to mimic release of nutrients from anoxic sediments, and qualitatively understand where ocean currents and mixing processes distribute the nutrients (i.e. the tracer) over a longer time-period. Anoxic sediments are known to release nutrients, such as phosphate and reduced iron, both of which have the potential to enhance productivity in the region – and initiate a positive feed-back loop (Bohlen et al. 2011; Scholz et al. 2014). At this time we were faced with a problem regarding our measurements: the liquid nitrogen generator broke down and we ran out of liquid nitrogen. Given that approximately 1/3 of the cruise participants depended in some way on measurements made with liquid nitrogen, plus others use liquid nitrogen to flash freeze samples, this was a serious concern. It was a hard call, but we decided to risk our schedule and go to port in Chimbote, Peru to buy 140 L of liquid nitrogen. This took approximately 1.75 days to accomplish, which required that we adjust our cruise plan in order to save time but still accomplish our major goals.

The last set of stations, 10-18, were designed to obtain contrasting measurements between strong upwelling and open ocean conditions (on shore/off shore transects). At station 11 and station 15, the OTIS and particle pumps were deployed simultaneously. These last particle pump deployments were successful. At station 12, a NAVIS float containing dissolved oxygen, temperature, and salinity sensors was successfully deployed. The float is currently in communication with researchers at GEOMAR and Villefranche, sending valid data every 10 days. Unfortunately, between stations 12 and 13, the trace metal tow fish was lost, but the

trace metal group was able to maintain most of their sampling program. Strong upwelling was detected around station 15, which was slightly further south than anticipated. After station 15, we had to divert our course again due to the presence of a Peruvian nature reserve, but arrived at our revised station 16 with enough time to include high resolution CTD casts in the sampling program for the first time. At our last station, station 18, we performed our longest program, during which time we deployed all instruments and included several high resolution casts. It was between this station and station 17 that we detected the strongest upwelling signal over the entire cruise track.

The R/V Sonne arrived at the pilot station at 8:00 on 22nd October, after 2 days of underway measurements in Chilean waters. Despite our challenges at sea and our shortened science schedule, we were able to accomplish most of our goals. This is clearly owed to the fantastic team work of the captain and crew onboard the R/V Sonne, the dedicated and patient work of the 37 ASTRA-OMZ scientists, and also to the much valued help of the two observers.

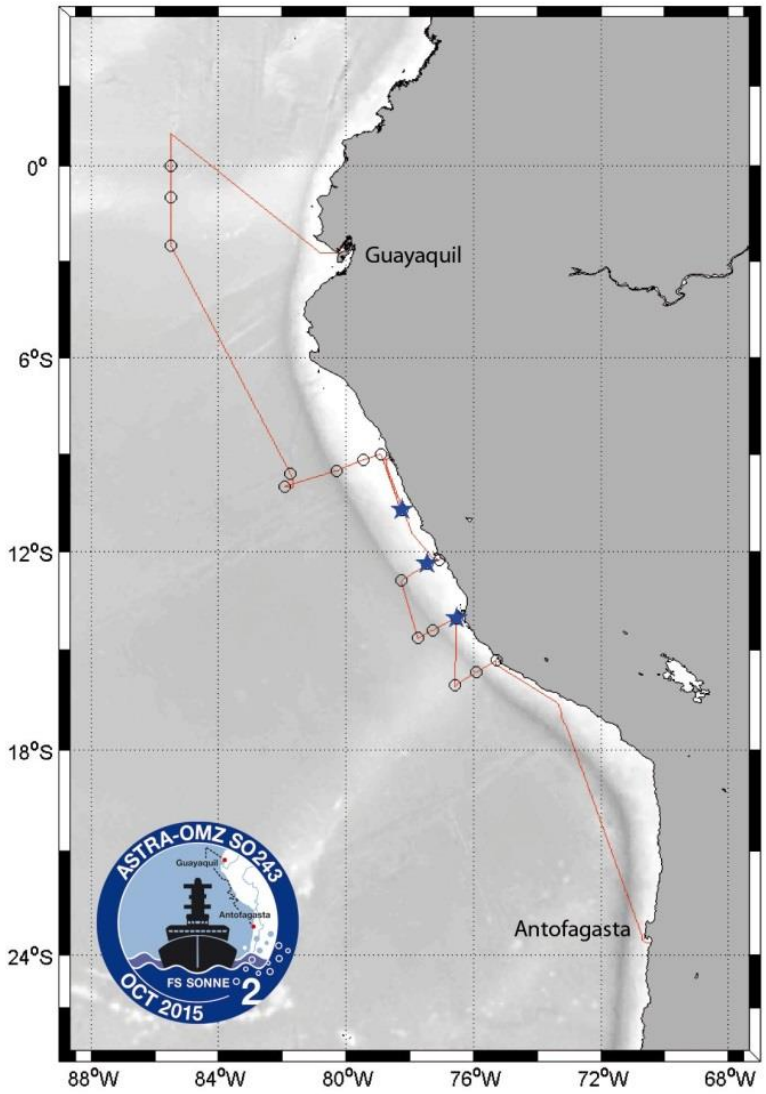

Figure 3.1. Cruise Track ASTRA-OMZ SO243 beginning in Guayaquil, Ecuador and ending in Antofagasta, Chile from 5. October to 22. October, 2015. Circles represent CTD stations and stars represent OTIS stations (see appendix for station list).

4. Aims of the Cruise

Dissolved oxygen (DO) concentrations in oceanic regions are declining due to global climate change, resulting in an expansion of oxygen minimum zones (OMZs) and DO decreases in existing OMZs (Keeling et al. 2010). As a principle determinant of redox state, DO availability plays a key role in regulating biogeochemical processes and nutrient cycles. The availability of redox sensitive trace metals important for various biological production pathways, such as those that lead to trace gas production, are also impacted by low DO conditions. The ASTRA-OMZ cruise, from Guayaquil to Antofagasta, provided an ideal opportunity to examine 1) the impact of DO in regulating trace gas distributions, and 2) how different biological (e.g. phytoplankton derived surfactants) and physical (e.g. upwelling) variables influence sea-to-air gas exchange. Processes within the shallow OMZ in the eastern tropical south Pacific (ETSP), which is connected to the Peruvian upwelling system and is characterized by high productivity, contribute to enhanced cycling of numerous biogenic trace gases and elevated concentrations of sea-surface surfactants, both of which directly influence atmospheric chemistry and climate. The subsequent impact of trace gases on atmospheric chemistry (e.g. oxidative processes, ozone formation/destruction) and climate (aerosol and cloud formation) will be determined. We expect that OMZs and the ETSP will enhance the production of certain compounds, such as iodocarbons, DMS, and N_2O, and perhaps lead to greater drawdown of CO_2. The combined effects of higher seawater concentrations of both trace gases and surfactants will have a confounding impact on trace gas fluxes.

We tested three hypotheses:

H1 – Trace element cycling will change as DO concentrations decrease;

H2 - The relative importance of the different N_2O production pathways will change as DO concentrations decrease; our results will support recent indications that archaea, as well as bacteria, produce N_2O via NH_4^+ oxidation, and we hypothesize that the relative importance of archaea vs. bacteria will increase as DO decreases;

H3 - Sea-to-air fluxes of trace gases will change with decreasing DO, especially in regions overlying shallow OMZs, and these fluxes will be modulated by biogeochemical/physical factors not currently included in flux calculations (e.g. surfactants).

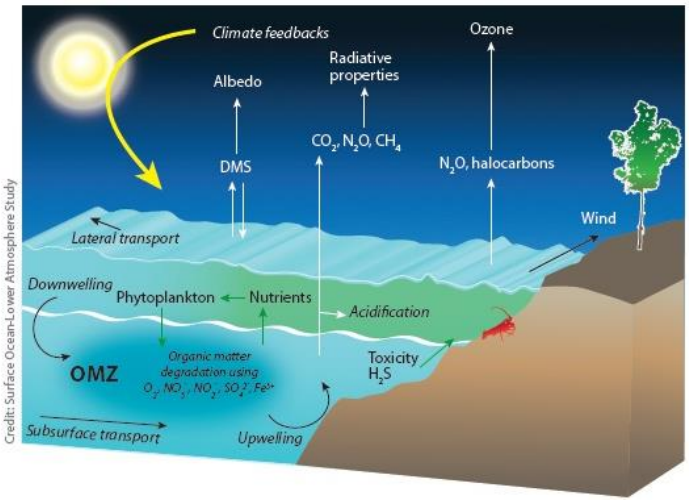

Figure 4.1. Surface Ocean Lower Atmosphere Study conceptual diagram outlining the main constituents and processes identified as important in eastern boundary upwelling systems and oxygen minimum zone re-search. These topics are all addressed by the ASTRA-OMZ cruise.

5. Agenda of the cruise

The ASTRA-OMZ cruise was a unique platform for a highly multidisciplinary approach. In addition to chemical oceanographers and atmospheric scientists, biological and physical oceanographers participated, providing us with ancillary measurements which are critical to helping us identify and unravel the key biological and physical processes which affect trace gas distributions. For example, phytoplankton influence trace gas cycling in the surface ocean (e.g. CO_2 uptake, and sulphur and halocarbon release) and phytoplankton composition and productivity work by the biological oceanographers will enable us to investigate how phytoplankton dynamics influence trace gas processes in the surface waters and in the underlying OMZ regions. From the physical standpoint, changes to circulation processes in the ocean have been proposed as one of the possible drivers of DO losses. To assess this requires an understanding of the mean circulation and the current bands which supply DO to OMZ regions. The goal of the hydrographic measurements is to derive the current band transports along the cruise track from continuous acoustic Doppler current profiler (ADCP) measurements. ADCP data from the R/V Sonne in October 2015 was compared to ADCP data from March 1993 (WOCE cruise), February 2009 (Meteor M77/4) and November 2012 (METEOR M90), to address unknown seasonal variations of the equatorial undercurrent east of the Galapagos Islands. ADCP and microstructure profiling work will also allow us to determine how different physical processes (diffusive vs. advective) contribute to gas transport from the OMZs to the ventilated surface waters. In addition, we performed a tracer release experiment on the Peruvian shelf (PESTRE) to quantify the rate of exchange and mixing, and advective pathways of bottom water over the time span of several months. This tracer release experiment will provide important information on the effective diapycnal diffusivity off the bottom boundary layer, and will allow for better understanding and knowledge of the integrated transport processes for the water in the bottom boundary layer.

Of course, determining the impact that an increase in climate relevant trace gas production will have for atmospheric chemistry requires an accurate understanding of the factors which affect sea-to-air gas exchange. Recent work has demonstrated that higher concentrations of surfactants at the sea-surface, which occur when phytoplankton biomass increases, may suppress gas transfer velocities (Kock et al. 2012). If this is the case, a major re-evaluation of gas transfer velocity parameters will be necessary, because conventional gas transfer velocity parameters do not take surfactants into account. Understanding the role of upwelling in transporting trace gases from intermediate depths to surface layer waters is also important, especially when these regimes are connected to OMZs, since atmospherically relevant trace gases (Bakker et al. 2014), as well as toxic gases, such as hydrogen sulphide (Schunck et al. 2013), may be rapidly transported into the mixed layer. Understanding the role that OMZs play in the formation of trace gases, as well as the factors that regulate their air-sea exchange, is critical if we are to accurately estimate the supply of trace gases to the atmosphere and begin to predict how this supply may change under future oceanic DO scenarios.

We used conventional methods, such as purge and trap gas chromatography coupled to various sensors, as well as more advanced continuous sampling instrumentation, such as ROS, to measure a suite of climate active trace gas cycling in the surface ocean. Isotope techniques were used to probe more deeply the sources and sinks of these gases. Surface

and atmospheric measurements of trace gas concentrations, along with physical structure (i.e. ozone- and radiosondes) and direct fluxes will be used to quantify emissions and investigate the processes that control their air-sea exchange and atmospheric distribution. State of the art techniques were employed to investigate the role of surfactants on air-sea trace gas exchange. The effects of DO, T and pH on trace metal speciation will be assessed. Additionally we will determine the fluxes of micronutrients (e.g. Fe, Co, Mn) and macronutrients (P, N, Si) to the surface ocean and their consequences for ocean productivity and trace gas production/consumption.

The following parameters were measured during SO243 (see appendix for station plan):

- Trace gases – Nitrogen compounds, methane, carbon compounds, sulphur-containing and halogen-containing compounds, non-methane hydrocarbons
- Isotope signatures of dissolved nitrogen species.
- Nutrient and oxygen concentrations
- Trace metals – Mn, Co, Ni, Cu, Zn, Cd, Pb; the speciation of Mn, Cu; iodide/iodate; Fe(II); Markers for lithogenic origin; ROS-, H_2O_2, superoxide, DOM
- Gas exchange between atmosphere and ocean – Eddy covariance fluxes, atmospheric structure, surface films (microlayer)
- Physical measurements – Tracer release, diapycnal and advective fluxes
- Biological measurements - Biooptical parameters, flow cytometry, identification of phytoplankton, phytoplankton group specific nutrient stoichiometry and rates of production

6. Settings of the working area

The Eastern Tropical South Pacific (ETSP) contains DO concentrations in the core of the OMZ are much lower (<5 µmol L-1) than are often observed in oceanic OMZs (Karstensen et al. 2008). As such, the ETSP OMZ serves as an ideal natural laboratory which can be used to provide insight into how biogeochemical conditions may change under future DO scenarios. For example the OMZ off of Peru is likely to be an N_2O production hotspot. A SOPRAN cruise (M91) showed that N_2O concentrations in the surface waters overlying the OMZ were often >300 nmol L-1, and at times were >900 nmol L-1 (>100 times atmospheric concentrations; Arévalo-Martínez et al. 2015). Secondly, the work area is an Eastern Boundary Upwelling System (EBUS), which is characterized by high productivity (Chavez & Messié 2009) and corresponds to enhanced cycling of numerous biogenic trace gases and elevated sea-surface surfactants (Žutić et al. 1981). The EBUS off of Peru exhibits a range of different biological and physical regimes that will be assessed for their impact on trace gas production and air-sea gas exchange. Furthermore, since the ETSP OMZ is connected to upwelling, we will be able to assess how trace gas transport from intermediate depths to surface waters may directly impact the atmosphere. Understanding how these types of physical and biological regimes impact the supply of trace gases to the surface waters, and then ventilation to the atmosphere, is central to determining how future formations of OMZs in different oceanic regions will contribute to atmospheric trace gas concentrations. Finally, one of the strongest El Niños on record began in 2015.Our cruise trace happened to pass right through one of the regions that is strongly impacted, however, we were there too early to observe the full influence of this strong El Niño. We did detect the transition to El Niño conditions, for example in the decreased upwelling off the coast of Peru (Stramma et al. 2016).

7. Work details and first results

7.1 Dissolved Nitrous Oxide Distributions and Production

Damian Grundle, Damian L. Arévalo-Martínez, Xiao Ma, Sun Mingshuang, Karen Stange

Objective

To understand how dissolved oxygen concentrations regulate the distribution, the production, and the production pathways of nitrous oxide in the ocean. Results from this work will help us to understand how the production of this greenhouse and ozone destroying gas may increase under future oxygen conditions in the ocean. To achieve these objectives we conducted discrete vertical profile sampling to measure dissolved N_2O concentrations and isotope signatures (^{15}N, ^{18}O and ^{15}N site-preference). In addition, at select depths, samples were also collected to measure N_2O production via the oxidation of NH_4^+ and the reduction of NO_2^- and NO_3^- using ^{15}N tracer techniques.

Methods

At every sampling station, replicate samples were collected from CTD-Niskin bottles which were fired at approximately 10-20 depths spanning the range of oxygen concentrations observed for the purpose of measuring N_2O concentrations and isotope signatures. All samples were collected following standard dissolved gas sampling techniques. N_2O concentrations were measured using a gas chromatograph with attached electron capture detector following the techniques outlined in the subsequent section (section 7.2). N_2O isotope signatures are currently being measured by isotope ratio mass spectrometry.

At approximately 3-5 sampling depths 4 sets of duplicate 160 ml samples were also collected following standard gas sampling techniques for the purpose of measuring N_2O production rates via each of the different production pathways. Following collection, the first three sets of duplicates were amended with ^{15}N-labeled NH_4^+ (N_2O production via NH_4^+ oxidation), NO_2^- (N_2O production via NO_2^- reduction), and NO_3^- (N_2O production via NO_3^- reduction), while the fourth set remained un-amended and served as controls. Samples were then incubated in the dark at near in situ temperature for a period of 24 hours, after which poisoning with mercuric chloride terminated the incubations. The final atom% ^{15}N in the product pool (i.e. N_2O will be measured by isotope ration mass spectrometry.

Preliminary and Expected Results

A preliminary analysis of the N_2O concentration data (range shown in Fig. 7.1.1) shows that the N_2O concentrations during our cruise were within the range of many of the highest values previously reported for oceanic N_2O 'hotspots' in the eastern tropical Pacific and Open Arabian Sea (S W A Naqvi et al. 1998; S. W. A. Naqvi et al. 1998). Furthermore, the N_2O vs. O_2 relationship (Fig. 7.1.1) shows that N_2O concentrations are inversely related to O_2 concentrations until O_2 becomes very low (less that approx. 5 µmol L^{-1}), at which point N_2O concentrations decrease, suggesting a switch from net N_2O production to net N_2O consumption. We expect that further analyses will show that the relationship between N_2O and O_2 will differ between offshore and coastal stations. Furthermore, the natural abundance

isotope data will provide us with insight into how the different N_2O production pathways (i.e. NH_4^+ oxidation, NO_2^- reduction and NO_3^- reduction) contribute to bulk N_2O concentrations under different O_2 conditions, and we expect that as O_2 decreases NO_2^- reduction, and eventually NO_3^- reduction will become more important sources of N_2O. The N_2O production experiments will provide us with critical insight, for the first time in the eastern tropical South Pacific, into how overall rates of N_2O production and the rates of N_2O formation via the different production pathways vary as O_2 concentrations change. These results will allow us to identify the O_2 threshold which induces a substantial increase in N_2O production in this region, and this will allow us to better understand how N_2O production may change under future O_2 conditions.

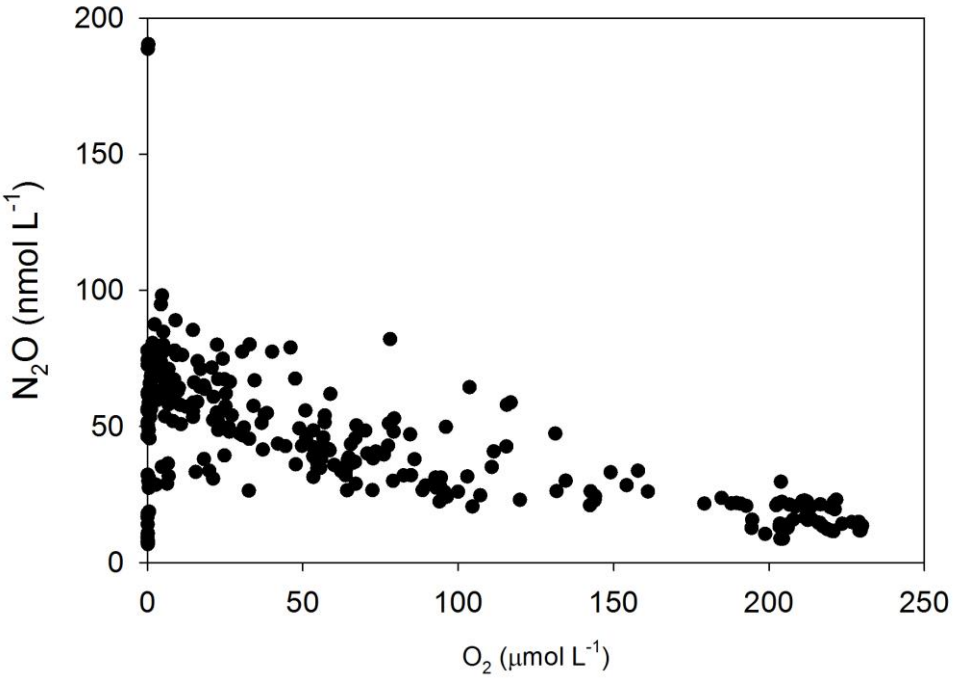

Figure 7.1.1. N_2O vs. O_2 concentrations (all data from discrete vertical measurements pooled) during SO243.

7.2 Oceanic greenhouse gases

Continous measurements: Damian L. Arévalo-Martínez and Tobias Steinhoff
Discrete samples: Damian L. Arévalo-Martínez, Xiao Ma, Sun Mingshuang, Karen Stange, Dennis Booge, Tim Fischer, Tobias Steinhoff

Objective/Intro

Given the climatic relevance of marine-derived greenhouse gases, the investigation of their distribution and emissions from key oceanic regions is a crucial need in our efforts to better understand potential responses of the ocean and the overlying atmosphere to environmental changes, such as warming and deoxygenation. Our main goal during the SO243 cruise was to perform a comprehensive survey of different trace gases both at the surface and in the water column within the coastal upwelling system and the associated oxygen minimum zone (OMZ) off Peru. In order to achieve this, we used a combination of continuous and discrete

measuring methods which are listed below, together with the most important preliminary results.

Methods

Surface oceanic and atmospheric measurements of N_2O, CO and CO_2 were performed by means of a continuous system based upon the off-axis integrated cavity output spectroscopy technique (DLT-100 N_2O/CO Analyzer, Los Gatos research Inc.) coupled to a CO_2 system based upon non-dispersive infrared detection from General Oceanics Inc. (Fig. 7.2.1) described in detail in Pierrot et al. (2009). Water was drawn on board by using a submersible pump installed in the ship's moonpool at 6 m depth and was subsequently conducted at a rate of about 3 L min^{-1} through the equilibrator. Sample air from the headspace of the equilibrator was continuously pumped through the instruments and then back to the equilibration chamber forming a closed loop. The air stream was dried before being injected into the analyzers in order to diminish interferences due to the water vapor content of the sample. In order to correct for potential warming of the seawater between intake and equilibrator the water temperature at the equilibrator was constantly monitored by means of a high accuracy digital thermometer (FLUKE 1523) and at the intake by a Seabird SBE37 high precision thermosalinograph. Ambient air measurements were accomplished by drawing air into the system from a suction point located at the ships mast at about 30 m high. Control measurements and calibration procedures were performed every ~6 and 24 h respectively, by means of 4 standard gas mixtures bracketing the expected seawater concentrations of N_2O, CO_2 and CO.

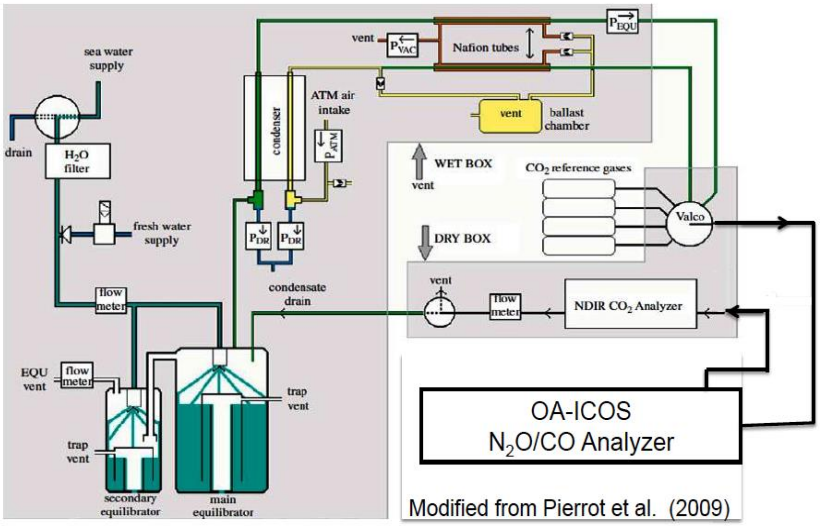

Figure 7.2.1. Schematic view of the analytical setup used for continuous measurements of N_2O, CO and CO_2 during the SO243 cruise.

Underway measurements of surface water O_2 and gas tension were carried out in a flow-through-box. The box was connected to the same water supply as the system above and the water flow was adjusted to approximately 20 L min^{-1}. The following instruments were implemented: Aanderaa Oxygen Optode and a Pro Oceanus Gas tension device. The gas tension device physically measures the total pressure of all dissolved gases, i.e, pN_2, pO_2, pH_2O, and pAr as well as minor trace gases below the instrument's accuracy. As water vapour (pH_2O) is a function of temperature and salinity, Argon pAr is constant, and Oxygen

pO_2 is measured by the oxygen optode, it effectively gives the pN_2, which is a prime indicator of physical processes of gas exchange, such as bubble processes, and unaffected by biology. It thus helps to separate biological and physical contributions to air-sea gas exchange of O_2. This is complemented by the biology-dominated pCO_2 measurements in water and air. In combination with information about the mixed layer from the CTD, the continuous underway measurements thus yield insight into major physical and biological processes at play in the surface ocean.

Discrete samples for N_2O, CO and CO_2 measurements were carried out in 12 h (N_2O, CO_2) or 6 h (CO) intervals by sampling from the same water stream that fed the continuous setup (see above). For N_2O, bubble-free triplicate samples were collected and immediately sealed by means of butyl stoppers and aluminum crimps. Subsequently a 10 mL headspace of helium and 50 µL of a saturated mercuric chloride ($HgCl_2$) solution were added. After an equilibration period of at least 2 hours the headspace sample was measured by means of a gas chromatograph equipped with an electron capture detector (GC/ECD). The GC was calibrated on a daily basis using dilutions of two standard gas mixtures. DIC/TA samples were collected in 500 mL glass bottles, preserved with $HgCl_2$ and then stored to be measured at the Chemical Oceanography Department of GEOMAR in Kiel (CH-Kiel). DIC/TA data together with ancillary parameters and the measured pCO_2 data will help to understand the carbonate system in the study area. These data will also be useful to interpret the air-sea flux data of CO_2 obtained by the eddy-covariance method (see section 7.8). CO samples were treated with 100 µL of a saturated $HgCl_2$ solution and then were stored in the dark. These samples will be measured at the CH-Kiel by means of a ta3000r GC/RGD (reduction gas detector) system which was recently established at GEOMAR. Fig. 7.2.2 shows an overview of the locations of the underway trace gas sampling during the cruise.

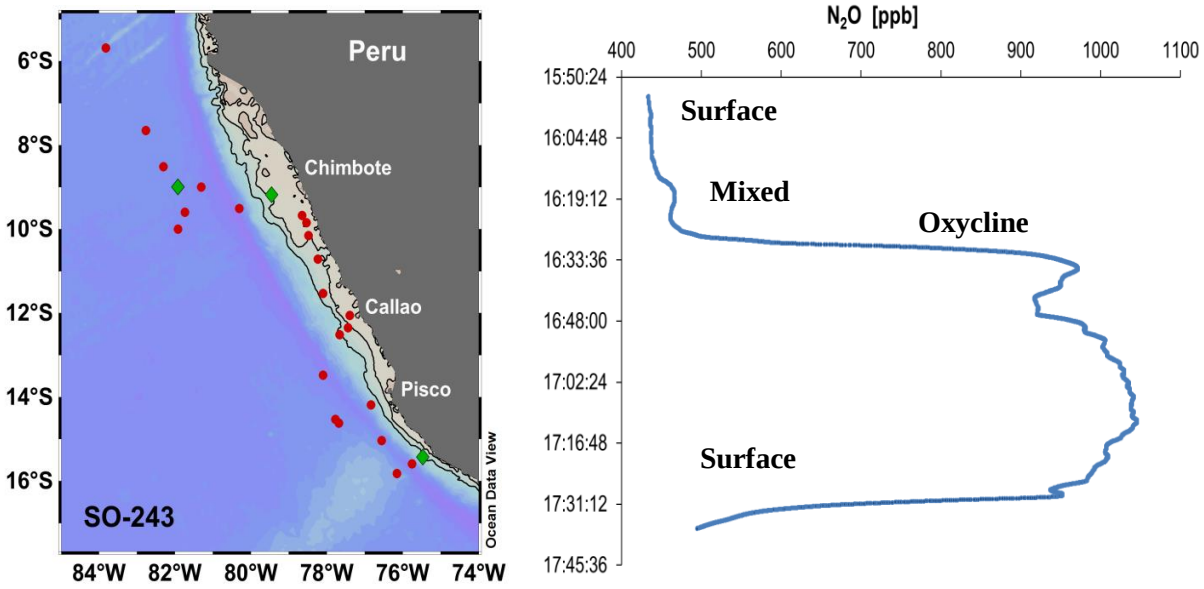

Figure 7.2.2. Sampling locations for underway N_2O, CO and DIC/TA measurements (left, red circles) and high resolution profiles of N_2O using the continuous pump profiler (CPP, left, green diamonds). The right panel shows a depth profile obtained with OA-ICOS and the CPP at 0°N, 85°W (not shown in the map). For further details on the CPP see section 7.4.

Preliminary Results

Preliminary results from continuous measurements show a strong source of N_2O and CO_2 from surface waters in the Peruvian upwelling, particularly in the near-coastal area between 9°S and 18°S where seawater values surpassed atmospheric equilibrium (~326 ppb) by one order of magnitude (Fig. 7.2.3, 7.2.4). In agreement with a recent survey which took place during the M91 cruise (December 2012), the highest N_2O values were consistent with the location of the upwelling centres off Chimbote, Callao, Pisco and San Juan, although in general surface N_2O during the SO243 cruise was lower, probably due to reduced extent of the upwelling events. Similarly, coastal waters during SO243 were a source of CO to the atmosphere, although in this case the diurnal variability is the most relevant signal (Fig. 7.2.3). Hence, as expected, enhanced/decreased CO values could be found during day-time/night-time.

CO and CH_4 (vertical N2O sampling is described in the previous section) sampling were performed in conjunction with several biological parameters and incubation work from other groups as well as with microstructure measurements. Samples were drawn directly from the CTD into glass vials of 20 - 100 mL and were processed as explained in the first section of this report. CO and CH_4 samples were preserved and stored for posterior analysis in Kiel. CH_4 analysis will be carried out by means of an analytical system similar to that used for N_2O during the cruise, but using a flame ionization detector (FID) instead of an ECD. DIC/TA samples were collected in 250 mL glass bottles, preserved with $HgCl_2$ and then stored to be measured at the Chemical Oceanography Department of GEOMAR in Kiel (CH-Kiel).

In addition to the rosette-CTD sampling, depth profiles of N_2O, and CO_2 were obtained in selected stations (Fig. 7.2.2) by using a continuous pump profiler developed by S. Lennartz (see section 7.4). This profiler was coupled to our OA-ICOS/NDIR $N_2O/CO/CO_2$ setup during the stations and allowed us to measure by the first time these three gases with such a high resolution. Preliminary results from one of the profiles in the northern part of the cruise track are shown in Fig. 7.2.2.

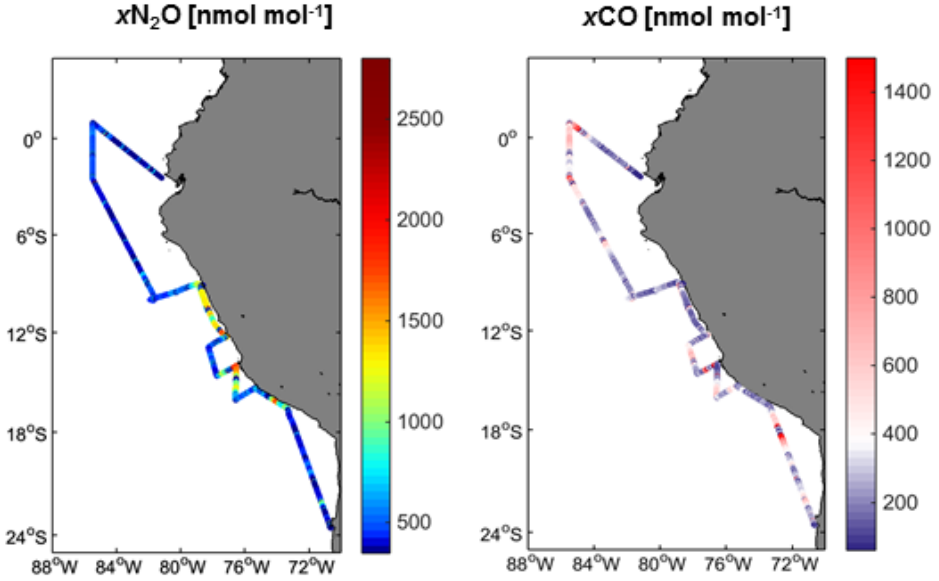

Figure 7.2.3. Preliminary data from along-track N_2O (left) and CO (right) measurements during the SO243 cruise expressed as gas molar fractions reported by the OA-ICOS analyser.

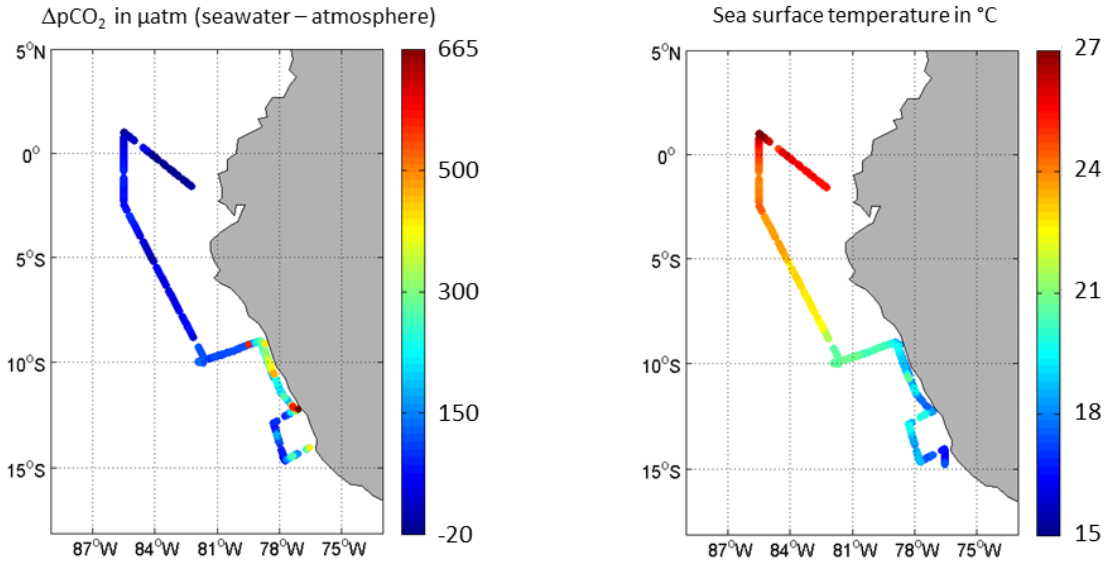

Figure 7.2.4. Preliminary results from along-track ΔpCO_2 (left) and SST (right) measurements during the SO243 cruise.

In order to investigate near-surface gradients of N_2O off the coast of Peru, three detailed surveys of the upper 10 m of the water column were carried out in selected stations on board of a Zodiac. Sampling was carried out as for the conventional depth profiles but by using either a single niskin bottle or a small submersible pump which could be lowered to the upper 15 - 150 cm of the water column. Preliminary results from the first zodiac sampling carried out during the cruise are shown in Fig. 7.2.5. Although a fairly large scatter between upper and lower samples of the profiles could be observed, the final concentration values are expected to be within the range of uncertainty of the measurement method (GC/ECD). Stations closer to the coast (such as off Callao and San Juan Bay), where the gradients tend to be higher, are yet to be analyzed.

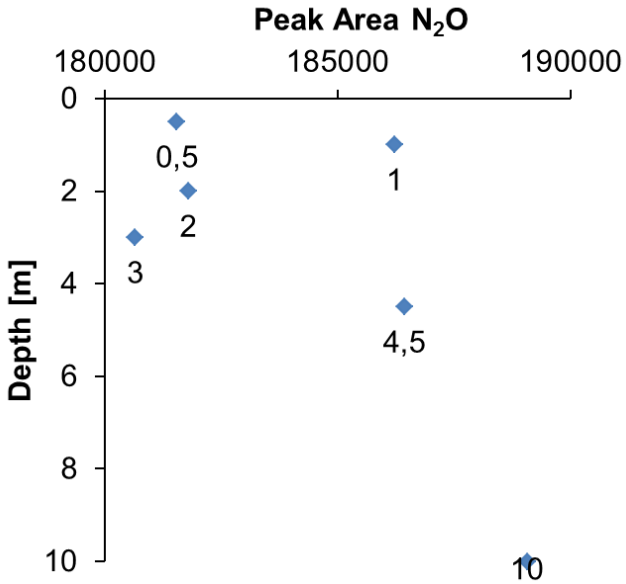

Figure 7.2.5. Preliminary results from the first near-surface N_2O sampling on board of the Zodiac. The numbers next to the blue symbols indicate the sampling depths.

During station 18, we performed nearly simultaneous sampling of N_2O from different platforms including continuous measurements with OA-ICOS both using the CPP and the pump installed at the ship's moonpool, discrete samples during the CPP deployment and Zodiac sampling. This, together with direct measurements of sea-air fluxes of N_2O by using an eddy covariance setup (see section 7.8) will help to reconcile the large uncertainties observed in the computed surface fluxes of this gas.

Expected results

Further calibration and data quality control are needed in order to compute the final CO_2, N_2O and CO seawater concentrations and this task will be carried out during the following months.

7.3 Dissolved isoprene and sulphur-containing gases (DMS/P/O, CS_2)

Cathleen Schlundt, Dennis Booge, Christa Marandino

Objective/Intro

Despite the low concentrations of short-lived trace gases in the atmosphere, their impact on local and global climate is crucial. Short-lived trace gases, for example isoprene and dimethylsulphide (DMS), are important precursors of secondary organic aerosol and cloud condensation nuclei in the remote marine boundary layer. These gases are produced by a complex interplay of bacteria and phytoplankton in the surface oceans and their emissions to the atmosphere are critically controlled by biotic activities and physical factors which are poorly quantified. The Peruvian shelf is of particular interest for trace gases due to the seasonal occurrence of upwelling and the oxygen minimum zone (OMZ). The upwelling transports nutrient rich deep water to the surface that initiate a strong phytoplankton bloom, most likely leading to elevated production of DMS and isoprene. In contrast, the activity of bacteria and phytoplankton might be reduced or changed in the OMZ, which might change the DMS and isoprene production. Our goal onthis cruise is to better understand the biological pathways of these gases, especially in these special marine regions, as well as monitoring their concentrations in the surface ocean, to evaluate their air-sea flux and finally their importance for the chemistry in the atmosphere.

Methods

We sampled surface seawater (5m) each hour or every three hours to analyse DMS/P/O, isoprene and CS_2. Additionally, we collected samples from different depths (microlayer to 1000 m) to obtain depth profiles of the trace gases. We sampled from the surface microlayer to 10 m depth in a high resolution (0.5 to 1 m steps) at three different stations. Furthermore, we collected samples in a high resolution (5 to 10 m steps) along the oxycline from oxic to suboxic water masses at two stations. Either the water was sampled by using Niskin bottles attached to a CTD or from a Niskin bottle submerged into the water from a Zodiac. All samples were directly measured on board by using a purge and trap system attached to a gas chromatograph and mass spectrometer (GC-MS) (Fig. 7.3.1). After trace gas analyses we prepared and stored the samples to analyse dimethylsulphoniopropionate (DMSP), the precursor of DMS and dimethylsulphoxide (DMSO) the oxidation product of DMS. Both compounds will be measured in the laboratory at our home institute, GEOMAR.

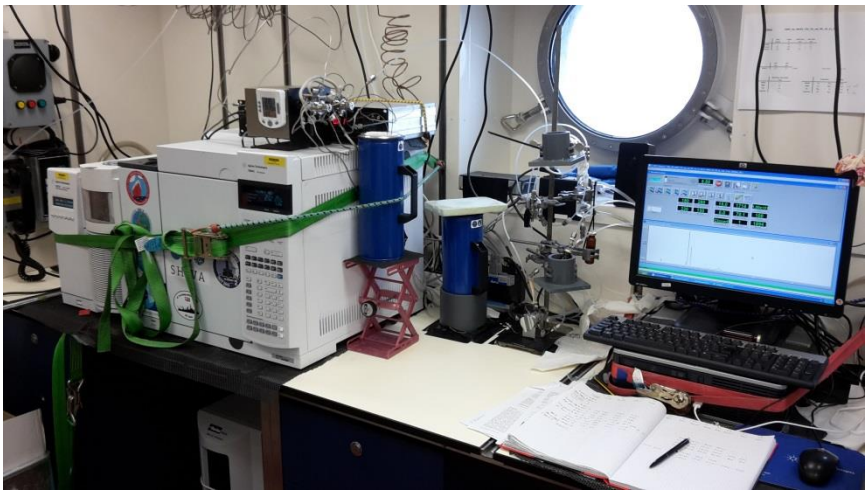

Figure 7.3.1. Purge and trap GC-MS on board R/V Sonne.

Preliminary results

Surprisingly, we detected less DMS (< 2nmol/L) in the coastal upwelling region (8°-12°S) than in the other parts of the cruise (Fig. 7.3.2). Highest surface concentrations could be detected while crossing the equator. In contrast, isoprene concentrations peaked in the upwelling region (8°-12°S). However, concentrations did not exceed 80 pmol/L. Mean concentrations outside the upwelling stayed very low, at 20-30 pmol/L. Both results show that the Peruvian upwelling is suppressed due to El Niño.

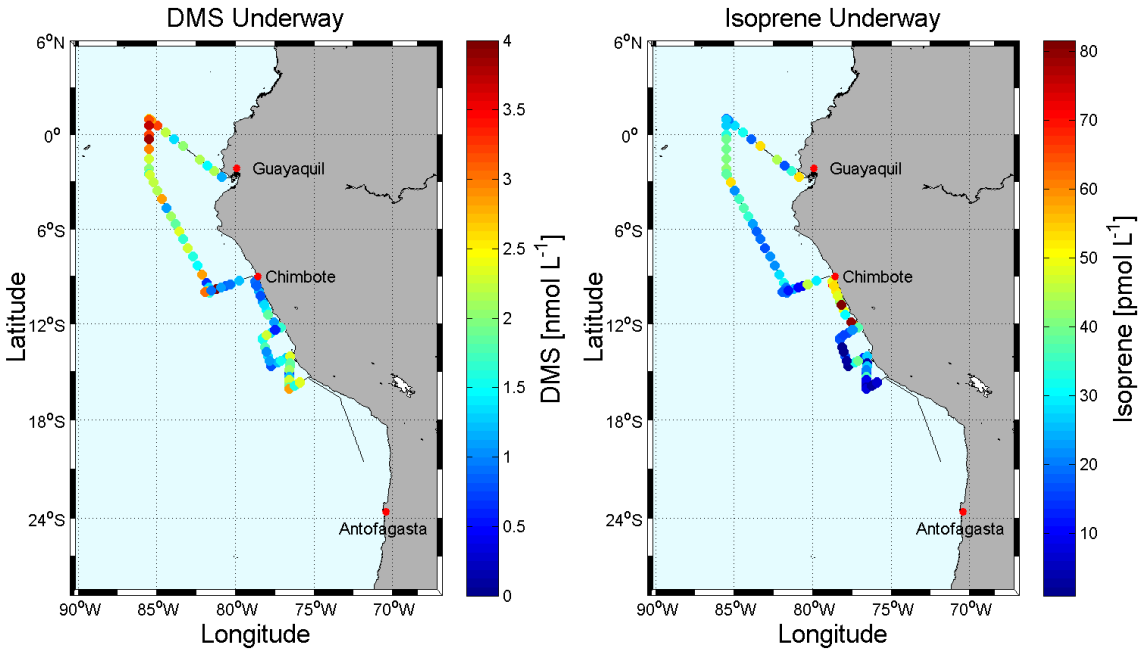

Figure 7.3.2. Hourly to 3 hourly underway measurements of DMS (left) und isoprene (right).

Expected results

We suppose elevated DMS and isoprene concentrations within the centre and/or at the edges of the upwelling were due to elevated productivity of phytoplankton and bacteria. It might be possible that we can observe a concentration gradient of the trace gases in the

surface seawater from eutrophic to oligotrophic regions. Furthermore, we assume a change in the concentrations of especially DMS and DMSO from oxic to anoxic water. It might be possible that DMSO is used as an oxygen donator and get be reduced to DMS in the OMZ by facultative anaerobic bacteria.

We observed in eastern Atlantic Ocean a close relationship between DMS and isoprene in nitrate depleted water. We suggested that certain microbes might be able to produce both DMS and isoprene under nitrate limitation. We hope to find the same relationship also in the eastern Pacific Ocean.

7.4 Underway measurements of carbonyl sulphide

CASCADE – Carbonyl Sulphide Cycling in Aphotic Depths (continuous pump)
Sinikka Lennartz, Christa Marandino

Objective/Intro

Carbonyl sulphide (OCS) is the most abundant sulphur gas in the atmosphere, and the ocean is thought to contribute the dominant part to its atmospheric budget. In the atmosphere, OCS acts as a greenhouse gas, but the warming effect is currently cancelled out by its contribution to aerosol formation in the stratospheric Junge layer, which increases the albedo of the planet. Recently, the potential of tropospheric OCS to constrain terrestrial gross primary production is discussed. OCS is taking up by plants during photosynthesis, but is not – as CO_2 – emitted by respiration. With a well explained atmospheric OCS budget, OCS can be used to quantify terrestrial gross primary production. However, the atmospheric budget of OCS is currently not well understood. A large missing source is assumed to be located in the tropical oceans. Our objective is thus to quantify air-sea gas exchange of OCS in the Peruvian upwelling region. By correlation with other parameters such as pigments, nutrients, temperature, dissolved organic sulphur (DOS) and fluorescent dissolved organic matter (FDOM), spatial and temporal variations will be analysed.

Another open question is the light-independent production of OCS. Within the project CASCADE (Carbonyl Sulphide Cycling in Aphotic Depths), continuous depth profiles of OCS were measured for the first time in an upwelling region. The objective here was to assess the correlation to other parameters such as light, oxygen, nutrients, pigments and CS_2 to better understand the light-independent cycling of carbonyl sulphide.

Methods

Underway sampling: OA-ICOS
Continuous (e.g. minutely) OCS mole fractions of OCS were measured in both surface water (5m, inlet in moon pool, 50 minutes per hour) and the marine boundary layer (ca. 30m, monkey deck, 10 minutes per hour). Therefore, water was pumped from the moon pool into a Weiss-type equilibrator, where the OCS concentration from the water equilibrates with the gas phase in the equilibrator. This equilibrated air was then circulated to the instrument and the mole fraction measured. The measurement principle is off-axis integrated cavity output spectroscopy (OA-ICOS). Together with simultaneously logged temperature, the concentration of OCS in the water can then be calculated using Henry's law.

Figure 7.4.1. Deployment of the continuous profiling pump.

Underway sampling of additional parameter: DOS/DOC, FDOM
In addition to the continuous OCS measurements, the underway system was sampled every 3-12 hours for DOS and FDOM. FDOM samples were measured directly after filtration (0.2 µm) onboard using a Fluorescence Spectrometer. DOS samples were filtered, acidified, extracted to PPL cartridges via solid phase extraction (SPE) and deep frozen. The samples will be measured at the Alfred-Wegener-Institute (K. Ksionzek, B. Koch). DOC samples were filtered and deep frozen for further analysis after the cruise.

Depth profiles: Continuous pump
For the depth profiles, the same equilibrator/OA-ICOS set-up is used, but the water supply came from a submersible pump lowered down to 135 m (Fig. 7.4.1). The pump was deployed at 4 stations (stations 2, 4, 7, and 18). The submersible pump was connected to 150 m of Teflon tubing to avoid contamination. Water was continuously pumped through the equilibrator at a flow rate of ca. 5 L per minute during the up- and the downcast. Additional sampling using the pumped water included DOS, FDOM, N_2O and O_2. Next to the pump, additional devices, such as a temperature-depth-logger and an oxygen optode, were connected to also obtain in-situ profiles.

Preliminary results

Underway measurements

The spatial distribution of OCS along the cruise track shows the highest concentrations at the coastal areas (Fig. 7.4.2). OCS showed a strong diurnal variation in the surface water, which coincides with global radiation and thus indicates the known photochemical production. OCS mole fractions in the seawater equilibrated air were higher than the atmospheric background mole fraction, which suggests that the cruise region is a strong source region for atmospheric OCS. OCS was supersaturated in the surface water and thus emitted to the atmosphere for, by far, most of the time of the cruise. This suggests that the role of upwelling areas should be considered in more detail in global budgets of OCS.

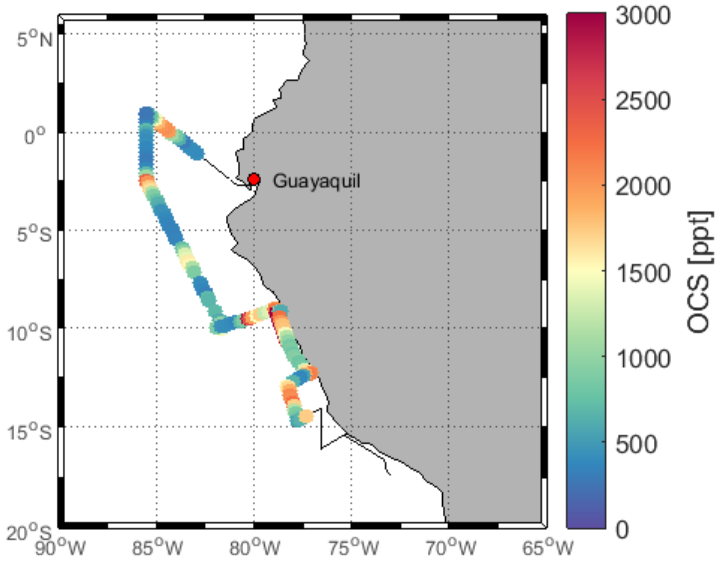

Figure 7.4.2.: *OCS in with seawater equilibrated air during SO243 ASTRA-OMZ. Note diurnal variations and higher concentrations towards the coast.*

Continuous depth profiles

The submersible pump connected to a Weiss-type equilibrator to measure OCS in an upwelling region with oxygen depleted waters was successfully deployed for the first time. OCS concentration correlated strongly with oxygen and decreased below detection limit in oxygen depleted zones.

Expected results

Underway measurements

OCS concentrations will be calculated out of the measured mole fractions. Together with the atmospheric measurements, the air-sea exchange of OCS will be calculated. The data will also be used in a 0D-box model to quantify production and consumption rates of the source and sink processes of oceanic OCS. Finally, global ocean climatologies of OCS will be validated using a database of OCS measurements, of which these measurements will be part.

Continuous depth profiles

The data for the continuous depth profiles will provide continuous information on OCS, O_2 (optode) and temperature, and discrete sampled of FDOM, DOS and O_2 with depth. From a corresponding CTD cast, samples of CS_2 and other biological, physical and chemical parameters were taken. To investigate the role of factors influencing OCS concentrations, the covariation with depth to these parameters will be investigated. The results will help to better constrain and parametrize light-independent production of OCS, which will be used to develop more skilful biogeochemical OCS models.

7.5 Halocarbons

Helmke Hepach, Sonja Endres, Gert Petrick, Birgit Quack

Objective/Intro

Halocarbons, short-chain hydrocarbons with one or more halogen atoms, are produced naturally in the ocean by biological and chemical processes. Highly productive ocean regions such as upwelling systems, where cool water rich in nutrients is brought up to the surface, have been identified as source regions for these compounds (Quack et al. 2007; Hepach et al. 2015). Microbial production and removal processes in the surface ocean are affecting the sea-air fluxes of the halocarbons, but the underlying processes and magnitude of the biogenic sources and sinks in the tropical East Pacific are poorly known. The brominated compounds bromoform ($CHBr_3$) and dibromomethane (CH_2Br_2) are considered as the main carriers of organic bromine into the atmosphere from the ocean, while the iodinated methyl iodide (CH_3I), chloroiodomethane (CH_2ClI), and diiodomethane (CH_2I_2) may carry significant amounts of iodine into the troposphere. Once these compounds reach the atmosphere, they can be degraded very rapidly and take part in numerous chemical processes in the troposphere such as the formation of aerosol and ultra-fine particles, HO_x and NO_x chemistry, and ozone chemistry. The tropics are of particular interest, since tropical deep convection can lift surface air rapidly into the stratosphere. This is especially important for the longer lived $CHBr_3$ (atmospheric lifetime of 24 days) and CH_2Br_2 (atmospheric lifetime of 120 days), which are involved in ozone destructing cycles, once they reach the stratosphere.

The Peruvian upwelling is one of the strongest upwelling systems in the world. During the M91 cruise from Callao to Callao in December 2012, we characterized the region for the first time with respect to halocarbons. Surprisingly, the strong upwelling was only a moderate source for $CHBr_3$ and CH_2Br_2, which have previously often been found as major halocarbons in the Atlantic upwelling systems. In contrast, very large concentrations of CH_3I, CH_2ClI and CH_2I_2 were observed, despite their shorter lifetimes in sea water. These led to high iodocarbon emissions, which contributed significantly to the tropospheric iodine loading above the tropical East Pacific. In contrast to M91, a strong El Niño occurred in 2015. It is unknown how this affects halocarbon production and emissions in the region. One goal of the ASTRA-OMZ cruise is therefore to characterize the upwelling system in different El Niño Southern Oscillation conditions with regard to halocarbons.

Methods

Halocarbons from underway and deep water samples were measured on two purge and trap systems during the cruise, each attached to a gas chromatograph and a mass spectrometric detector (Fig. 7.5.1). About 50 mL of the sample were purged for 40 to 45 minutes using a stream of helium of 30 mL min^{-1} with concurrent heating to 70 °C. The trace gases were trapped on stainless steel tubing in liquid nitrogen. After the purging time, the sample was desorbed at 100 °C and injected into the GCs. Underway samples were measured using a gas chromatograph equipped with an ECD (electron capture detector), while CTD and incubation samples were measured using GC-MS (combined gas chromatography and mass spectrometry). In total, 120 underway samples and about 90 samples were measured from the CTD and surface gradient stations. In cooperation with Sonja Endres, deuterated dibromomethane and carbon 13 labelled bromoform was measured in addition to the natural compounds in 80 samples to determine bromocarbon cycling. At four selected stations along the cruise track, seawater was incubated with ^{13}C- and D-labelled substrate to study the microbial degradation of brominated halocarbons. The unfiltered seawater was amended with the substrate and incubated at 20°C in the dark for up to 10 days. Glucose, phosphate, and treated ship wastewater were added to some bottles to stimulate microbial growth. Samples were collected regularly for bacterial and phytoplankton abundance, nutrients, bacterial community composition, bromocarbons, carbohydrate, amino acid and dissolved organic matter concentrations. Control incubations included seawater only and artificial seawater or ultrapure water with ^{13}C-labelled substrate. Experimental data are compared to measured depth profiles of microbial biomass, as well as bromocarbon and organic matter concentrations. In total, 105 incubation bottles were sampled in four experiments and the bromocarbons were measured during the cruise. All biological parameters will be analyzed in the home laboratory at GEOMAR in Kiel.

Figure 7.5.1. Halocarbon GC-MS system on board ASTRA-OMZ SO243.

Preliminary results

First evaluation of the data shows very different results than M91 (Fig. 7.5.2). While the most intense upwelling was observed in the north, strongest upwelling cells during ASTRA-OMZ occurred in the southern part of Peruvian waters. Both surface and deeper water was characterized by much larger concentrations of bromocarbons than of iodocarbons during ASTRA-OMZ, which stands in contrast to the previous M91 cruise. Many CTD stations appeared to be well mixed with respect to the upper water column with much less halocarbon concentrations in the lower, oxygen depleted water masses. However, in contrast to M91, not all OMZs were completely depleted in halocarbons. The very surface of the water column was in two out of three surface gradient profiles completely mixed, indicating no influence of surface production/depletion of halocarbons at these stations. These were also characterized by comparatively high wind speeds. During low wind speeds at the last station, station 18, the surface gradient profile showed varying concentrations in the upper 5m of the water column with maxima at 2 to 3 m depth, which show that high productivity may strongly influence the very upper water column. These data will be further evaluated at GEOMAR. In the incubation experiments a sligth conversion of ^{13}C-labelled bromoform to dibromomethane was observed in some experiments over the course of some days, which may yield an in situ conversion rate for the Peruvian upwelling.

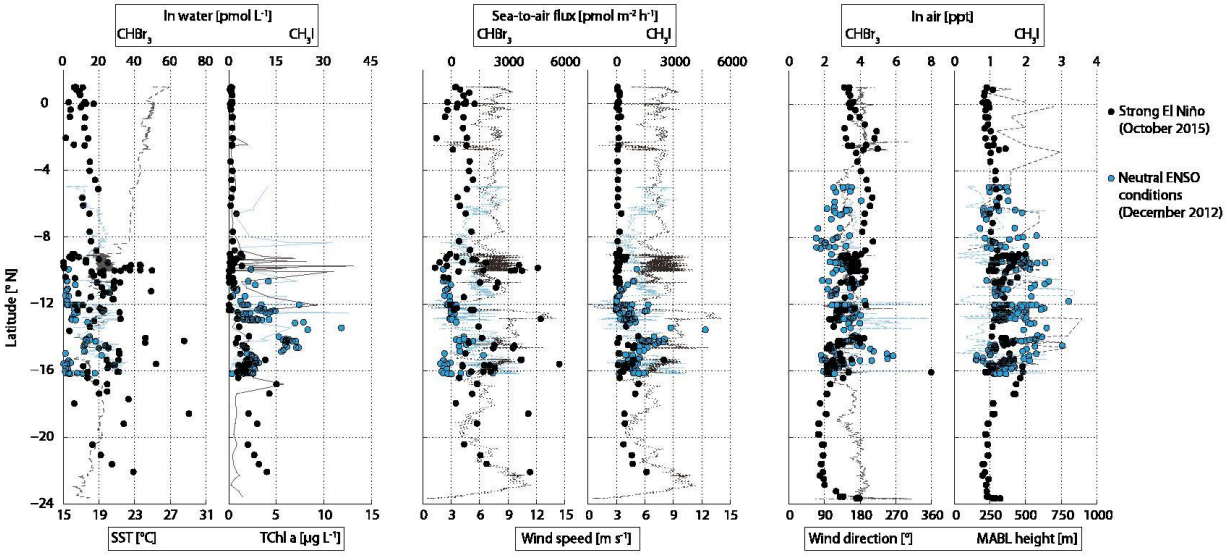

Figure 7.5.2. Comparisson of M91 (blue) and ASTRA-OMZ (black) halocarbon data, left) surface ocean concentrations; middle) sea-to-air fluxes; right) atmospheric mixing ratios.

Expected results

Our results will be compared to several other biogeochemical and physical parameters including DOM (dissolved organic matter) measurements, phytoplankton species composition, nutrients, oxygen and physical parameters, such as sea surface temperature and salinity. This will help to identify possible source organisms and processes related to halocarbon production and their oceanic emissions. The water column distribution of halocarbons along with metadata will help interpret the surface water distributions. Emissions will be calculated using the results of the surface water measurements in conjunction with the atmospheric data, which were sampled in parallel every three hours along the cruise track.

We expect higher bromocarbon emissions during ASTRA-OMZ than during the previous M91 cruise and potentially much lower emissions for CH_3I, CH_2ClI and CH_2I_2. The data from the incubation experiments will be used to determine bromocarbon cycling in the tropical East Pacific.

7.6 Trace elements

Christian Schlosser, Insa Rapp, Thomas Browning and Martha Gledhill

Objective/Intro

Trace metals such as iron (Fe), cobalt (Co) and manganese (Mn) are essential elements for all organisms and therefore play a pivotal role in the functioning and structure of marine ecosystems and the oceanic fixation of carbon and nitrogen (Boyd & Ellwood 2010). The important role of trace elements is due to their obligatory requirement in enzymes required to drive the biological carbon and nitrogen cycles (Falkowski et al. 2008). In the Eastern Tropical South Pacific (ETSP) the main of source of trace metals to the ocean are the shelf and slope sediments, with enhanced concentrations of trace metals often associated with the oxygen minimum zone (Loescher et al. 2014; Chever et al. 2015; Dale et al. 2015). Although inputs can be high from the shelf, concentrations of metals are known to decrease rapidly offshore (Bruland et al. 2005) so that productivity in waters adjacent to the OMZ can be limited by Fe or possibly other trace nutrients, such as Co. The mechanisms controlling the loss of trace metals from the upwelled low oxygen waters of the ETSP are not well constrained. The objectives of our work on the ASTRA-OMZ cruise were, therefore, to understand processes controlling the loss/retention of trace metals (particularly Fe) in near shore waters of the ETSP, to investigate the phytoplankton community response to gradients in trace metal (particularly Fe and Co) distributions, and to investigate the distribution of biologically produced Fe compounds (heme *b* and siderophores) in the ETSP.

This part of the cruise is a contribution to the second phase of the SFB754 project “Climate - Biogeochemistry Interactions in the Tropical Ocean”.

Methods

Samples for trace metal analysis were collected to depths of up to 1200 m using trace metal clean sampling equipment comprising a set of 12 GoFlo (General Oceanics) mounted on a Kevlar wire (Fig. 7.6.1). Underway samples were collected using a tow fish equipped with trace metal clean tubing and a Teflon bellows pump for transferring a constant supply of water to the clean container. Samples were processed in a class 1000 clean container.

Figure 7.6.1. Deployment of a GoFlo bottle at the Kevlar wire.

Particulate, dissolved and soluble trace metals

Underway samples for trace metal analysis were collected every 1.5 hours from the tow fish deployed at 2-3 m water depth. Dissolved samples (DFe) were filtered by an 0.8/0.2 µm Acropak 1000 cartridge filter and transferred into 125 mL acid washed low density polyethylene (LDPE) bottles. Total dissolvable (unfiltered) samples (TDFe) collected every 3 hours were stored in 125 mL LDPE bottles and acidified similarly with 140 µL HCl (UpA grade Romil) to pH 1.9. Dissolved water samples from the water column were filtered by an 0.8/0.2 µm Acropak 500 cartridge filter and transferred into 125 mL acid washed low density polyethylene (LDPE) bottles. Total dissolvable (unfiltered) samples were stored in 125 ml bottles. Soluble samples were filtered through a 0.02 µm Whatman filter and filled in 60 mL acid washed LDPE bottles. All water samples were acidified to pH1.9 using UpA grade HCl from Romil, Iodate and iodide samples (I^-) from the water column were stored in 100 ml opaque Nalgene bottles and stored frozen at -20°C. The particulate fraction of ~ 4 L was collected on 0.2 µm 25mm polyether sulphone (PES) filters using 0.2 bar N_2 overpressure and then stored frozen for later analysis at -20°C. Unfiltered surface and water column samples for Fe(II) and hydrogenperoxide (H_2O_2) analyses (Fe(II)/H_2O_2) were collected and analysed immediately on board by luminol chemoluminescence using a flow injection analyser and a method outlined by Croot and Laan (2002). For nano molar nutrient analysis (nuts), 60 mL of 0.2 µm filtered surface seawater collected by the tow fish, were stored in 15 mL vials and shipped frozen to the GEOMAR, Kiel, for later analysis in the lab. Table 11.3.1

(see appendix) shows all collected samples from the 51 tow fish stations. Table 11.3.2 (see appendix) all samples retrieved from the 13 Go-Flo deployments.

Phytoplankton chlorophyll-a biomass, community composition and nutrient stress status
Sample collection for this suite of measurements was carried out every ~1.5 hours of steaming time or between CTD stations. 3 hour time points matched up with the coordinated moon pool sampling strategy of the various working groups on the cruise (see master sampling sheet for times/locations/Bedford numbers). The total number of sampling points is 117.

- *Chlorophyll-a concentrations:* 100 mL samples were filtered onto Macherey-Nagel GFF filter pads and extracted for 12-24 hours in 10 mL 90% acetone in a -20 °C freezer in the dark before measurement on a Turner Designs trilogy fluorometer following the method of Welschmeyer (1994).

- *Analytical flow cytometry:* 1.87mL of seawater was mixed with 0.125mL 16% paraformaldehyde yielding a final paraformaldehyde concentration of 1%. Mixing was carried out using vortex, after which samples were left for 10 minutes at room temperature in the dark before transfer to a -80 °C freezer. Samples will be analysed on a FACSort flow cytometer (Beckton-Dickinson, UK) following the method of e.g. Davey et al. (2008), with the intention of analysing for nanophytoplankton, picophytoplankton, Synechococcus, Prochlorococcus and total bacterial cell counts.

- *Fast Repetition Rate fluorometry (FRRf):* A FASTOcean fluorometer (Sensor ID: 14-9740-003) with integrated FASTact laboratory system (both Chelsea Technologies LTD., UK) was used to measure in vitro variable fluorescence of phytoplankton samples after a 30 minute dark acclimation period (with temperature maintained by submersion in continuously flowing water from the ship's underway system). Fluorescence light curves were also ran following a protocol of progressively increasing light intensities between 20 and 2000 µmol photons m^{-2} s^{-1} (as described in Browning et al. (2014). Blank filtrates (0.2 µm filtrates) were measured for virtually all samples. All FRRf data will be blank-corrected and fluorescence parameters recalculated upon return to GEOMAR.

- *Incubation experiments:* Five 48 hour duration on-deck incubation experiments were carried out in 1L trace-metal-clean polycarbonate bottles. Seawater was collected at night time using the trace-metal-clean towed-fish described previously. Filling times were approximately ~30 minutes for 1L bottle experiments (total volume = 18L). Bottled seawater was spiked with the following combination of nutrients/trace metals: Fe, Co, Fe+Co, Fe+ vitamin B12

Final incubation concentrations of Fe and Co were 2 nM and 100 pM vitamin B12. Initial conditions were sampled in 1L bottles for all experiments at 3 time points throughout the bottle filling procedure. Triplicate control bottles (1L) with no nutrients added were also collected alongside all treatment experiments.

Bottles were placed in on-deck incubators connected to the ships underway flow-through system to continuously maintain temperatures at that of sea surface waters. Incubators were screened with Blue Lagoon screening (Lee Filters), which maintained irradiance at ~30% of

that of the surface. After 48 hours incubation, experiments were taken down and measurements made for:

Chlorophyll-a concentrations (1 replicate per treatment bottle), FRRf (single acquisitions for each triplicate bottle; fluorescence light curves for pooled treated samples), analytical flow cytometry, particulate B12 concentrations (pooled treatments), protein analysis (control and Fe-treated samples only).

Heme b concentrations in the ETSP

Heme *b* was sampled at three hourly intervals whilst the ship was underway (see appendix Tab. 11.3.3 and 11.3.4). One to 1.5 liters were filtered onto glass fiber filters (25mm). Filters were frozen at -70°C for later analysis. Filters for POC/PON analysis were also collected on precombusted GF/F filters (25mm) and frozen at -20°C. Samples were collected from the ship board underway seawater system. At stations, depth profiles from the surface 100 m were obtained from the in situ pump in the moon pool (5 m) and from the shallow CTD cast (> 5m). Heme *b* is detected in particulate material collected on glass fibre filters (nominal cut off 0.7 µm; (Gledhill et al. 2013; Gledhill 2014) Samples were frozen at -80 °C and will be analysed in the laboratory at GEOMAR by high performance liquid chromatography - electrospray ionisation – mass spectrometry (HPLC-ESI-MS; Gledhill 2014).

Siderophore distributions in the ETSP

Extraction and preconcentration of dissolved and particulate siderophores: Seawater (20 L) was collected from a high volume continuous pumping system at three depths – surface, the chlorophyll maximum and from within the oxycline (see appendix Tab. 11.3.5). Samples were filtered and particles collected using 0.2 µm CellTrap membrane filters. Particles were eluted from the filters and frozen at -80 °C for later analysis of particulate siderophores after extraction into ethanol. Dissolved hydroxamate siderophores were concentrated onto polystyrene divinyl benzene polymeric resin (ISOLUTE ENV+ solid phase extraction cartridge), dissolved catecholate and mixed ligand siderophores onto modified hydrophilic cartridges (HLB, Waters Oasis) and were frozen at -20 °C. Siderophores will be quantified by high performance liquid chromatography – inductively coupled plasma – mass spectrometry (HPLC-ICP-MS) and identified HPLC – ESI-MS (Mawji, Gledhill, Milton, et al. 2008).

Remineralisation incubations: An incubation experiment was carried out using seawater collected from the trace metal clean towfish on the 9th October 2015 at 19:15 UTC. Seawater was sampled into trace metal clean gas tight bags, enriched with dead isotopically labelled (^{54}Fe and ^{57}Fe) *Emiliania huxleyii* cells and incubated for 5 days in the dark at ambient surface water temperatures. Unenriched seawater served as a control. Incubations were sampled for siderophores, particulate iron and dissolved iron after 5 days. Siderophores in the incubations will be quantified by high performance liquid chromatography – inductively coupled plasma – mass spectrometry (HPLC-ICP-MS) and identified and characterized by HPLC - electrospray ionization – mass spectrometry (ESI-MS) (Mawji, Gledhill, Milton, et al. 2008; Mawji, Gledhill, Worsfold, et al. 2008). Iron concentrations will determined by ICP-MS following digestion and/or preconcentration.

Preliminary results

Preliminary results of H_2O_2 and Fe(II) indicate the photoreductive production of both compounds in the upper water column (Fig. 7.6.2). The outflow of Fe(II) containing sediment porewaters represent a secondary Fe source.

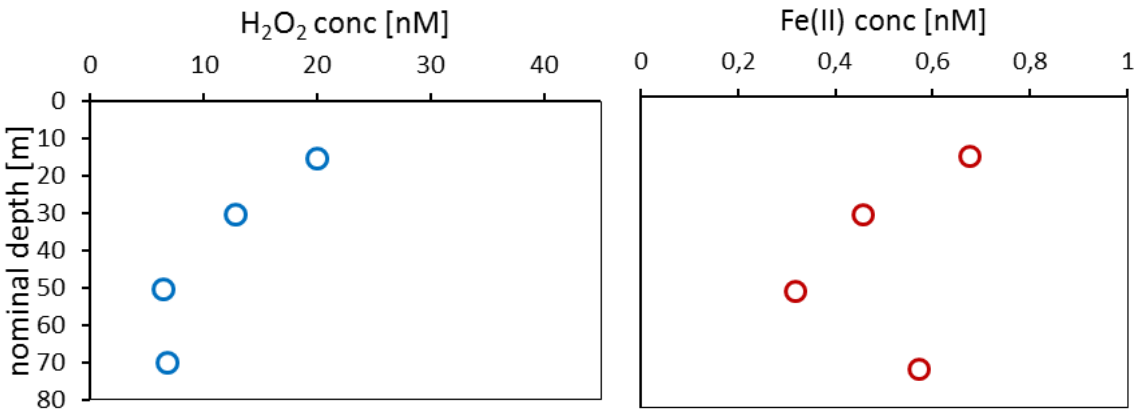

Figure 7.6.2. Hydrogen peroxide and Fe(II) concentration in the water column of Station 8

Expected results

Heme *b*

Heme *b* is an iron containing prosthetic group of hemoproteins which are ubiquitous to life and essential to photosynthesis, respiration and many redox processes within the cell. Investigations of heme b concentrations in particulate material from the field indicate that both the absolute abundance and the abundance relative to biomass indicators such as particulate organic carbon and chlorophyll *a* are related to ambient iron concentrations in surface ocean waters (Gledhill et al. 2013; Honey et al. 2013). This is the first study of heme *b* distributions undertaken in the Pacific Ocean, and the first to investigate heme *b* in a region influenced by upwelling and strong gradients in iron concentrations arising from oxygen depletion in the water column. There is thus potential for variability in heme *b* distributions connected with gradients in iron concentrations and also possibly with changes in iron demands for microbial metabolism within oxygen depleted waters.

Siderophores

Siderophores are produced by bacteria as part of a high affinity iron uptake mechanism. Siderophores are the only characterised fraction of the dissolved iron pool, and they appear to be present at low to undetectable concentrations in seawater. The exact role of siderophores in bacterial iron uptake is not fully known, but it is likely that bacteria produce siderophores when they are iron, but not carbon limited. They are thus likely to play an important role in influencing bacterial community composition and possibly also be involved in an “arms race” for iron in productive regions. To date there have been relatively few studies of siderophore concentrations in the ocean. Picomolar concentrations have been measured in the surface waters of the Atlantic Ocean, and concentrations were observed to increase in equatorial regions, where bacterial numbers and POC concentrations were higher (Mawji, Gledhill, Milton, et al. 2008). No studies in upwelling regions or in the South Eastern Pacific have yet been reported and little is known of how siderophore concentrations might vary with depth. On SO243, we will therefore undertake the first survey of siderophores

in the Peruvian upwelling regime. In addition, we have taken large volume samples from 3 depths in order to investigate siderophore abundance in relation to chlorophyll distributions in the water column. Siderophore production in the remineralisation experiment will be used to aid the identification of siderophores in seawater samples.

7.7 Nutrients and Oxygen

Martina Lohmann, Hanna Campen and Damian Grundle

Objective/Intro

Dissolved nutrients (i.e. nitrate, nitrite, silicate and phosphate) and oxygen were measured on-board SO243 for the purpose of understanding vertical and horizontal nutrient and oxygen distributions distributions. The availability of nutrients and oxygen play a key role in regulating a number of the biogeochemical processes that were measured during the cruise, so these were critical ancillary measurements that will be used in the interpretation of results from many of the core projects conducted during SO243.

Methods

Nutrients: Samples for the measurement of dissolved nutrients were collected at all stations during SO243, and at times during multiple CTD casts at a station. Samples were also collected from the underway system. In total, 450 samples were collected from CTD casts and 120 samples were collected from the underway system, for a total of 570 nutrient samples collected during the cruise. With the exception of the last 13 underway samples, which were frozen and measured upon returning to GEOMAR, all nutrient samples were measured fresh at sea with a QuAAtro auto-analyzer from SEAL Analytical. Nitrite was measured following reaction with sulphanilamide to form a diazo compound. Nitrate was measured as nitrite following reduction on a cadmium coil. Phosphate was measured after reaction with molybdate and antimony ions. Silicate was measured by forming a silico-molybdate complex which was subsequently reduced to molybdenum blue. Based on the measurement of 59 triplicate samples, the precision of the nutrient measurements was calculated to be ±0.03 µmol L^{-1}, ±0.13 µmol L^{-1}, ±0.01 µmol L^{-1} and ±0.13 µmol L^{-1}, for nitrite, nitrate, phosphate and silicate, respectively.

Oxygen: Samples for the measurement of dissolved oxygen concentrations were collected from CTD-Niskin bottles at all stations and from the underway sampling system using the overflow technique. Following collection and fixation, samples were stored in the dark before being measured by manual end-point determination within 10 hours following the protocol outlined by Hansen (1999). Based on the measurements of 48 replicate (duplicates and triplicates) samples, the precision of the dissolved oxygen measurements was calculated to be ±0.24 µmol L^{-1}.

Preliminary results

Dissolved nutrient and oxygen concentration data are currently being used in the interpretation of findings from many of the core projects conducted during SO243, and a full description of the nutrient and oxygen results is beyond the scope of the cruise results. Interestingly, however, while the vertical distribution of dissolved nutrients and oxygen concentrations were similar to those reported from previous work in the ETSP, the overall bulk nutrient and oxygen concentrations were noticeably different at times. For example, as reported in Stramma et al., (2016), near surface oxygen concentrations were at times higher

during SO243 than during previous cruises. Strong upwelling along the Peruvian coastline typically brings very low oxygen waters from the core of the OMZ up to the near surface waters, however, during SO243 upwelling was reduced due to developing El Niño conditions and this led to less low oxygen water being mixed into the near surface waters (Stramma et al. 2016). Likewise, nitrate concentrations and N:P ratios were also higher at times in the near surface waters during SO243 when compared to previous cruises in the same region (Stramma et al. 2016). Again, strong upwelling usually brings low nitrate water characterized by low N:P ratios from the core of the OMZ (low nitrate and N:P due to denitrification in the OMZ) into the near surface waters. The reduction in upwelling as a result of the developing El Niño during SO243 suppressed the upward flux of low nitrate and low N:P waters, however, and these results highlight the potential biogeochemical implications of El Niño conditions in the near surface waters of the coast of Peru (Stramma et al. 2016).

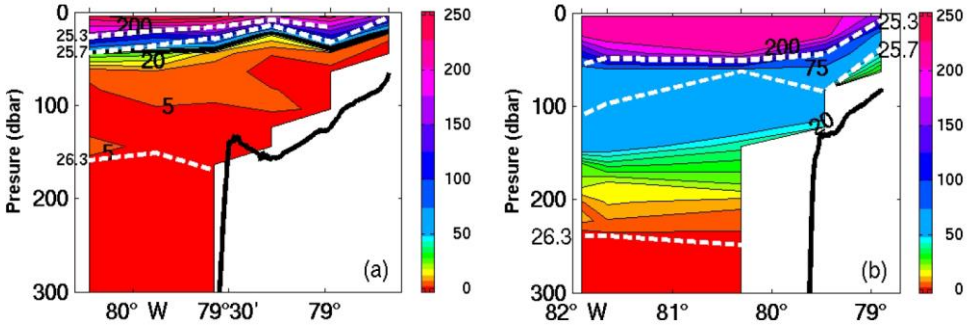

Figure 7.7.1. Oxygen section (color; in µmol kg^{-1}; same color scale in both frames) at ~9°S off the Peruvian shelf for December 2012 (a) and October 2015 (b). Three selected isopycnals are included as white dashed lines. Please note that the section in October 2015 reaches further west than in December 2012 (figure from Stramma et al. 2016).

7.8 Eddy covariance

Alex Zavarsky, Tobias Steinhoff, Damian Arevalo and Christa Marandino

Objective/Intro

In order to investigate the ocean's role in the atmospheric budget of climate active trace gases, we deployed an eddy covariance (EC) direct flux measurement system onboard R/V Sonne. EC can be used to perform emission/deposition measurements without the typical pitfalls associated with bulk flux calculations, as well as to constrain the main forcing on air-sea gas exchange. Using the direct flux (*F*) from EC, $F = \rho \langle w'c' \rangle$, we can attempt to improve the gas transfer parameterization (*k*) used in bulk formulas, $F = (HCw - Ca)$, where ρ is density, w' are the fast fluctuations in vertical wind speed, c' are the fast fluctuations in atmospheric gas concentrations (brackets denote time average), C_w and C_a are water and air concentrations, respectively, and H is the Henry's law solubility constant. Our goal was to measure dimethylsulphide (DMS), isoprene, acetone, CO_2 and N_2O flux. Measurements started with favorable wind conditions after Station 1. For the first time ever direct N_2O fluxes were measured in the marine environment.

Methods

Atmospheric levels of DMS, isoprene and acetone were measured using an atmospheric pressure chemical ionization mass spectrometer (AP-CIMS). Additionally CO_2 and N_2O measurements were taken using optical measurement techniques at a frequency of 5 Hz. Air was sampled through a ½" tube from a mast welded to the bow (approximately 14 m above the sea surface) at a flow rate of 40 l min^{-1}. To obtain turbulent wind speed measurements and sensible heat flux, a sonic anemometer was placed at the bow mast. A GPS and inertial navigation system (INS) was used for motion correction (Fig. 7.8.1).

Figure 7.8.1. Eddy covariance mast on the bow of R/V Sonne in the port of Guayaquil.

Preliminary results

Due to the high presence of ammonia in the air, the sensitivity of the AP-CIMS was at its limits for eddy covariance flux measurements. Still with home post-processing it will be possible to obtain flux measurements. For N_2O and CO_2 first data quality checks exceeded the expectations and soon direct flux data, for the first time for N_2O, will be available (Fig. 7.8.2).

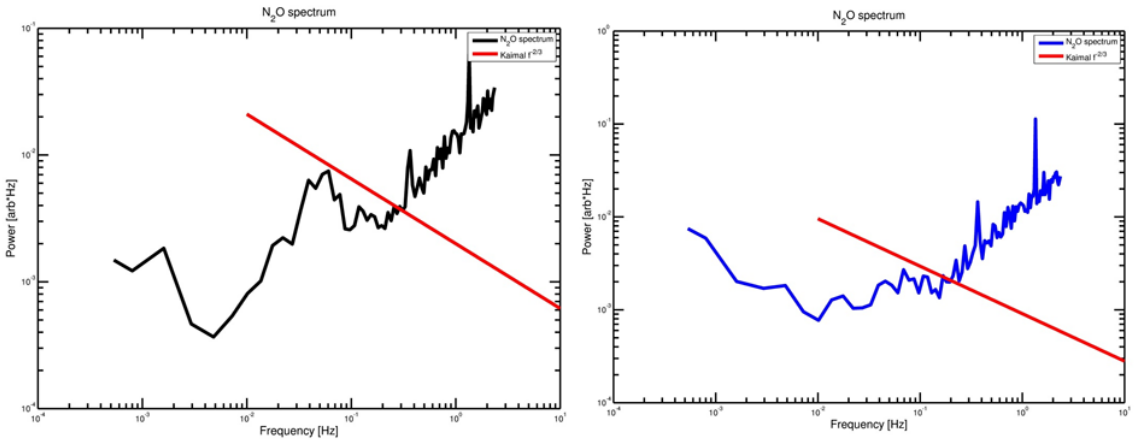

Figure 7.8.2. N_2O power spectra. Left: Data from a period with large sea to air gradient. Right: Data from a period with a small sea to air gradient. The red line indicates the inertial subrange from Kaimal et al., (1972).

Expected results

It will be interesting to see if the predicted high fluxes of N_2O can be reproduced by a direct flux measurement. The fluxes of CO_2 and DMS will be used to investigate the influence of solubility on the gas exchange processes. If there should be high discrepancies between various flux measurement methods, we will try to find reasons by comparing our results to those from the other working groups on the ship. Especially, the work of Birthe Zäncker (section 7.14) will be used to understand how the presence or absence of the sea surface microlayer influences gas exchange.

7.9 Atmospheric physics

Kirstin Krüger, Alina Fiehn, Birgit Quack and Elliot Atlas

Objective/Intro

The Peruvian upwelling area is a known source for very short lived halocarbons like bromoform, dibromomethane and methyl iodide. They play an important role for the tropospheric and stratospheric halogen burden and ozone budget. Here we are interested in how meteorological conditions and in particular El Niño affect the halocarbon abundance in the marine atmospheric boundary layer (MABL) and what their contribution to the free troposphere and stratosphere is.

Methods

Regular radio- and ozonesonde launches have been carried out to monitor the atmospheric structure and composition along the cruise track in order to compare with marine trace gas abundance above the Peruvian upwelling (Fig. 7.9.1). The radiosonde profiles were delivered to the Global Telecommunication System in real time to improve the weather and meteorological reanalyses products, which will later be used to calculate the air mass origin and transport with high resolution Lagrangian transport modelling of various marine trace gases. For this, regular air canister samples have been taken to determine more than 50 different trace gases concentrations. Available meteorological instruments on board of the R/V SONNE (DSHIP data) are accompanied by continuous precipitation and irregular aerosol optical depth (AOD) measurements. 66 radiosondes were launched on standard WMO times (00, 06, 12, 18 UTC). Additionally, 4 ozonsondes were started above the Humboldt Current and the Peruvian upwelling. 140 air canisters were filled with air (40 psi) along the cruise track at 3 hourly resolution. For precipitation measurements an ODM470 disdrometer from University of Hamburg, which was employed on the radar deck of RV SONNE, was available. Whenever sunny and cloud free, AOD was measured with the Microtops instruments from NASA Goddard.

Figure 7.9.1. Preparation to launch a radiosonde from the aft deck of R/V Sonne.

Preliminary results

The radiosondes launches illustrate a tropical atmosphere (Fig. 7.9.2) with the surface trade wind system, trade inversion layer, westerly wind of the Hadley cell in the upper troposphere, a high and cold tropopause and the quasi –biennial oscillation (QBO) of the inner tropical stratospheric zonal wind. A pronounced inversion layer at approximate 1 km altitude is striking, which is accompanied with an accumulation of high relative humidity and moderate to fresh southerly winds below this inversion. Convective activity was limited and very few precipitation events were detected on 15th October and 20th October. Figure 7.9.3 displays the preliminary ozonesonde profiles launched within the Humboldt Current and Peruvian upwelling. The profile on 10th October 2015 reveals tropical high ozone levels whereas the following three ozone launches show lower subtropical ozone all four profiles maximizing at around 27 km altitude. Tropospheric ozone levels reveal distinct fluctuations within 9.5°S and 16.5°S latitude, which will be further analysed together with halocarbon measurements and trajectory calculations. Back in the home laboratories we will revise the radiosonde and ozonesonde data and analyse the MABL and trade inversion layers (height and

characteristic) as well as the tropopause heights. The air canisters will be shipped back to RSMAS/ University of Miami where they will be analysed for more than 50 trace gases.

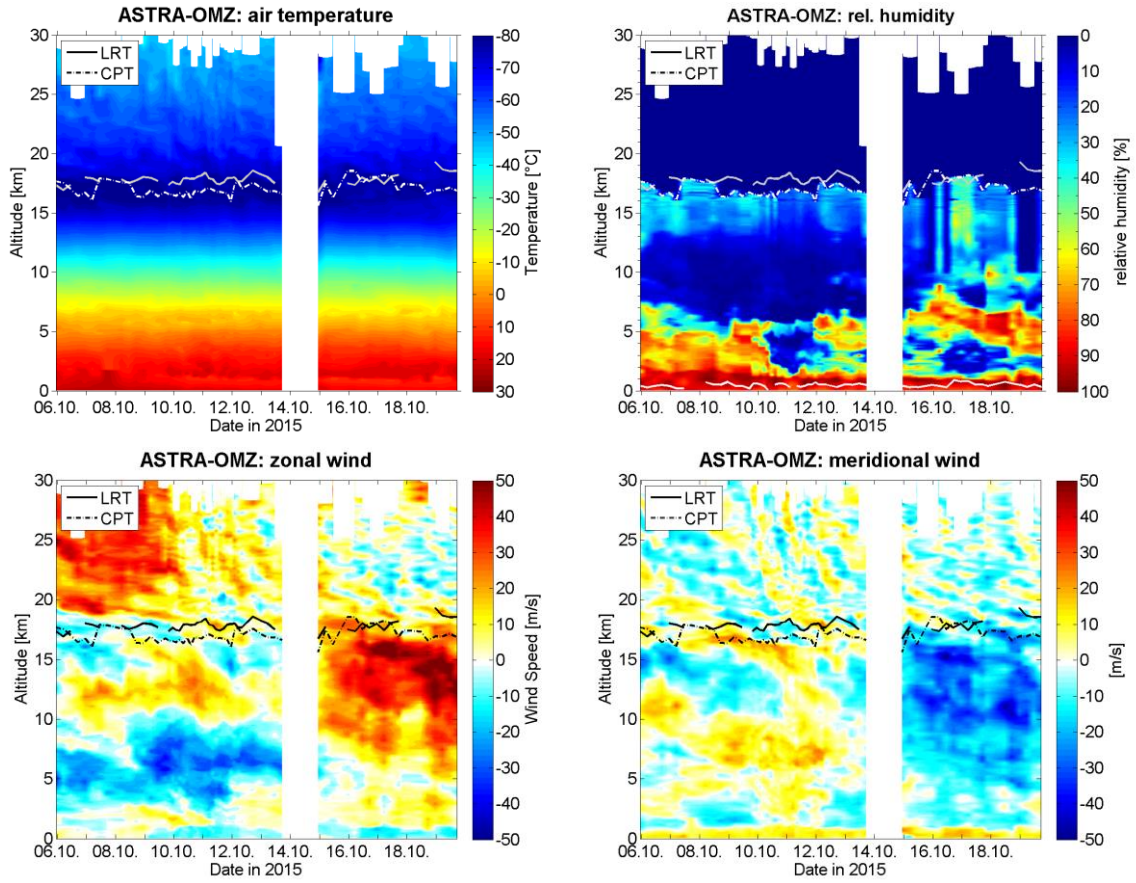

Figure 7.9.2. Temperature (deg C), relative humidity (in %), zonal wind (m/s) and meridional wind (m/s). Radiosonde launches along ASTRA-OMZ cruise were centred on 00, 06, 12, 18 UTC. The white gap marks the radiosonde launch break at Chimbote harbour.

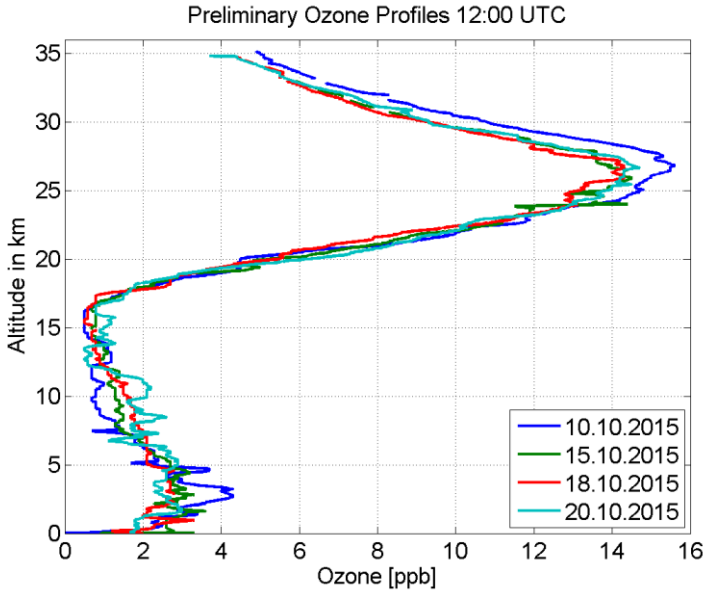

Figure 7.9.3. Ozone mixing ratios [in mPa] for the troposphere (to 17 km altitude) and the stratosphere (above 17 km altitude) launched within the Humboldt Current and Peruvian upwelling at 12 UTC on 10th, 15th, 18th, and 20th October 2015.

Expected results

Finally, we will analyse the air mass origin and flow for the marine trace gases, including a characterisation of the typical atmospheric regimes during ASTRA-OMZ impacting the trace gas distribution. For this we will compare the SO243 cruise during October 2015 with the M91 December 2012 cruise, thus also focussing on the current El Niño versus normal conditions. We will also analyse the halocarbon transport from the ocean surface taking their derived sea-to-air fluxes based on surface water and atmospheric measurements from the halocarbon group and calculate their contribution to the troposphere and stratosphere (see section 7.5). The ozonesonde profiles will be analysed and related to the observed halocarbon abundances. Marine trace gas concentrations will be analysed along the cruise track, including major anthropogenic and natural components.

7.10 Deliberate tracer release with the OTIS and transient tracers

T. Tanhua, T. Stöven, M. Müller, A. Pinck

Objective/Intro:

This part of the cruise is a contribution to the proposed 3rd phase of the project SFB754, Climate - Biogeochemistry Interactions in the Tropical Ocean. Previous research efforts conducted during SFB754 in the Peruvian shelf Oxygen Minimum Zone (OMZ) region have demonstrated that sediment-ocean interface processes are potentially very important for the biogeochemistry of the OMZ and possibly for the development of the OMZ itself. The anoxic sediments of the OMZs have the potential to release significant amounts of reactive nitrogen, phosphorous, reduced iron (Fe2+) and silicate to the benthic boundary layer. These substances, if brought to the photic zone, exert a significant positive feedback mechanism on surface water primary production with the potential to maintain, or increase, the extent of suboxic waters. Fluxes from the sediment and the surface/interior ocean hold the potential to be important for the development of the OMZs, and quantification of these fluxes are important for the overall oxygen/nutrient budget of the OMZs. However, the mixing and pathways of the water from the benthic boundary layer and how it connects with the interior ocean in the OMZ or to the surface ocean above the OMZ are poorly characterized. Existing regional models show divergent solutions and direct observations of some of the regional scale exchange mechanisms, time scales and rates would help to evaluate choices of resolution and sub-grid-scale parameterization. To address this, we are conducting a tracer release experiment on the Peruvian shelf. Transient tracers in the water column, such as CFCs, are also measured to understand the physical mixing processes in the region.

Methods:

For the tracer release we used the Ocean Tracer Injection System (OTIS) of GEOMAR. This system has been successfully used for 3 previous tracer release experiments by the GEOMAR group. Whereas the OTIS in normally towed behind the research vessel at a set density level (in order to quantify diapycnal and isopycnal dispersion), for this experiment the OTIS was deployed in a different mode of operation; the OTIS was deployed on the bottom and released the tracer on a fixed position during each release. For this purpose the buoyancy devices on the OTIS was removed (to provide negative buoyancy) and the OTIS was equipped with four “legs”, each of them with two 50×55 cm plates to prevent the OTIS

from sinking into the sediment. This way the OTIS should sit 60 cm above the bottom during release.

Figure 7.10.1. Deployment of the OTIS from the A-frame.

The inert gas CF_3SF_5 was used as tracer; this was loaded on three cylinders on the OTIS prior to deployment, a fourth cylinder was loaded with a primer that was pumped through the system during deployment and recovery. The tracer/primer was pumped through two dual-head HPLC pumps, typically set to ~3200 psi pressure, to a set of six 25 µm ID orifices on each pump (i.e. a total of 12 orifices). Due to the fine-tip of the orifices, a fraction of the orifices usually clogged during injection, and was the rate-limiting factor during releases.

The OTIS was deployed at three positions during the cruise (Tab. 7.10.1). During each of those, the ship was directed to a water depth of 250 meters after reaching the approximate release positions; releasing at the same depth during on all three sites was important. During the OTIS stations, the OTIS was lowered to the bottom from the A-frame on the 18 mm conducting cable. Six 10L buoyancy balls were attached to the wire between ~15 and 35 m above the OTIS to provide positive buoyancy for the lower part of the cable. Once the OTIS reached the bottom an additional 20 meters of wire was paid out. Following this the ship moved 50 meters forward, in 10 meter increments, at the same time as the wire was paid out. This way enough slack was provided in the wire to prevent any movement to the OTIS during deployment; the buoyancy on the wire effectively prevented kinks in the wire from developing. All three deployments were successful. A CTD station was always performed immediately before the OTIS deployment.

Table 7.10.1. Information on the three tracer release sites. The timing refers to time when tracer was pumped.

Position	Start Time (UTC)	Duration	Amount	CTD#
10°42.9'S 78°14.1'W	Oct 13, 01:15	10h 48min	25 kg	19
12°21.8'S 77°26.2'W	Oct 15, 21:48	8h 16min	28 kg	22
14° 02.2'S 76°31.7'W	Oct 18, 01:13	7h 55min	15.5 kg	30

The CTD on the OTIS recorded salinity, temperature and oxygen (and pressure) for the duration of the tracer releases. Significant variability in potential density (σ_Θ) over time is evident for all three sites, with a general trend of slowly decreasing density interrupted by rapid increases, Figure 7.11.1. These events of rapidly changing densities are also visible on the sADCP data with east setting currents rising to over 0.1 ms^{-1} (from close to zero zonal velocity) during these events.

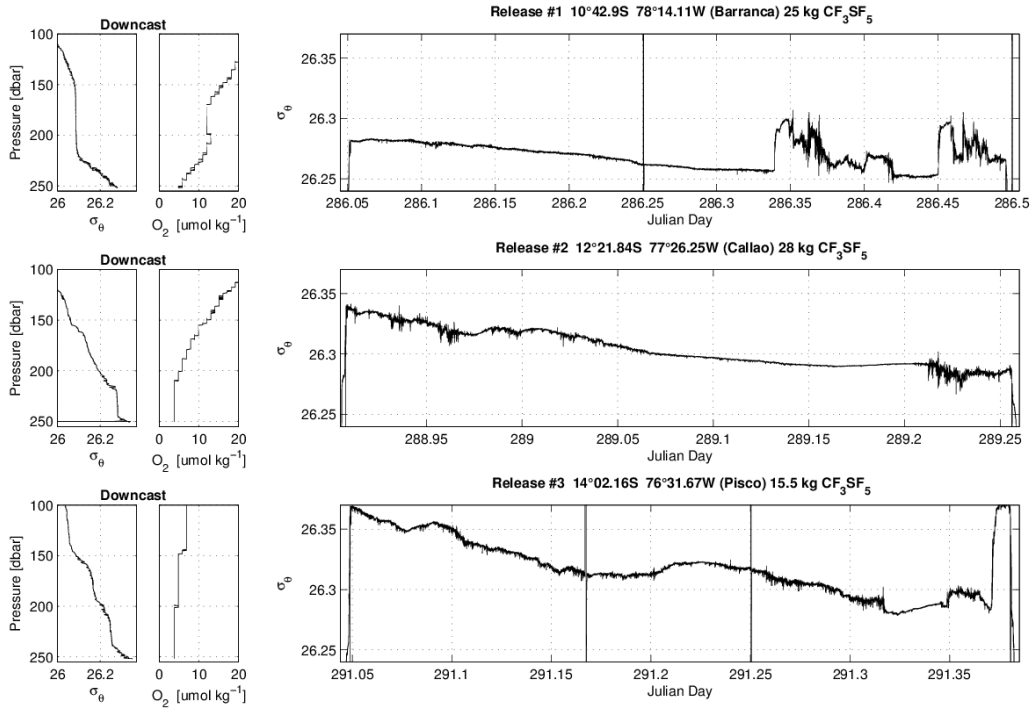

Figure 7.10.2. Left panels: density and oxygen profiles from the OTIS "downcast". Right panels: potential density during the OTIS deployment. Preliminary calibrated data

For the transient tracer measurements, water samples for the determination of dichluorodifluoromethane (CFC-12) and sulphur hexafluoride (SF_6) concentrations were collected from the Niskin bottles using 300 ml glass ampules. The ampules were directly attached to the Niskin bottles with a stainless steel tubing system to prevent contact with the atmosphere during the sampling process (e.g. Stöven, 2011). The ampules were flushed with 3 times the volume during sampling. The samples were cooled in a water bath at ~0°C to prevent outgassing of the trace gases before they were flame sealed and stored in aluminum boxes during the cruise; flame sealing was always performed immediately after sampling.

The measurements of the samples were conducted onshore in the tracer lab at GEOMAR Helmholtz Centre for Ocean Research Kiel. The two transient tracers were simultaneously analyzed using a purge and trap GC-ECD system as described in Stöven (2011). In total 110 samples from six stations were taken (see appendix Tab. 11.3.6).

7.11 Hydrographic observations (CTD and salinity measurements)

Lothar Stramma, Tim Fischer, Rudolf Link

Objective/Intro

There is increasing concern today that climate change will lead to decreasing dissolved oxygen (DO) levels in the ocean with large impact on marine habitat and ecosystems. Volumes of the interior ocean that are relatively poor in oxygen are often called oxygen minimum zones (OMZs). Climate model runs over centuries predict an overall decline in oxygen concentration and a consequent expansion of the mid-depth OMZ's under global warming conditions. These OMZs cover the upper ocean from about 100 to 900 m depth in the eastern Pacific. The recently reported expansion of OMZs in the World Ocean has major implications for biogeochemical cycles.

In the Pacific near the equator, the Equatorial Undercurrent, Northern and Southern Subsurface Countercurrents and the Northern and Southern Intermediate Countercurrents all carry water that is oxygen richer than adjacent westwards flows, thereby providing a net oxygen supply to the eastern Pacific OMZs. To investigate circulation changes and related oxygen changes first the mean circulation especially of the current bands which supply oxygen to the OMZ need to be understood. A comprehensive observational data set suitable for describing the structure and pathways of the EUC east of the Galapagos Islands (~92°W) does not exist.

In earlier investigations we could show that in most regions of the tropical Pacific the oxygen content in the 200-700 dbar layer has declined. An investigation of the Meteor M77/4 data from February 2009 indicated that the decreasing oxygen trend in the equatorial channel became stagnant.

The goal of the CTD-O_2 measurements combined with the ADCP data on Sonne 243 was to investigate the water mass and oxygen transport in the zonal equatorial current bands to understand the supply paths of the OMZ. In addition the CTD-O_2 data will be used to extend the investigation of long-term (~ 50 years) oxygen trends into present time and determine whether the recently observed stagnation in deoxygenation is continuous. Off Peru the CTD-O_2 measurements will be used to investigate upwelling on the shelf. As an El Niño developed during 2015 a new aim added was to investigate a possible weakening of the upwelling due to the El Niño (Stramma et al. 2016).

Methods

CTD-calibration

During SO243 a total of 39 CTD-profiles on 18 stations were collected, often with 2 profiles at one location to cover the amount of water needed from the rosette by the different scientific groups (Fig. 7.11.1). On the first 2 deep stations (1200 and 1000 m depth) below 500 m

depth the bottles could be release, however no confirmation was received from the CTD deck unit. The problem could be resolved and did not appear again on later stations.

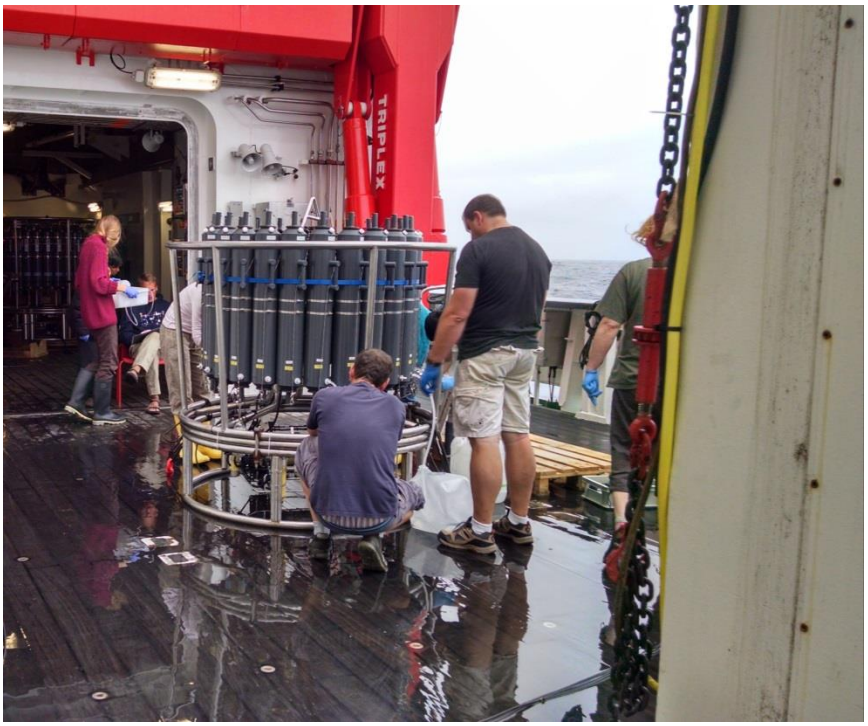

Figure 7.11.1. Sampling the Niskin bottles of the CTD rosette.

Data acquisition was done using Seabird Seasave software version 7.23.1. The CTD was mounted on the GO3 rosette frame with a 24 bottle rosette sampling system with 10 l bottles. Only the CTD SBE02 was used (Tab. 7.11.1). In addition the SBE07 was shipped to R/V Sonne as backup, but was never used. The final calibration of the CTD data was done using the primary set of sensors.

Table 7.11.1. Sensors used for the SBE 02 CTD.

Device	Model number	Serial number
CTD deck unit	SBE 11 plus	SN 11P25213-0581
CTD underwater unit	SBE 9 plus (SBE02)	SN 09P24785-0612
Pressure Sensor	Digiquarz	SN 80024
Pump, primary	SBE 5T	SN 3851
Pump, second	SBE 5T	SN 1991
Temperature, primary	SBE 3	SN 2463
Temperature, second	SBE 3	SN 5806
Conductivity, primary	SBE 4	SN 3373
Conductivity, second	SBE 4	SN 3379
Oxygen, primary	SBE 43	SN 1312
Oxygen, second	SBE 43	SN 2591
Fluorescence	Wetlabs, ECO CDOM	SN 2687
Altimeter	Valeport VA500	SN 48832
Fluorescence	Dr. Haardt	SN %
Fluorescence	Trios MicroFlu	SN 1145

The GEOMAR Guildline Autosal salinometer #8 (operated by L. Stramma) was used for CTD conductivity cell calibration. The Guildline Autosal salinometer #4 was available as backup, but had not been used for measurements on this cruise. Calibration during operation was done in two ways: IAPSO Standard Seawater (P157, K15=0.99985) was measured at the beginning of the salinometer use and 3 times at the end of the measurements. In addition, a so called “substandard” (essentially a large volume of water with constant but unknown salinity), obtained from deep bottles from the first deep CTD cast was used to track the stability of the system. The standard water and the substandard measurements showed that no drift appeared during the measurements. Hence the AS8 was stable during the entire measurement time as well as from one measurement day to the next.

The preliminary conductivity calibration at the end of the cruise of the downcast data was performed using a linear fit with respect to conductivity, temperature, and pressure. For the CTD profiles the calibration was: C_corrected = C_observed -0.001962 + 1.5113e-07 * P – 1.927e-05 * T + 5.8152e-04 * C). Using 67% of the 102 samples for calibration a r.m.s. of 0.0011 PSU for salinity was found for the downcast.

Samples for the determination of dissolved oxygen after Winkler (1888) were taken from a total of 28 CTD casts to calibrate the oxygen sensors (SBE 43) and to support chemical and biological CTD data (see section 7.7). On most CTD casts on several depths samples for dissolved oxygen were taken yielding a total of 155 samples for the entire cruise. The CTD oxygen sensor calibration was performed similarly to the conductivity calibration. The resulting calibration correction for the oxygen sensor was: : o_corrected = o_observed (µmol kg^{-1}) + 0.10713 + 0.0024487 * P + 0.12363 * T + 0.020098 * O. Using 67% of the 155 samples for calibration a r.m.s. of 0.8 µmol O_2 kg^{-1} was determined as uncertainty of the calibration.

Preliminary results

As a strong El Niño developed in 2015 it was of special interest to investigate whether the upwelling off Peru has weakened or even terminated. The comparison of the oxygen distribution measured at about 9°S on the RV Sonne cruise in October 2015 with the oxygen distribution from the RV Meteor cruise M91 in December 2012 (Fig. 7.11.2) showed that the upwelling in October 2015 was very weak. Low oxygen water with less than 5 µmol kg^{-1} was located below about 50 m depth in December 2012 while it was located only below 250 m in October 2015.

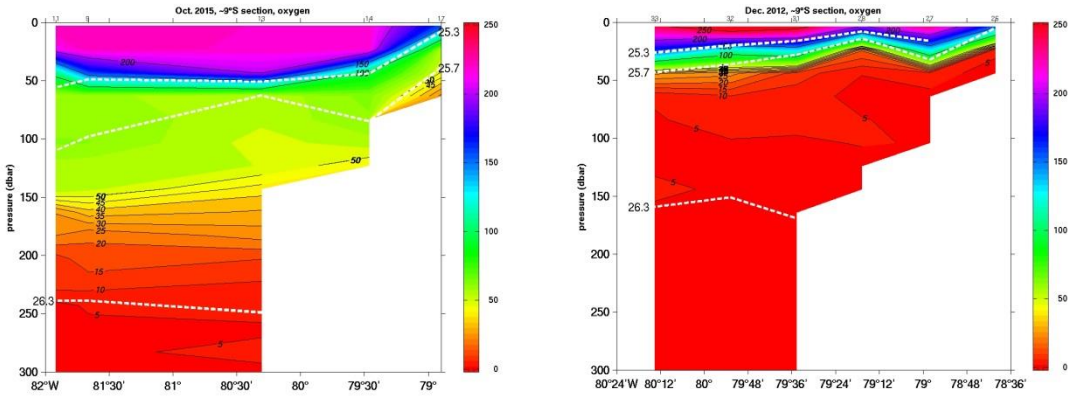

Figure 7.11.2. Oxygen distribution at about 9°S in October 2015 (left) and December 2012 (right) with the same color scale for oxygen. Selected density contours are included as dashed white lines.

Further south in October 2015 the upwelling signal was still strong. At the section at about 12°S the oxygen with less than 5 µmol kg^{-1} reached up to 50 m depth at the near-coastal station. However, the oxygen depth was observed to move up and down by wave influence. On the easternmost station of the ~16°S section the oxycline depths shifted upward by about 20 m between the downcast and the upcast.

Earlier observations showed higher oxygen values in the eastern and equatorial Pacific in the upper 300 to 350 m at times of El Niño conditions. The comparison of the oxygen profiles at the equator in October 2015 at El Niño conditions showed higher oxygen in the upper 300 m compared to February 2009 and in the upper 130 m compared to November 2012 (Figure 7.11.3). The potential temperature in October 2015 was higher in the entire upper 300 m compared to the two earlier cruises. Salinity was lower in the upper 40 m, but higher between 40 m and 300 m in October 2015. Except for the upper 10 m the density was lower to 250 m depth in October 2015. The higher oxygen distribution in 2015 as well as the changes in water temperature, salinity and density indicate the influence of El Niño, however it appears we were there during the onset (Stramma et al. 2016).

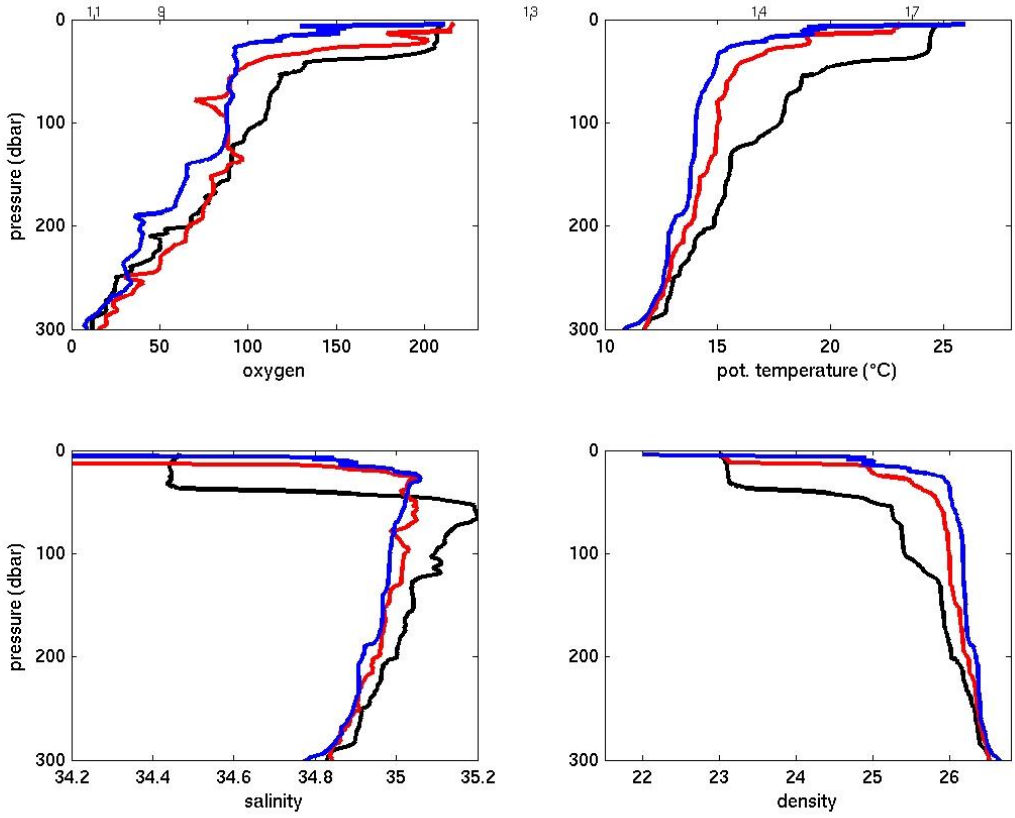

Figure 7.11.3. Pressure profiles in February 2009 (blue lines), in November 2012 (red lines) and in October 2015 (black lines) for oxygen (in µmol/kg), for temperature, salinity and density.

7.12 Microstructure and current measurements

T. Fischer, R. Link, L. Stramma

A MSS90-D microstructure profiler (#026) of Sea and Sun Technology (Fig. 7.12.1) was used to infer turbulent dissipation rate and diapycnal diffusivity, aiming at calculating diapycnal fluxes of several solutes including oxygen and nitrous oxide (N_2O). The loosely tethered profiler was equipped with 3 airfoil shear sensors and a fast thermistor, as well as with a pressure, a conductivity, and a temperature sensor. Profiler sink velocity was adjusted to 0.6 m s^{-1}. In total 43 profiles to usually 300m depth were recorded at 14 ship stations, generally 3 microstructure profiles following a CTD cast. The system worked well throughout the cruise and there were no technical issues beyond maintenance.

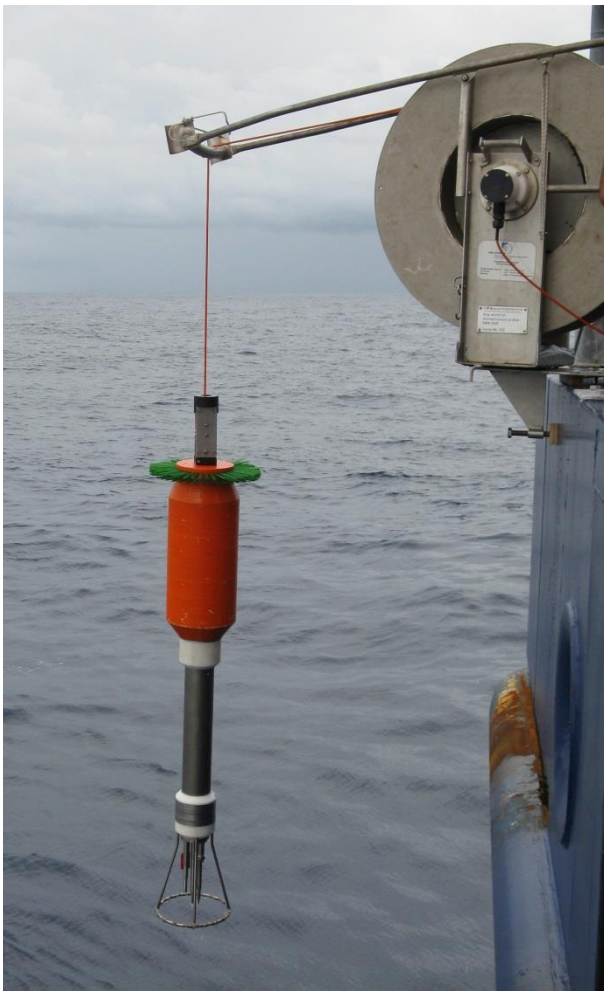

Figure 7.12.1. Deployment of microstructure sonde of the aft deck.

For properly operating the system and smooth deployment and recovery of the microstructure probe, the winch was fixed at the port side aft railing close to the corner, making it necessary to unmount parts of the wire frame first. The railing is broader and thicker than on other research vessels, which forced some constructive adaptations of the winch mounting.

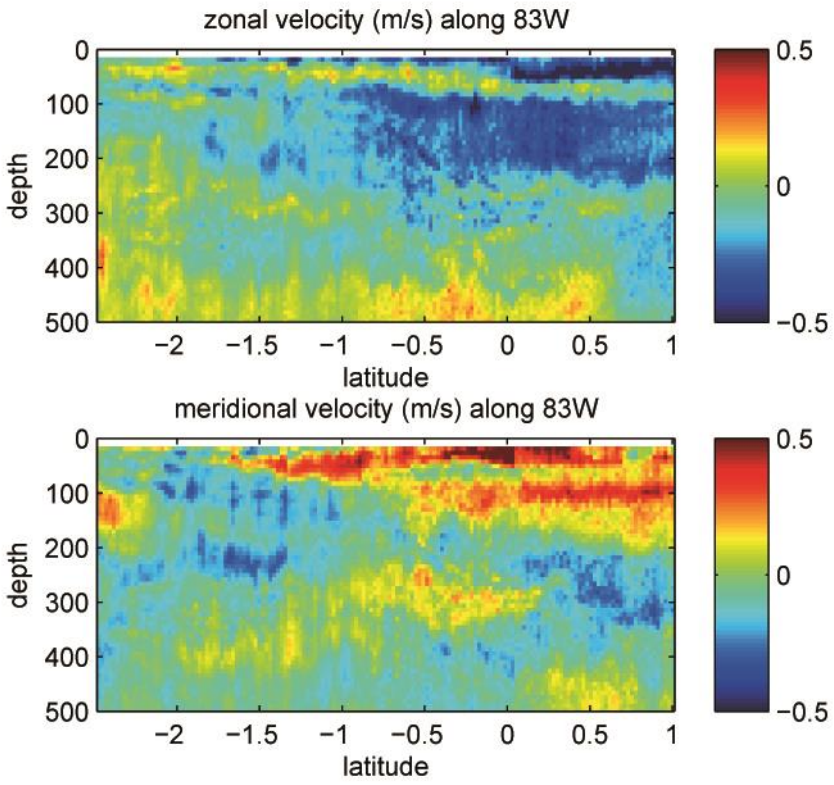

Figure 7.12.2. Current velocities when crossing the equator, from the 75kHz Ocean Surveyor.

Shipboard current measurements

Two vessel mounted Acoustic Doppler Current Profilers (ADCP) continuously recorded vertical profiles of current velocities: a 75kHz RDI Ocean Surveyor (OS75) and a 38kHz RDI Ocean Surveyor (OS38) mounted in the ship's hull (Fig. 7.12.2). The two instruments are closely located and each aligned to zero degrees, which caused some interference, but nevertheless did not much deteriorate the velocity data after post-processing. Each of the two instruments was run in the more robust narrowband mode. The two configurations were: OS75) 100 bins of 8m, pinging at 25 per minute, range 650m; OS38) 55 bins of 32m, pinging at 20 per minute, range 1300m. During the entire cruise the navigation data was of high quality. Acoustic interference from navigational acoustic devices could not be detected. The only other scientific acoustic device working was the 12 kHz multibeam echosounder, which also did not interfere. The bow thruster operating on stations only rarely deteriorated the ADCP performance, contrary to the experience from other research vessels.

7.13 Biological Control of the Ocean's C:N:P ratio

Mike Lomas

Support for participation in this cruise comes from "Biological Control of the Ocean's C:N:P ratio" NSF Climate Research Investigations Award Nbr. 1045966. Scientists ashore, beside M. Lomas, who will be involved in the analysis of the samples/data are Steven Baer and LeAnn Whitney (Bigelow Laboratory) and Adam Martiny (University of California at Irvine).

Objective/Intro

One of the fundamental patterns of ocean biogeochemistry is the Redfield ratio. Redfield identified the similarity between the N:P ratio of plankton living in the surface ocean and that of dissolved nitrate and phosphate in the deep ocean. He hypothesized that the deep ocean nutrient concentrations were controlled by the elemental requirements of the surface plankton. This concept has been extended to include other elements like carbon (C) and remains a central tenet for our understanding of ocean biogeochemistry.

Despite this importance, there is no obvious mechanism for the globally consistent C:N:P ratio of 106:16:1 (i.e. Redfield ratio), and there is substantial elemental variation among ocean taxa. Although the data are sparse, recent field surveys of plankton C:N:P ratios furthermore indicate significant deviations in different ocean regions. These observations suggest that on local/regional and perhaps seasonal scales, the planktonic C:N:P ratio is not constant in the ocean and can increase or decrease depending on the biodiversity of ocean plankton across biogeographic conditions. This has at least two important implications. First, on the global scale, Broecker and Henderson (1998) have proposed that an increased plankton C:N:P ratio and thus increased CO_2 uptake in the ocean could explain the glacial to inter-glacial variation in atmospheric CO_2 concentration. Second, geochemical estimates of N_2 fixation are critically dependent upon an assumed N:P ratio (specifically the Redfield ratio). Recently, it has been argued that our understanding (or lack thereof) of cellular elemental stoichiometry has a large influence on our ability to estimate the global N budget. Thus, knowing how biodiversity regulates the elemental composition of the ocean (C:N:P) is important for understanding Earth's climate – in the past, present, and future.

The following conceptual model guides the research in which the samples collected on this cruise are framed (Fig 7.13.1):

1. The C:N:P ratio of a cell is constrained by the broad *taxonomic* group to which it belongs, which affects whether it has an outer shell, its size, functional metabolism, membrane lipid composition, etc.
2. Within a taxon, there is a high *genetic* diversity. Some of this genetic diversity is potentially laterally transferred or can be lost within taxa and confers various functional abilities (organic phosphate assimilation, nitrate assimilation, photoheterotrophy, etc.). This *functional* diversity provides further flexibility to a cell to respond to varying nutrient supply rates/ratios and affects a cell's C:N:P ratio.
3. Given these taxonomic and genetic constraints, a cell is physiologically plastic and modifies how it allocates cellular resources in response to nutrient supply rates and ratios in the environment.
4. The microbial diversity (taxonomic, genetic, and functional) of the surface ocean varies over time and space, driven by many factors in addition to nutrients. The sum of this mixture composes the ecosystem C:N:P, the ratio that Redfield describes.

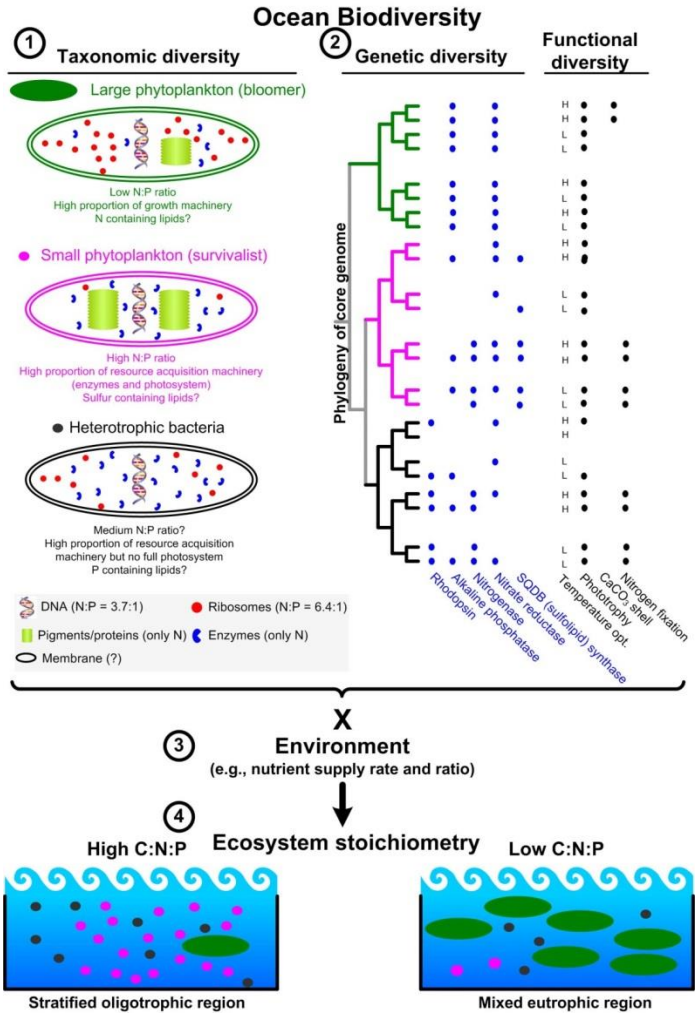

Figure 7.13.1. Predicted integrated role of ocean taxonomic (here defined as broad phylogenetic groups), genetic, and functional biodiversity on ocean C:N:P ratios. Number refers to our four questions and associated objectives. Parts of the figure are inspired by Arrigo.

Based upon this conceptual model we have the following science questions:
Q1: How does ocean taxonomic biodiversity impact C:N:P ratios?
Q2: What is the range of gene content diversity within taxa and how does this diversity impact C:N:P ratios?
Q3: Given taxonomic, genetic, and functional constraints, how do cells physiologically adjust their cellular C:N:P ratio in response to nutrient supply rates andratios?
Q4: What is the integrated effect of biodiversity and environmental variation on the ecosystem C:N:P ratio?

Methods

Methods related to the analysis of samples collected on the cruise are given below:

Bulk Particulate organic carbon (POC), nitrogen (PON), and phosphorus (PPhos). Bulk POC/PON and PPhos samples are filtered onto precombusted (450^{o}C, 5 hours) Whatman GF/F glass fiber filters, as separate samples, and stored frozen (-20^{o}C). POC/PON samples

are analyzed according to standard JGOFS protocols, while PPhos samples are analyzed as in Lomas et al., (2009).

Population-specific POC, PON, PP. We will measure the C:N:P ratios of specific plankton groups (i.e., *Prochlorococcus*, *Synechococcus*, picoeukaryotes, heterotrophic bacteria, N_2-fixing bacteria, diatoms, and, *Coccolithophores*) in the field. For pico- and nanoplankton populations, heterotrophs and autotrophs, samples are concentrated and flow cytometrically sorted. Populations are filtered onto precombusted GF-75 filters (nominal pore size 0.3 µm), treated with oxalate rinse, and analyzed for C:N:P.

RNA preparation and transcriptome sequencing. Approximately 1.5 L of sample volume was gently filtered over 5 µm, 47 mm polycarbonate filter and then through a Sterivex 0.2 µm. Filters were stored in lysis buffer, flash frozen, and stored at -80°C until analyzed. Total RNA will be extracted using the Qiagen RNeasy Mini Kit (Venlo, Netherlands) according to the manufacturer's protocol, with the following exceptions: cells will be lysed using 0.5 mm zirconia/silica beads (BioSpec, Bartlesville, OK, USA) mixed with the lysis buffer and vortexed until the solution looked homogenous. The lysis solution will be then put over Qiashredder columns (Qiagen) to remove any large cell material that could clog the spin columns. To aid in the removal of DNA, two DNase digestions are performed. First, Qiagen's RNase-free DNase Set (an on-column treatment) was used according to the manufacturer's instructions. The RNA samples from within a treatment are then combined. The second DNA removal step is conducted using the Turbo DNA-free kit (Life Technologies) according to the manufacturer's protocol. The RNA is then quantified in duplicate using the Qubit Fluorometer (Life Technologies); RNA quality is assessed by gel electrophoresis.

RNA sequencing libraries are generated from 1 ug of RNA with 100 base pair paired-end reads sequenced using an Illumina HiSeq 2000. Reads are analyzed following the JGI pipeline. First, read quality is assessed using BBDuk where artifact sequences were detected by kmer matching (kmer=25) and trimmed. Reads are then quality trimmed using the phred trimming method at Q6 and finally, reads under 25 bases removed. Counts will be used to generate gene counts which are subsequently used to evaluate differential expression between samples/stations. DESeq2 will be used to determine differential expression; significantly differentially expressed genes are those with a p-value < 0.05 and a fold change > 2.

Preliminary results:

No samples were analysed on board and therefore there are no preliminary results specific to this cruise.

Expected results

Samples for bulk and taxon-resolved particulate organic matter were collected at 4 depths at every CTD station. In addition, RNA/DNA samples were collected from the near surface (CTD or underway system) and the subsurface chlorophyll maximum depth. From these we expect to present a spatial and profile map of ecosystem and phytoplankton stoichiometry for this cruise. In addition, at several stations we conducted ^{15}N incubation experiments in collaboration with Damian Grundle (section 7.1). From these incubations we will be able to

quantify rates of nitrification (through isotope dilution in the final fluid sample). These data will also be used in the estimation of efficiency of N_2O production in conjunction with Damian's incubation experiments. All data will be permanently archived as the Biological and Chemical Oceanography Data Management Office in the US, as this project was a US NSF funded project. However, all data will be made freely available to other cruise participants, should they wish, in efforts to provide a more robust dataset for the cruise

7.14 Biogenic characterization of the sea surface microlayer

Birthe Zäncker and Jon Roa

Objective/Intro

The Sea Surface Microlayer (SML) occurs on all water bodies and covers approximately 70 % of the Earth's surface. It is the boundary layer between the ocean and the atmosphere with a gel-like structure containing carbohydrates, amino acids and proteinacous, as well as polysaccharidic, gels.

The position of the SML directly at the boundary between the ocean and the atmosphere makes it a potentially important factor in air-sea exchange processes. Previous studies have found that surfactants in the SML can affect the gas transport (section 7.8). The composition of sea spray aerosols (SSA) emitted from the ocean is influenced by the organic constitution of the SML. Gel particles provide a habitat for microorganisms, potentially favoring biofilm-forming bacteria and thus making the microbial community in the SML distinct from the community in the underlying water.

Methods

A total of 11 stations were sampled during the cruise. A Zodiac was used to sample the sea surface microlayer with a hydrophilic glass plate and the bulk water at 20 cm (Fig. 7.14.1). Furthermore 3 depths from the CTD (surface (~5m), deep chlorophyll a maximum and oxygen minimum zone) were sampled.

Figure 7.14.1. Microlayer sampling on the zodiac.

Cell abundances and DNA extraction
At each Zodiac station, samples were collected from the surface microlayer, the underlying water and from the Niskin rosette for the analyses of bacterial and phytoplankton cell abundance via flow cytometry. Therefore, 4 ml sample were fixed with 200µl 25% glutardlutadialdehyde (GDA). These data will enable a detailed description of the vertical distribution of those organisms.

Furthermore, samples for bacterial DNA (400 ml seawater filtered onto a 0.2 µm Durapore membrane filter) were taken.

Dissolved organic matter
Carbohydrates and amino acids are valuable tracers of biological production and decomposition processes. Highly sensitive IC- and HPLC-techniques will be applied to analyze concentrations and compositions of amino acids (AA) and carbohydrates (CHO) in DOM. Furthermore, total and dissolved organic carbon (T/DOC) were analyzed. All parameters for DOM were size-fractionated: 100 kDa, 1000 kDa and 0.45 µm for DOC, 10 kDa, 100 kDa, 1000 kDa and 0.45 µm for AA and CHO.

Gel particles
Gel particles represent important microbial habitats and comprise significant fractions of extracellular carbon and nitrogen. Transparent exopolymer particles (TEP) and Coomassie-stainable particles (CSP) will be determined colorimetrically and microscopically using semi-automated image analysis.

FISH, cLSM and live/dead staining
Samples were fixed with 1 % formaldehyde for 1 h and filtered onto Whatman polycarbonate filters (47 mm diameter, 0.2 µm pore size) and stored at -20°C for analysis using Fluorescence *in situ* hybridization (FISH). Samples for analysis with confocal laser scanning

microscopy (cLSM) were filtered onto black Whatman polycarbonate filters (25 mm diameter, 0.2 µm pore size) and stored at -20°C.

The ThermoFisher Scientific live/dead BacLight kit was used according to the manufacturer's instructions to determine the amount of living cells in the samples.

Overview of biogeochemical parameters measured:

- dissolved organic carbon (DOC)
- dissolved organic nitrogen (DON)
- transparent exopolymer particles (TEP)
- Coomassie stainable particles (CSP)
- dissolved hydrolysable amino acids
- total and dissolved carbohydrates
- overview of biological parameters
- phytoplankton and bacterial cell numbers by flow cytometry
- genetic analyses of bacterial community
- fluorescence *in situ* hybridization (FISH)
- live/dead staining

Preliminary results

No samples were analyzed during the cruise and therefore there are no preliminary results.

Expected results

We will analyze the DOM composition and the microbial community of the SML as compared to the directly underlying water (20 cm) and the deeper water (5 m and deeper). Furthermore, we will look at the spatial distribution patterns of DOM and bacteria between different stations. We will also compare our data to the data collected during the Meteor M91 cruise in December 2012.

In addition, we will look at the SML using cLSM and epifluorescence microscopy and different staining techniques (live/dead staining, FISH) to analyse the distribution patterns.

7.15 Optical properties of phytoplankton, particulate and dissolved organic matter

Astrid Bracher and Rüdiger Röttgers

Objective/Intro

Marine phytoplankton is the basis of the marine food web and also a main driver of biogeochemical fluxes, thus, an important source of dissolved and particulate organic substances, including volatile organic substances (e.g. DMS, isoprene, halocarbons, sections 7.3 and 7.5). On this cruise we broadened our sampling frequency of phytoplankton, particulate and chromophoric dissolved organic matter (CDOM) abundance and composition by taking continuous optical measurements which directly give information on inherent and apparent optical properties (IOPs, and AOPs, respectively). These can later be inverted to extract information on the above listed parameters. Additionally, light absorption by CDOM can be used to identify specific dissolved pigments in the water column especially in the

oxygen minimum layer and the surface microlayer. The specific objectives of our working group on the SO243 ASTRA-OMZ cruise were: 1) to collect a high spatially and temporally resolved dataset on phytoplankton (total and composition) and its degradation products at the surface and the full euphotic zone using continuous optical observations during the cruise and from ocean colour remote sensing develop; 2) validate (global and regional) algorithms and associated radiative transfer models in accordance to the previous objective by using discrete water samples for pigment analysis and absorption measurements; 3) to identify bio-physical-chemical coupling with cooperation partners from ASTRA by using this comprehensive data sets to detect shifts in phytoplankton community biomass and composition and the factors driving the variability and changes in phytoplankton community and CDOM absorption; 4) link to oceanic emissions of trace gases (mainly DMS, isoprene, halocarbons); 5) measure CDOM absorption in the water column from the surface microlayer through the euphotic zone down to the oxygen minimum and to collect DOM extracts from the deeper waters for identification of specific dissolved pigments.

Methods

Methods to obtain quantity and composition of phytoplankton, other particulates and chromophoric dissolved organic matter (CDOM)

Continuous and discrete measurements of inherent optical properties (IOPs) with a hyperspectral spectrophotometer: For the continuous underway surface sampling an in-situ–spectrophotometer (AC-S; Wetlabs) was operated in flow-through mode to obtain total and particulate matter attenuation and absorption of surface water. The instrument was mounted to a seawater supply taking water from about 5m depth from the ship's moonpool. A second AC-S instrument was mounted on a steel frame together with a depth sensor (and a set of radiometers) and operated during 14 CTD stations (all but except station 3, 4, 9 and 11). The frame was lowered down to maximally 90 m with a continuous speed of 0.1 m/s or during daylight with additionally stops at 2, 4, 6, 8, 10, 12.5, 15, 20, 25 and 30 m. to allow a better collection of radiometric data.

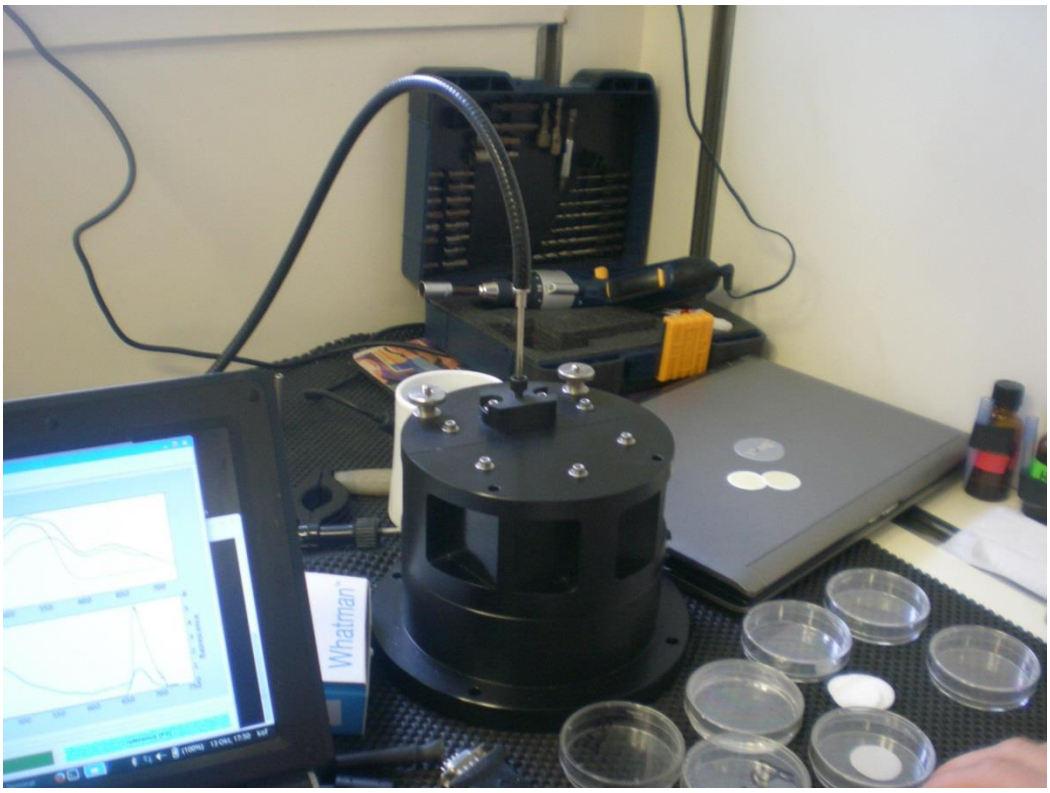

Figure 7.15.1. Set-up of portable lab unit of phytoplankton and particulate absorption measurements using a QFT-ICAM (Quantitative Filtration Technique Integrative Cavitiy Absorption Measurements) from Röttgers et al. (2016).

Discrete measurements of IOPs (absorption) at water samples were performed 1) for samples from the underway surface sampling (as for the AC-s flow-through system at 5 m depth sampled by a pump through the ship's moonpool) at an interval of 3 hours, 2) for samples from the CTD sampling at 6 to 7 depths within the top 100 m at 17 stations (all stations except Station 4), and 3) for samples from the surface microlayer sampling at 11 stations. The light absorption coefficient of the sum of particulate and dissolved matter was determined onboard using a Point-Source Integrating-Cavity Absorption Measurement Device (PSICAM) developed by Röttgers et al. (2005) according to the method by Röttgers et al. (2007). Water samples for CDOM absorption analysis were filtered through 0.2 µm filters and analyzed onboard with a 2.5-m path length liquid waveguide capillary cell system (LWCC, WPI). The particulate absorption is later obtained by subtracting LWCC results from PSICAM results. In addition, total particulate and phytoplankton absorption coefficients were determined with the quantitative filter techniques using sample filtered onto glass-fiber filters QFT-ICAM and measuring them in a portable QFT integrating cavity setup following Röttgers et al. (in review Ocean Express) (Fig. 7.15.1). Particulate and phytoplankton absorption was also determined for Tom Browning's experiments (a total of 5) where the influence of iron limitation was investigated (section 7.6).

Samples for determination of phytoplankton pigment concentrations and composition were taken at a 3-hourly interval from the underway-sampling system, and from 6-7 depths at 17 (all stations except Station 4) CTD-stations. These water samples were filtered on board immediately after sampling and the filters were thermally shocked in liquid nitrogen and then stored in the -80°C freezer. The samples were sent back to AWI with a dry shipper and then

wanalyzed within the next three months by High Performance Liquid Chromatography Technique (HPLC) at AWI following Taylor et al. (2011).

Radiometric measurements to obtain apparent optical properties: At the 10 daylight stations (except for station 3) we measured continuously hyperspectral upwelling radiance and downwelling irradiance down to maximally 90 m with 1-min. stops at 2, 4, 6, 8, 10, 12.5, 15, 20, 25 and 30 m to improve data quality. TRIOS Ramses radiance and irradiance sensors were mounted on the same steel frame (in addition to the AC-s in situ spectrophotometer) in downward and upward 90° direction, respectively. The data will be corrected by changes in solar irradiance, which was measured continuously during the cruise on the ship's helicopter deck where measurements can be taken without shading by the ship.

DOM extracts were collected at some stations from depths of the oxygen minimum or close to the maximum depths at coastal stations. Therefore 25 L of water was run through 1g PPL cartridges following the procedure of (Dittmar et al. 2008). The cartridges were dried with nitrogen and frozen at - 20 °C.

Algorithms (following e.g. Bracher et al., 2008, 2015; Chase et al., 2014; Hansell et al., 2012; Kostadinov et al., 2009), to extract later from the IOPs and AOPs the particulate composition, including a characterization of the phytoplankton community structure and status on photoacclimation, will be adapted to the region and maybe further developed by using the discrete water sample measurements (also for validation).

Preliminary results

On board we sampled, filtered, and keep at -80°C 180 pigment samples. 207, 217 and 349 measurements of total absorption, of phytoplankton absorption, and of CDOM absorption were directly measured on board. We took DOM extracts at 9 stations from the depth around the OMZ and measured continuous profiles of IOPs and of AOPs at 14 and 10 CTD stations, respectively. At 11 stations the SML was sampled and the particulate and CDOM absorption coefficient was determined for the SML and the underlying water. Solar irradiance was measured continuously from 4th October to 21st October and surface IOPs from 4th October afternoon to 14th October afternoon and from 15th afternoon to 22nd morning.

Expected results

We expect to obtain from the continuous IOPs information on phytoplankton and other particulates, but also to some respect in the profiles from the AOPs determined from the radiometric data. In addition the AOPs of reflectance and diffuse attenuation coefficient will be used for validating ocean color remote sensing data (probably from MODIS and VIIRS). Those validated datasets, using the discrete sample detailed measurements, will help to identify changes in phytoplankton community and its degradation products and elucidate thes link to biogeochemical fluxes, especially regarding the volatile organic compounds emissions to the atmosphere. The DOM extracts will be used to identify a specific pigment found in the OMZ.

7.16 Transfer and remineralization of biogenic elements in OMZs

Frederic Le Moigne

Objective/Intro

Climate models predict a decline in dissolved oxygen concentration and a consequent expansion of the Oxygen Minimum Zones (OMZ) in the future ocean. One crucial biogeochemical mechanism is the process by which of carbon is transferred into the deep ocean, the biological carbon pump (BCP). There is currently little consensus on the fate of sinking OM and the efficiency of the BCP in OMZ areas. Previous particles flux studies have shown that the BCP is more efficient in suboxic zones relative to surrounding well oxygenated waters. However, incubations performed on sinking material collected in oxic and suboxic areas have observed similar remineralisation rate in both conditions, suggesting that suboxic conditions do not enhance the transfer of sinking OM through the mesopelagic zone. This project will assess how different oxygen conditions and surface productivity impact C:N:P remineralization rate of sinking particles.

Methods

Sampling

Three free *in situ* pump deployments were performed at station 3, 11, 15 (see appendix Fig. 7.16.1). Pumps were deployed with OTIS except at station 3. Deployments dates, depths and splits for subsequent analysis/experiments are given in Table 11.3.7.

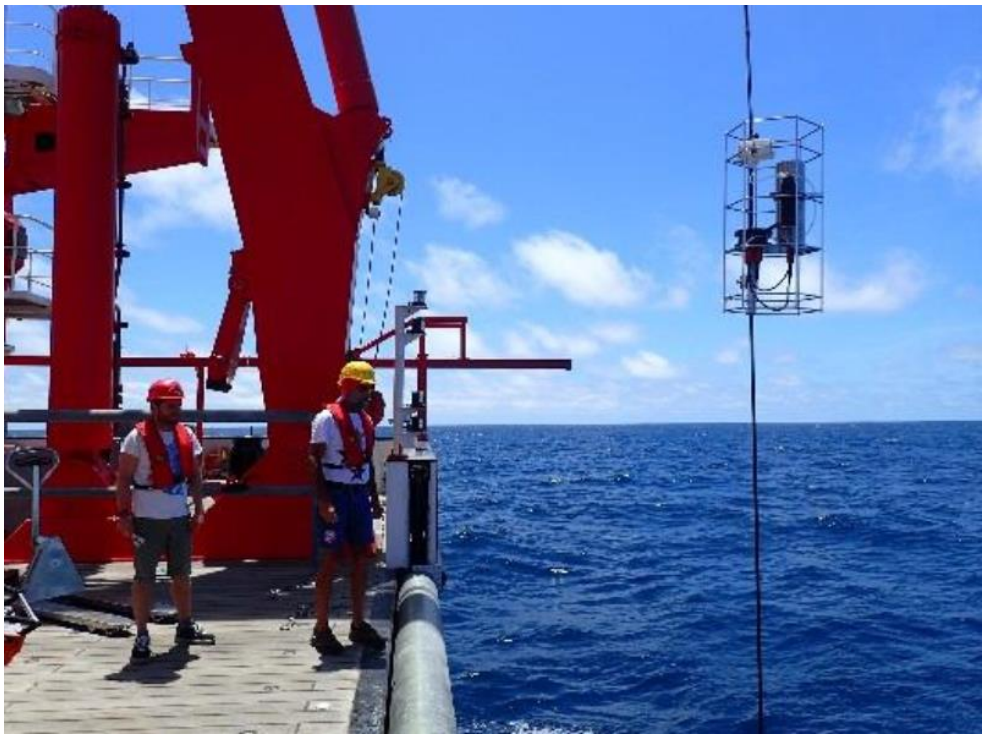

Figure 7.16.1. Deployment of particle in-situ pumps off the A-frame above the OTIS.

Incubations

Two distinct incubations were performed using material from stations 11 and 15 described above (Fig. 7.16.2). After splitting, pump material was incubated in 1.2L gas tight bottles fixed on a rotating plankton wheel (2 rpm) at constant temperature (22°C). Oxygen concentrations in some of the bottles were manipulated and lowered using a gas mix of 0.1283% CO_2 in pure N_2. Oxygen treatments, time steps for both incubations are summarized in Table 11.3.8 (appendix).

Figure 7.16.2. Incubation bottle (left) showing collected particles (middle) and rotating plankton wheel (right).

Expected results

Particles were incubated for several days and the evolution of various remineralisation parameters as well as the stoichiometry (C:N:P) of the particulate organic, the dissolved organic and the dissolved inorganic pools will be monitored. For instance, the evolution of nitrate and phosphate will provide results of the net C:N:P remineralisation rate. In addition, degradation index (amino-acids and sugars) will be monitored in order to quantify the rate at which N rich OM is consumed relative to C rich OM.

8. Acknoweledgements

Many thanks to the captain and crew of the R/V Sonne. Their work and help on board was outstanding. We would also like to thank the Control Station of German Research Vessels, Briese Schiffahrt, and the German Federal Foreign Office in Peru for all of their logistical support during SO243. This work was (and continues to be) funded by the BMBF (Project 03G0243A) and the DFG (GR4731/2-1, MA6297/2-1) with additional funding from GEOMAR Helmholtz Centre for Ocean Research Kiel, the Future Ocean Excellence Cluster in Kiel, and the DFG funded Collaborative Research Center 754. The chief scientist contributed with her Helmholtz Young Investigator Group TRASE-EC, funded by the Helmholtz Association through the President's Initiative and Networking Fund.

9. References

Arévalo-Martínez, D.L. et al., 2015. Massive nitrous oxide emissions from the tropical South Pacific Ocean. *Nature Geoscience*, 8(June), pp.530–533. Available at: http://www.nature.com/doifinder/10.1038/ngeo2469.

Bakker, D.C.E. et al., 2014. An update to the surface ocean CO2 atlas (SOCAT version 2). *Earth System Science Data*, 6(1), pp.69–90.

Bohlen, L. et al., 2011. Benthic nitrogen cycling traversing the Peruvian oxygen minimum zone. *Geochimica et Cosmochimica Acta*, 75(20), pp.6094–6111.

Boyd, P.W. & Ellwood, M.J., 2010. The biogeochemical cycle of iron in the ocean. *Nat. Geosci.*, 3, pp.675–682.

Bracher, A. et al., 2008. Quantitative observation of cyanobacteria and diatoms from space using PhytoDOAS on SCIAMACHY data. *Biogeosciences Discussions*, 5, pp.4559–4590.

Bracher, A. et al., 2015. Using empirical orthogonal functions derived from remote-sensing reflectance for the prediction of phytoplankton pigment concentrations. *Ocean Science*, 11(1), pp.139–158.

Broecker, W.S. & Henderson, G.M., 1998. The sequence of events surrounding termination II and their implications for the causes of glacial interglacial CO2changes. *Paleoceanography*, 13(4), pp.352–364. Available at: http://dx.doi.org/10.1029/98PA00920.

Browning, T.J., Bouman, H.A. & Moore, C.M., 2014. Satellite detected fluorescence: decoupling non-photochemical quenching from iron stress signals in the Southern Ocean. *Global Biochem. Cycles*, 28.

Bruland, K.W. et al., 2005. Iron, macronutrients and diatom blooms in the Peru upwelling regime: brown and blue waters of Peru. *Marine Chemistry*, 93(2-4), pp.81–103. Available at: http://linkinghub.elsevier.com/retrieve/pii/S0304420304001859 [Accessed September 19, 2013].

Chase, A. et al., 2014. Decomposition of in situ particulate absorption spectra. *Methods in Oceanography*, 7(2013), pp.110–124. Available at: http://dx.doi.org/10.1016/j.mio.2014.02.002.

Chavez, F.P. & Messié, M., 2009. A comparison of Eastern Boundary Upwelling Ecosystems. *Progr. Oceanogr.*, 83, pp.80–96.

Chever, F. et al., 2015. Total dissolvable and dissolved iron isotopes in the water column of the Peru upwelling regime. *Geochimica et Cosmochimica Acta*, 162(August), pp.66–82.

Croot, P.L. & Laan, P., 2002. Continuous shipboard determination of Fe(II) in Polar waters using flow injection analysis with chemiluminescence detection. *Anal. Chimi. Acta*, 466, pp.261–273.

Dale, A.W. et al., 2015. A revised global estimate of dissolved iron fluxes from marine sediments. *Global Biogeochem. Cycl.*, 29(5), pp.691–707.

Davey, M. et al., 2008. Nutrient limitation of picophytoplankton photosynthesis and growth in the tropical North Atlantic. *Limnol. Oceanogr.: Methods*, 53(5), pp.1722–1733.

Dittmar, T. et al., 2008. A simple and efficient method for the solid-phase extraction of dissolved organic matter (SPE-DOM) from seawater. *Limnology and Oceanography*, 6(6), pp.230–235. Available at: http://onlinelibrary.wiley.com/doi/10.4319/lom.2008.6.230/pdf.

Falkowski, P.G., Fenchel, T. & Delong, E.F., 2008. The Microbial Engines That Drive Earth 's Biogeochemical Cycles. *Science*, 320(5879), pp.1034–1039. Available at: http://www.ncbi.nlm.nih.gov/pubmed/18497287.

Gledhill, M. et al., 2013. Distributions of particulate Heme b in the Atlantic and Southern Oceans - Implications for electron transport in phytoplankton. *Global Biogeochemical Cycles*, 27(4), pp.1072–1082.

Gledhill, M., 2014. The detection of iron protoporphyrin (heme b) in phytoplankton and marine particulate material by electrospray ionisation mass spectrometry - comparison

with diode array detection. *Analytica Chimica Acta*, 841, pp.33–43. Available at: http://dx.doi.org/10.1016/j.aca.2014.06.045.
Hansell, D. a., Carlson, C. a. & Schlitzer, R., 2012. Net removal of major marine dissolved organic carbon fractions in the subsurface ocean. *Global Biogeochemical Cycles*, 26(1), pp.1–9. Available at: http://www.agu.org/pubs/crossref/2012/2011GB004069.shtml [Accessed February 8, 2012].
Hansen, H.P., 1999. Determinationof oxygen. In K. Grasshoff, K. Kremling, & M. Erhardt, eds. *Methods of seawater analysis*. Weinheim, Germany: Verlag Chemie, pp. 75–90.
Hepach, H. et al., 2015. Halocarbon emissions and sources in the equatorial Atlantic Cold Tongue. *Biogeosciences*, 12(21), pp.6369–6387.
Honey, D.J. et al., 2013. Heme b in marine phytoplankton and particulate material from the North Atlantic Ocean. *Marine Ecology Progress Series*, 483, pp.1–17.
Kaimal, J.C. et al., 1972. Spectral characteristics of surface-layer turbulence. *Quarterly Journal of the Royal Meteorological Society*, 98(417), pp.563–589. Available at: http://doi.wiley.com/10.1002/qj.49709841707.
Karstensen, J., Stramma, L. & Visbeck, M., 2008. Oxygen minimum zones in the eastern tropical Atlantic and Pacific oceans. *Progress In Oceanography*, 77(4), pp.331–350. Available at: http://linkinghub.elsevier.com/retrieve/pii/S0079661108000670 [Accessed August 5, 2011].
Keeling, R.E., Körtzinger, A. & Gruber, N., 2010. Ocean deoxygenation in a warming world. *Annual review of marine science*, 2, pp.199–229. Available at: http://www.ncbi.nlm.nih.gov/pubmed/21141663.
Kock, A. et al., 2012. Sea-to-air and diapycnal nitrous oxide fluxes in the eastern tropical North Atlantic Ocean. *Biogeosciences*, 9(3), pp.957–964.
Kostadinov, T.S., Siegel, D.A. & Maritorena, S., 2009. Retrieval of the particle size distribution from satellite ocean color observations. *Journal of Geophysical Research: Oceans*, 114(9), pp.1–22.
Loescher, C.R. et al., 2014. Facets of diazotrophy in the oxygen minimum zone waters off Peru. *The ISME journal*, pp.1–13. Available at: http://www.ncbi.nlm.nih.gov/pubmed/24813564.
Lomas, M.W. et al., 2010. Sargasso Sea phosphorus biogeochemistry: an important role for dissolved organic phosphorus (DOP). *Biogeosciences Discussions*, 6, pp.10137–10175.
Mawji, E., Gledhill, M., Worsfold, P.J., et al., 2008. Collision-induced dissociation of three groups of hydroxamate siderophores: ferrioxamines, ferrichromes and coprogens/fusigens. *Rapid communications in mass spectrometry : RCM*, 22, pp.2195–2202.
Mawji, E., Gledhill, M., Milton, J.A., et al., 2008. Hydroxamate Siderophores: Occurance and Importance in the Atlantic Ocean. *Environmental science & technology*, 42(xx), pp.8675–8680.
Naqvi, S.W.A. et al., 1998. Budgetary and biogeochemical implications of N2O signatures in the Arabian Sea. *Nature*, 394(JULY), pp.462–464.
Naqvi, S.W.A. et al., 1998. Nitrogen isotopic studies in the suboxic Arabian Sea. *Proceedings of the Indian Academy of Sciences-Earth and Planetary Sciences*, 107(4), pp.367–378. Available at: <Go to ISI>://WOS:000079181800014.
Pierrot, D. et al., 2009. Recommendations for autonomous underway pCO2 measuring systems and data-reduction routines. *Deep-Sea Research Part II: Topical Studies in Oceanography*, 56(8-10), pp.512–522.
Quack, B. et al., 2007. Bromoform and dibromomethane above the Mauritanian upwelling: Atmospheric distributions and oceanic emissions. *Journal of Geophysical Research Atmospheres*, 112(9), pp.1–9.
Röttgers, R. et al., 2005. Practical test of a point-source integrating cavity absorption meter: the performance of different collector assemblies. *Appl. Opt.*, 44(26), pp.5549–5560.
Röttgers, R., Doxaran, D. & Dupouy, C., 2016. Quantitative filter technique measurements of spectral light absorption by aquatic particles using a portable integrating cavity absorption meter (QFT-ICAM). *Optics Express*, 24(2), pp.A1–A20. Available at:

http://www.opticsexpress.org/abstract.cfm?URI=oe-24-2-A1.
Röttgers, R., Häse, C. & Doerffer, R., 2007. Determination of the particulate absorption of microalgae using a point-source integrating-cavity absorption meter: verification with a photometric technique, improvements for pigment bleaching, and correction for chlorophyll fluorescence. *Limnology and Oceanography: Methods*, 5(1), pp.1–12. Available at: http://dx.doi.org/10.4319/lom.2007.5.1.
Scholz, F. et al., 2014. The impact of ocean deoxygenation on iron release from continental margin sediments. *Nature Geoscience*, 7(May), pp.433–437. Available at: http://www.nature.com/doifinder/10.1038/ngeo2162.
Schunck, H. et al., 2013. Giant Hydrogen Sulfide Plume in the Oxygen Minimum Zone off Peru Supports Chemolithoautotrophy. *PloS one*, 8(8), p.e68661. Available at: http://www.pubmedcentral.nih.gov/articlerender.fcgi?artid=3749208&tool=pmcentrez&rendertype=abstract [Accessed September 19, 2013].
Stöven, T., 2011. *Ventilation processes of the Mediterranean Sea based on CFC-12 and SF6 measurements*. Christian-Albrechts-Universität Kiel. Available at: http://oceanrep.geomar.de/id/eprint/13936.
Stramma, L. et al., 2016. Transition to El Niño conditions in the eastern tropical Pacific in October 2015. *Ocean Science Discussions*, pp.1–30. Available at: http://www.ocean-sci-discuss.net/os-2016-14/.
Taylor, B.B. et al., 2011. Bio-optical provinces in the eastern Atlantic Ocean and their biogeographical relevance. *Biogeosciences*, 8(12), pp.3609–3629. Available at: http://www.biogeosciences.net/8/3609/2011/ [Accessed September 28, 2013].
Winkler, L.W., 1888. Die Bestimmung des im Wasser gelösten Sauerstoffes. *Berichte der deutschen chemischen Gesellschaft*, 21(2), pp.2843–2854. Available at: http://doi.wiley.com/10.1002/cber.188802102122 [Accessed August 17, 2016].
Žutić, V. et al., 1981. Surfactant production by marine phytoplankton. *Marine Chemistry*, 10(6), pp.505–520. Available at: http://linkinghub.elsevier.com/retrieve/pii/0304420381900049.

10. Abbreviations

AA	Amino acids
ADCP	Acoustic Doppler current profiler
AOD	Aerosol optical depth
AOP	Apparent optical properties
AP-CIMS	Atmospheric pressure chemical ionization mass spectrometer
ASTRA-OMZ	Air Sea Interaction of Trace Elements in Oxygen Minimum Zones
BCP	Biological carbon pump
BMBF	Federal Ministry of Education and Research
C	Conductivity
c'	Fast fluctuations in atmospheric gas concentrations
C_a	Concentration in air
CASCADE	Carbonyl Sulphide Cycling in Aphotic Depths
Cd	Cadmium
CDOM	Chromophoric dissolved organic matter
CFC-12	Dichlorodifluoromethane
CH_2Br_2	Dibromomethane
CH_2I_2	Diiodomethane
CH_2I_2	Diiodomethane
CH_3I	Methyl iodide
CH_4	Methane
$CHBr_3$	Bromoform
CHO	Carbohydrates
cLSM	Confocal laser scanning microscopy
Co	Cobalt
CO	Carbon monoxide
CO_2	Carbon dioxide
CPP	Continous pump profiler
CS_2	Carbonyl sulphide
CSP	Coomassie-stainable particles
CTD	Conductivity-temperature-depth-sonde
Cu	Copper
C_w	Concentration in water
DFe	Dissolved iron
DFG	German Research Foundation
DIC	Dissolved inorganic carbon
DMS	Dimethyl sulphide
DMSO	Dimethylsulphoxide
DMSP	Dimethylsulphoniopropionate

DNA	Deoxyribonucleic acid
DO	Dissolved oxygen
DOC	Dissolved organic carbon
DOM	Dissolved organic matter
DOS	Ddissolved organic sulphur
EBUS	Eastern boundary upwelling systems
EC	Eddy covariance
ECD	Electron capture detector
ESI	Electrospray ionization
ETSP	Eastern tropical south Pacific
EUC	Equatorial undercurrent
F	Flux
FDOM	Fluorescent dissolved organic matter
Fe	Iron
FID	Flame ionization detector
FISH	Fluorescence *in situ* hybridization
FRRF	*Fast Repetition Rate fluorometry*
GC	Gas chromatograpg
GDA	Glutardlutadialdehyde
H	Henty's law solubility constant
H_2O_2	Hydrogen peroxide
HCl	Hydrochloric acid
$HgCl_2$	Mercury chloride
HOx	Hydrogen oxide radicals
HPLC	High performance liquid chromatography
ICP	Inductively coupled plasma
INS	Inertial navigation system
IOP	Inherent optical properties
k	Gas tranfer coefficient
LDPE	Low density polyethylene
LWCC	Liquid waveguide capillary cell
MABL	Marine atmospheric boundary layer
Mn	Manganese
MS	Mass spectrometer
N	Nitrogen
N2O	Nitrous oxide
NDIR	Non dispersive infra-red
NH_4^+	Ammonium
Ni	Nickel
NO_2^-	Nitrite
NO_3^-	Nitrate
NOx	Mono-nitrogen radicals
O_2	Oxygen
OA-ICOS	Off-axis integrated cavity output spectroscopy
OCS	Carbonyl sulphide

OMZ	Oxygen minimum zone
OMZ	Organic matter
OTIS	Ocean tracer injection system
P	Phosphor
pAr	Partial pressure of argon
Pb	Lead
pCO_2	Partial pressure of carbon dioxide
PES	Polyether sulphone
PESTRE	Peruvian shelf tracer release experiment
pH_2O	Partial pressure of water
pN_2	Partial pressure of nitrogen
pO_2	Partial pressure of ogygen
POC	Particulate organic carbon
PON	Particulate organic nitrogen
P_{phos}	Particulate organic phosphorus
PSICAM	Point-Source Integrating-Cavity Absorption Measurement Device
QBO	Quasi –biennial oscillation
QFT-ICAM	Quantitative Filtration Technique Integrative Cavitiy Absorption Measurements
RAMSES	Hyperspectral Radiance and Irradiance Sensor
RGD	Reduction gas detector
RNA	Ribonucleic acid
ROS	Reactive oxygen species
SF_6	Sulfur hexafluoride
Si	Silicate
SML	Surface micro layer
SOLAS	Surface Ocean Lower Atmosphere Study
SPE	Solid phase extraction
TA	Total alkalinity
TDFe	Total dissolfed iron
TEP	Transparent exopolymer particles
TOC	Total organic carbon
UTC	Universal Time Coordinated
w'	Fast fluctuation in wind speed
WMO	World meteorological organization
WOCE	World ocean circulation experiment
Zn	Zink
ρ	Density

11. Appendices

11.1 Participating Institutions

GEOMAR	GEOMAR Helmholtz Centre for Ocean research Kiel, Germany
AWI	Alfred-Wegener-Institute for Polar Research, Bremerhaven, Germany
HZG	Helmholtz Centre Geesthacht, Centre for Materials and Coastal Research, Geesthacht, Germany
UiO	University of Oslo, Oslo, Norway
Bigelow	Bigelow Laboratory for Ocean Sciences, East Boothbay, USA
UMass	University of Massachusetts, Dartmouth, USA
Miami	Rosenstiel School of Marine & Atmospheric Science, Miami, USA
IMARPE	Intituto del Mar del Peru, Callao, Peru

11.2 Station list

Leg	Station/ event	Time [UTC]	Latitude [°N]	Longitude [°E]	Gear	Notes
SO243	1-1	2015-10-07 00:39:00.0	-0.9998	-85.5003	CTD	
SO243	1-2	2015-10-07 01:15:00.0	1.0000	-85.5000	Light meter	
SO243	1-3	2015-10-07 02:16:00.0	1.0000	-85.5001	CTD	
SO243	1-4	2015-10-07 04:17:00.0	1.0001	-85.5001	Microstructure | MSS	
SO243	2-1	2015-10-07 14:56:00.0	0.0001	-85.5001	Pump	continous profiling pump
SO243	2-1	2015-10-07 17:49:00.0	0.0001	-85.5001	Pump	
SO243	2-2	2015-10-07 17:56:00.0	-0.0001	-85.5001	Microstructure | MSS	
SO243	2-3	2015-10-07 19:22:00.0	0.0000	-85.5001	CTD	
SO243	2-4	2015-10-07 22:04:00.0	0.0000	-85.5000	Light meter	
SO243	2-5	2015-10-07 22:55:00.0	0.0000	-85.5001	CTD	
SO243	2-6	2015-10-08 01:06:00.0	-0.0001	-85.5001	water sampler | WS [Wasserschoe…]	
SO243	2	2015-10-07 15:06:00.0	0.0000	-85.5001	Rubber boat, Zodiak | ZODIAK	
SO243	3-1	2015-10-08 16:14:00.0	-2.5000	-85.5000	CTD	
SO243	3-1	2015-10-08 16:48:00.0	-2.5000	-85.5000	CTD	
SO243	3-2	2015-10-08 18:09:00.0	-2.5000	-85.4999	Pump	Particle pump
SO243	3	2015-10-08 16:24:00.0	-2.5000	-85.5000	Rubber boat, Zodiak | ZODIAK	
SO243	4-1	2015-10-10 12:40:00.0	-9.5947	-81.7528	CTD	
SO243	4-2	2015-10-10 14:20:00.0	-9.7001	-81.7000	CTD	
SO243	4-3	2015-10-10 15:28:00.0	-9.7746	-81.6537	CTD	
SO243	4-4	2015-10-10 17:24:00.0	-10.0443	-81.6591	CTD	
SO243	5-1	2015-10-10 19:17:00.0	-9.9993	-81.9169	CTD	
SO243	5-1	2015-10-10 19:29:00.0	-9.9995	-81.9167	CTD	
SO243	5-2	2015-10-10 19:52:00.0	-9.9995	-81.9168	Light meter	
SO243	5-3	2015-10-10 20:51:00.0	-9.9995	-81.9167	CTD	
SO243	5-4	2015-10-10 22:08:00.0	-9.9994	-81.9168	Microstructure | MSS	
SO243	5-5	2015-10-10 23:37:00.0	-10.0000	-81.9171	Go-Flo Bottles | GoFlo	
SO243	5-6	2015-10-11 02:27:00.0	-10.0000	-81.9167	Pump	

Leg	Station/ event	Time [UTC]	Latitude [°N]	Longitude [°E]	Gear	Notes
SO243	5	2015-10-10 19:27:00.0	-9.9993	-81.9169	Rubber boat, Zodiak | ZODIAK	
SO243	6-1	2015-10-11 13:08:00.0	-9.5134	-80.3076	CTD	
SO243	6-2	2015-10-11 13:41:00.0	-9.5133	-80.3074	Light meter	
SO243	6-3	2015-10-11 14:48:00.0	-9.5132	-80.3074	CTD	
SO243	6-4	2015-10-11 16:00:00.0	-9.5133	-80.3073	Microstructure | MSS	
SO243	6-5	2015-10-11 17:29:00.0	-9.5128	-80.3076	Go-Flo Bottles | GoFlo	
SO243	7-1	2015-10-12 01:05:00.0	-9.1828	-79.4632	CTD	
SO243	7-2	2015-10-12 01:42:00.0	-9.1835	-79.4639	Light meter	
SO243	7-3	2015-10-12 02:04:00.0	-9.1835	-79.4638	CTD	
SO243	7-4	2015-10-12 03:07:00.0	-9.1835	-79.4638	CTD	
SO243	7-5	2015-10-12 03:41:00.0	-9.1834	-79.4638	Microstructure | MSS	
SO243	7-6	2015-10-12 04:40:00.0	-9.1834	-79.4639	Go-Flo Bottles | GoFlo	
SO243	7-7	2015-10-12 05:27:00.0	-9.1835	-79.4638	Pump	continous profiling pump
SO243	8-1	2015-10-12 10:47:00.0	-9.0000	-78.9000	CTD	
SO243	8-1	2015-10-12 11:01:00.0	-9.0000	-78.9001	CTD	
SO243	8-2	2015-10-12 11:16:00.0	-9.0000	-78.9001	Microstructure | MSS	
SO243	8-3	2015-10-12 12:12:00.0	-9.0000	-78.9000	CTD	
SO243	8-4	2015-10-12 12:52:00.0	-9.0001	-78.9000	Go-Flo Bottles | GoFlo	
SO243	8-5	2015-10-12 13:19:00.0	-9.0000	-78.9000	Light meter	
SO243	8	2015-10-12 10:57:00.0	-9.0000	-78.9000	Rubber boat, Zodiak | ZODIAK	
SO243	9-1	2015-10-12 23:50:00.0	-10.7151	-78.2352	CTD	
SO243	9-2	2015-10-13 00:42:00.0	-10.7153	-78.2349	Ocean Tracer Injection System | OTIS	
SO243	10-1	2015-10-15 15:50:00.0	-12.2537	-77.0773	CTD	
SO243	10-1	2015-10-15 16:05:00.0	-12.2535	-77.0774	CTD	
SO243	10-2	2015-10-15 16:17:00.0	-12.2535	-77.0774	Light meter	
SO243	10-3	2015-10-15 16:48:00.0	-12.2535	-77.0774	Go-Flo Bottles | GoFlo	
SO243	10-4	2015-10-15 17:35:00.0	-12.2535	-77.0774	CTD	
SO243	10-5	2015-10-15 18:05:00.0	-12.2535	-77.0774	Microstructure | MSS	

Leg	Station/ event	Time [UTC]	Latitude [°N]	Longitude [°E]	Gear	Notes
SO243	10	2015-10-15 16:01:00.0	-12.2537	-77.0773	Rubber boat, Zodiak | ZODIAK	
SO243	11-1	2015-10-15 20:27:00.0	-12.3640	-77.4375	CTD	
SO243	11-1	2015-10-15 21:02:00.0	-12.3640	-77.4375	CTD	
SO243	11-2	2015-10-15 21:04:00.0	-12.3639	-77.4376	Ocean Tracer Injection System | OTIS	
SO243	11	2015-10-15 20:37:00.0	-12.3640	-77.4375	Rubber boat, Zodiak | ZODIAK	
SO243	11	2015-10-15 21:05:00.0	-12.3639	-77.4376	Pump	Particle Pump
SO243	12-1	2015-10-16 11:40:00.0	-12.8926	-78.2722	CTD	
SO243	12-2	2015-10-16 12:58:00.0	-12.8927	-78.2720	Go-Flo Bottles | GoFlo	
SO243	12-3	2015-10-16 15:05:00.0	-12.8927	-78.2720	CTD	
SO243	12-4	2015-10-16 15:37:00.0	-12.8928	-78.2720	Light meter	
SO243	12-5	2015-10-16 16:16:00.0	-12.8927	-78.2720	Microstructure | MSS	
SO243	12-6	2015-10-16 17:15:00.0	-12.9024	-78.2674	Float	
SO243	13-1	2015-10-17 02:44:00.0	-14.6266	-77.7468	CTD	
SO243	13-1	2015-10-17 05:22:00.0	-14.6497	-77.7341	CTD	
SO243	13-2	2015-10-17 03:14:00.0	-14.6265	-77.7468	Microstructure | MSS	
SO243	13-3	2015-10-17 04:38:00.0	-14.6490	-77.7345	Light meter	
SO243	13-4	2015-10-17 06:34:00.0	-14.6497	-77.7341	Go-Flo Bottles | GoFlo	
SO243	13-5	2015-10-17 08:43:00.0	-14.6496	-77.7340	CTD	
SO243	14-1	2015-10-17 12:00:00.0	-14.4032	-77.2811	CTD	
SO243	14-1	2015-10-17 12:47:00.0	-14.4033	-77.2812	CTD	
SO243	14-2	2015-10-17 13:24:00.0	-14.4033	-77.2811	Light meter	
SO243	14-3	2015-10-17 14:17:00.0	-14.4033	-77.2812	CTD	
SO243	14-4	2015-10-17 14:48:00.0	-14.4033	-77.2812	Go-Flo Bottles | GoFlo	
SO243	14-4	2015-10-17 17:58:00.0	-14.4036	-77.2809	water sampler | WS [Wasserschoe…]	
SO243	14-5	2015-10-17 17:00:00.0	-14.4035	-77.2810	Microstructure | MSS	
SO243	14	2015-10-17 12:10:00.0	-14.4032	-77.2811	Rubber boat, Zodiak | ZODIAK	
SO243	15-1	2015-10-17 22:00:00.0	-14.0360	-76.5278	CTD	
SO243	15-2	2015-10-17 22:31:00.0	-14.0361	-76.5278	Light meter	

Leg	Station/ event	Time [UTC]	Latitude [°N]	Longitude [°E]	Gear	Notes
SO243	15-3	2015-10-17 23:03:00.0	-14.0360	-76.5277	CTD	
SO243	15-4	2015-10-17 23:38:00.0	-14.0361	-76.5278	Go-Flo Bottles | GoFlo	
SO243	15-5	2015-10-18 00:38:00.0	-14.0361	-76.5278	Ocean Tracer Injection System | OTIS	
SO243	15	2015-10-17 21:10:00.0	-14.0360	-76.5278	Rubber boat, Zodiak | ZODIAK	
SO243	15	2015-10-18 00:39:00.0	-14.0361	-76.5278	Pump	Particle Pump
SO243	16-1	2015-10-18 19:03:00.0	-16.0748	-76.5789	CTD	
SO243	16-1	2015-10-18 19:15:00.0	-16.0750	-76.5790	CTD	
SO243	16-2	2015-10-18 19:34:00.0	-16.0750	-76.5790	Light meter	
SO243	16-3	2015-10-18 20:17:00.0	-16.0751	-76.5790	CTD	
SO243	16-4	2015-10-18 21:32:00.0	-16.0751	-76.5789	Go-Flo Bottles | GoFlo	
SO243	16-5	2015-10-18 23:57:00.0	-16.0751	-76.5790	CTD	
SO243	16-6	2015-10-19 01:36:00.0	-16.0751	-76.5788	Microstructure | MSS	
SO243	16	2015-10-18 19:13:00.0	-16.0748	-76.5789	Rubber boat, Zodiak | ZODIAK	
SO243	17-1	2015-10-19 06:52:00.0	-15.6737	-75.8951	CTD	
SO243	17-2	2015-10-19 08:05:00.0	-15.6737	-75.8951	Light meter	
SO243	17-3	2015-10-19 08:57:00.0	-15.6737	-75.8950	CTD	
SO243	17-4	2015-10-19 09:34:00.0	-15.6737	-75.8950	Go-Flo Bottles | GoFlo	
SO243	17-5	2015-10-19 12:04:00.0	-15.6681	-75.8987	Microstructure | MSS	
SO243	17-5	2015-10-19 12:51:00.0	-15.6769	-75.8932	Microstructure | MSS	
SO243	17	2015-10-19 12:14:00.0	-15.6681	-75.8987	Rubber boat, Zodiak | ZODIAK	
SO243	18-1	2015-10-19 17:43:00.0	-15.3186	-75.2746	CTD	
SO243	18-1	2015-10-19 18:08:00.0	-15.3184	-75.2745	CTD	
SO243	18-2	2015-10-19 18:11:00.0	-15.3184	-75.2744	Light meter	
SO243	18-3	2015-10-19 18:52:00.0	-15.3184	-75.2745	CTD	
SO243	18-4	2015-10-19 19:26:00.0	-15.3185	-75.2745	Pump	continous profile pump
SO243	18-5	2015-10-19 21:54:00.0	-15.3185	-75.2745	CTD	
SO243	18-6	2015-10-19 23:20:00.0	-15.3185	-75.2745	Go-Flo Bottles | GoFlo	
SO243	18-7	2015-10-20 00:34:00.0	-15.3184	-75.2745	CTD	

Leg	Station/ event	Time [UTC]	Latitude [°N]	Longitude [°E]	Gear	Notes
SO243	18-8	2015-10-20 01:11:00.0	-15.3184	-75.2745	Microstructure | MSS	
SO243	18	2015-10-19 17:53:00.0	-15.3186	-75.2746	Rubber boat, Zodiak | ZODIAK	

11.3 List of selected samples

Table 11.3.1. Trace metal clean surface samples collected by the tow fish

ID	Betford #	Date	Time (UTC)	DFe	TDFe	Nuts	Fe(II)/H2O2
1	259052	05.10.2015	23:00	X	X	X	
1,5		06.10.2015	00:30	X		X	
2	259053	06.10.2015	02:00	X	X	X	X
2,5		06.10.2015	03:30	X		X	X
3	259054	06.10.2015	05:00	X	X	X	
3,5		06.10.2015	06:30	X		X	
4	259055	06.10.2015	08:00	X	X	X	
4,5		06.10.2015	09:30	X		X	
5	259056	06.10.2015	11:00	X	X	X	
5,5		06.10.2015	12:30	X		X	
6	259057	06.10.2015	14:05	X	X	X	
6,5		06.10.2015	15:40	X		X	X
7	259058	06.10.2015	16:55	X	X	X	
7,5		06.10.2015	18:35	X		X	
8	259059	06.10.2015	20:05	X	X	X	X
8,5		06.10.2015	21:30	X		X	
9	259060	06.10.2015	23:00	X	X	X	X
9,5		07.10.2015	00:20	X	X	X	X
10	259064	07.10.2015	11:01	X	X	X	
10,5		07.10.2015	12:30	X	X	X	
11	259065	07.10.2015	14:00	X	X	X	
11,5		08.10.2015	06:47	X		X	
12	259071	08.10.2015	08:50	X	X	X	X
12,5		08.10.2015	09:50	X		X	
13	259072	08.10.2015	11:00	X	X	X	
13,5		08.10.2015	12:30	X		X	
15	259073	08.10.2015	14:00	X	X	X	
15,5		08.10.2015	15:30	X		X	
16	259076	08.10.2015	21:30	X		X	X
17		08.10.2015	23:10	X	X	X	X
17,5		09.10.2015	00:35	X		X	X
18	259077	09.10.2015	02:00	X	X	X	X
18,5		09.10.2015	15:25	X	X	X	
19	259082	09.10.2015	17:00	X	X	X	X
19,5		09.10.2015	18:30	X		X	X
24	259083	09.10.2015	20:05	X	X	X	X
24,5		09.10.2015	21:30	X		X	
25	259084	09.10.2015	23:00	X	X	X	X
25,5		10.10.2015	00:30	X		X	X
26	259085	10.10.2015	02:00	X	X	X	X
26,5		10.10.2015	03:33	X		X	X
27	259086	10.10.2015	05:00	X	X	X	X
27,5		10.10.2015	06:30	X		X	
28	259087	10.10.2015	08:00	X	X	X	
29		10.10.2015	11:00	X	X	X	
29,5		10.10.2015	12:30	X	X	X	
30		10.10.2015	13:56	X	X	X	
30,5		10.10.2015	15:17	X	X	X	X
31		10.10.2015	17:10	X	X	X	

ID	Betford #	Date	Time (UTC)	DFe	TDFe	Nuts	Fe(II)/H2O2
31,5		10.10.2015	18:35	X		X	X
32	Station	10.10.2015	Stn 6	X	X	X	X
41,5		15.10.2015	00:31	X	X	X	
42		15.10.2015	02:00	X	X	X	
42,5		15.10.2015	03:30	X		X	
43		15.10.2015	05:00	X	X	X	
43,5		15.10.2015	06:35	X		X	
44		15.10.2015	07:55	X	X	X	
44,5		15.10.2015	09:27	X		X	
45		15.10.2015	11:00	X	X	X	
45,5		15.10.2015	12:30	X		X	
46		15.10.2015	14:00	X	X	X	
46,25		15.10.2015	14:38	X	X	X	X
46,5	Station	15.10.2015	15:30	X	X	X	X
47		15.10.2015	20:00	X	X	X	X
48		16.10.2015	08:00	X	X	X	
48,5		16.10.2015	09:25	X		X	
49	Station	16.10.2015	11:05	X	X	X	X
49,5		16.10.2015	18:35	X		X	
50		16.10.2015	20:05	X	X	X	X
50,5		16.10.2015	21:30	X		X	
51		16.10.2015	23:00	X	X	X	X

Table 11.3.2. Shows the volume in mL of trace metal clean water column samples collected at the 13 different sites for dissolved (DFe), total dissolvable (TDFe), soluble (SFe), iodite/iodate (IO3/I), and Fe(II)/H_2O_2. The water volume passed through the 0.2 µm PES filters for the particulate trace metal fraction are shown in litre (L).

Station	Date	Lat	Long	~Depth	DFe	TDFe	SFe	PFe	IO3/I	Fe(II)
					(mL)	(mL)	(mL)	(L)	(mL)	(mL)
243-2	08.10.2015	0,00	-85,50	22	125	125	60	2	30	100
				35	125	125	60	4	30	100
				50	125	125	60	2,9	30	100
				105	125	125	60	4,1	30	100
				200	125	125	60	3,85	30	100
				300	125	125	60	2,3	30	100
				350	125	125	60	0,8	30	100
				420	125	125	60	1,1	30	100
				600	125	125	60	1,2	30	100
				800	125	125	60	3	30	100
				1000	125	125	60	3,9	30	100
				1200	125	125	60	1,1	30	100
243_5	10.10.2015	-10,00	-81,92	20	125	125	60	1,84	30	100
				40	125	125	60	3	30	100
				80	125	125	60	4	30	100
				150	125	125	60	4	30	100
				200	125	125	60	4	30	100
				240	125	125	60	3,1	30	100
				300	125	125	60	2,7	30	100
				400	125	125	60	2,95	30	100
				600	125	125	60	4	30	100
				800	125	125	60	4	30	100
				1000	125	125	60	3,95	30	100
243_6	11.10.2015	-9,51	-80,31	20	125	125	60	1,45	30	100
				100	125	125	60	2,8	30	100
				150	125	125	60	4	30	100
				200	125	125	60	4	30	100
				250	125	125	60	3,1	30	100
				300	125	125	60	3,5	30	100
				400	125	125	60	2,6	30	100
				500	125	125	60	2,9	30	100
				600	125	125	60	4,5	30	100
				800	125	125	60	3,1	30	100
				1000	125	125	60	4	30	100
243_7	12.10.2015	-9,51	-80,31	10	125	125	60	4,05	30	100
				30	125	125	60	4	30	100
				50	125	125	60	4	30	100

Station	Date	Lat	Long	~Depth	DFe	TDFe	SFe	PFe	IO3/I	Fe(II)
				75	125	125	60	4	30	100
				100	125	125	60	1,5	30	100
				120	125	125	60	1,9	30	100
243_8	12.10.2015	-9,00	-78,90	15	125	125	60	4,05	30	100
				30	125	125	60	4	30	100
				50	125	125	60	4	30	100
				70	125	125	60	4	30	100
243_10	12.10.2015	-12,25	-77,08	5	125	125	60	2	30	100
				15	125	125	60	4,3	30	100
				25	125	125	60	2,5	30	100
				35	125	125	60	4,2	30	100
				50	125	125	60	3,55	30	100
				65	125	125	60	3,8	30	100
243_12	16.10.2015	-12,89	-78,27	15	125	125	60	3,95	30	100
				30	125	125	60	2,65	30	100
				45	125	125	60	3,7	30	100
				60	125	125	60	4,45	30	100
				100	125	125	60	3,55	30	100
				150	125	125	60	3,4	30	100
				200	125	125	60	2	30	100
				300	125	125	60	3	30	100
				400	125	125	60	2,7	30	100
				500	125	125	60	4,8	30	100
				750	125	125	60	4,2	30	100
				1000	125	125	60	4	30	100
243_13	17.10.2015	-14,65	-77,73	20	125	125	60	1,6	30	100
				40	125	125	60	2,1	30	100
				70	125	125	60	2,7	30	100
				100	125	125	60	3,1	30	100
				150	125	125	60	2,1	30	100
				250	125	125	60	2,9	30	100
				350	125	125	60	3,4	30	100
				475	125	125	60	3,2	30	100
				600	125	125	60	2,3	30	100
				700	125	125	60	4,1	30	100
				850	125	125	60	4	30	100
				1000	125	125	60	4,5	30	100
243_14	17.10.2015	-14,40	-77,28	10	125	125	60	2,55	30	100
				30	125	125	60	3,4	30	100
				50	125	125	60	4	30	100
				70	125	125	60	3,9	30	100

Station	Date	Lat	Long	~Depth	DFe	TDFe	SFe	PFe	IO3/I	Fe(II)
				115	125	125	60	4,2	30	100
				140	125	125	60	3,4	30	100
				200	125	125	60	3,2	30	100
				300	125	125	60	3	30	100
				400	125	125	60	2,95	30	100
				500	125	125	60	5,4	30	100
				750	125	125	60	4,3	30	100
				1000	125	125	60	3,36	30	100
243_15	17.10.2015	-14,04	-76,53	10	125	125	60	4	30	100
				50	125	125	60	4,1	30	100
				100	125	125	60	3,7	30	100
				150	125	125	60	3,2	30	100
				220	125	125	60	3,4	30	100
243_16	18.10.2015	-16,08	-76,58	5	125	125	60	1,5	30	100
				15	125	125	60	3,2	30	100
				30	125	125	60	2,9	30	100
				62	125	125	60	4	30	100
				80	125	125	60	2,03	30	100
				140	125	125	60	3	30	100
				200	125	125	60	3,15	30	100
				300	125	125	60	3,3	30	100
				400	125	125	60	4	30	100
				500	125	125	60	3,1	30	100
				750	125	125	60	4	30	100
				1000	125	125	60	4	30	100
243_17	19.10.2015	-16,08	-76,58	15	125	125	60	1,6	30	100
				50	125	125	60	2,85	30	100
				100	125	125	60	2,9	30	100
				200	125	125	60	3,6	30	100
				310	125	125	60	3	30	100
				380	125	125	60	3,2	30	100
				480	125	125	60	3,8	30	100
				580	125	125	60	1,1	30	100
				750	125	125	60	2,7	30	100
				1000	125	125	60	4,3	30	100
243_18	19.10.2015	-15,32	-75,27	10	125	125	60	1,65	30	100
				20	125	125	60	1,75	30	100
				30	125	125	60	4,4	30	100
				50	125	125	60	3,4	30	100
				75	125	125	60	2,6	30	100
				105	125	125	60	2,6	30	100

Table 11.3.3. Time and depths of underway samples obtained for heme *b* and POC analysis

Date and Time (Local)	Date and time (UTC)	Bedford number	Depth (m)	Heme *b* (volume filtered, L)	POC/N (volume filtered, L)
05.10.2015 18:00	05.10.2015 23:00	259052	6	2	2
05.10.2015 21:00	06.10.2015 02:00	259053	6	1	0.5
06.10.2015 00:00	06.10.2015 05:00	259054	6	1	0.5
06.10.2015 03:00	06.10.2015 08:00	259055	6	1.5	0.5
06.10.2015 06:00	06.10.2015 11:00	259056	6	1	0.5
06.10.2015 09:00	06.10.2015 14:00	259057	6	1	0.5
06.10.2015 12:00	06.10.2015 17:00	259058	6	1.5	0.5
06.10.2015 15:00	06.10.2015 20:00	259059	6	1.5	0.5
06.10.2015 18:00	06.10.2015 23:00	259060	6	1.5	0.5
07.10.2015 06:00	07.10.2015 11:00	259064	6	1.5	0.5
07.10.2015 09:00	07.10.2015 14:00	259065	6		0.5
08.10.2015 00:00	08.10.2015 05:00	259070	6	1.5	0.5
08.10.2015 03:00	08.10.2015 08:00	259071	6	1.5	0.5
08.10.2015 06:00	08.10.2015 11:00	259072	6	1.5	0.5
08.10.2015 09:00	08.10.2015 14:00	259073	6	1.5	0.5
08.10.2015 18:00	09.10.2015 02:00	259076	6	1.26	0.5
08.10.2015 21:00	09.10.2015 05:00	259077	6	1.45	0.5
09.10.2015 00:00	09.10.2015 08:00	259078	6	1.5	0.5
09.10.2015 03:00	09.10.2015 11:00	259079	6	1.5	0.5
09.10.2015 06:00	09.10.2015 14:00	259080	6	1.5	0.5
09.10.2015 09:00	09.10.2015 17:00	259081	6	1.5	0.5
09.10.2015 12:00	09.10.2015 20:00	259082	6	1.5	0.5
09.10.2015 15:00	09.10.2015 23:00	259083	6	1.5	0.5
09.10.2015 18:00	10.10.2015 02:00	259084	6	1.5	0.5
09.10.2015 21:00	10.10.2015 05:00	259085	6	1.5	0.5
09.10.2015 00:20	10.10.2015 08:00	259086	6	1.5	0.5
09.10.2015 03:40	10.10.2015 11:00	259087	6	1.5	0.5
09.10.2015 07:00	10.10.2015 14:00	259088	6	1.5	0.5
09.10.2015 10:00	10.10.2015 17:00	259089	6	1.5	0.5
11.10.2015 04:00	11.10.2015 11:00	259095	6	1.5	0.5
11.10.2015 07:00	11.10.2015 14:00	259096	6	1.5	0.5
11.10.2015 19:00	11.10.2015 23:00	259100	6	1.5	0.5
12.10.2015 13:00	12.10.2015 17:00	259106	6	1	0.2
12.10.2015 16:00	12.10.2015 20:00	259107	6	1	0.2
12.10.2015 19:00	12.10.2015 23:00	259108	6	1	0.2
13.10.2015 10:00	13.10.2015 14:00	259113	6	1	0.2
13.10.2015 13:00	13.10.2015 17:00	259114	6	1	0.2
13.10.2015 16:00	13.10.2015 20:00	259115	6	1	0.2
14.10.2015 22:00	15.10.2015 02:00	259125	6	1	0.2
15.10.2015 01:00	15.10.2015 05:00	259126	6	1	0.2
15.10.2015 04:00	15.10.2015 08:00	259127	6	1	0.2
15.10.2015 07:00	15.10.2015 11:00	259128	6	1	0.2

Date and Time (Local)	Date and time (UTC)	Bedford number	Depth (m)	Heme *b* (volume filtered, L)	POC/N (volume filtered, L)
15.10.2015 10:00	15.10.2015 14:00	259129	6	1	0.3
15.10.2015 16:00	15.10.2015 20:00	259131	6	1	0.2
16.10.2015 04:00	16.10.2015 08:00	259135	6	1	0.4
16.10.2015 07:00	16.10.2015 11:00	259136	6	1.5	0.5
16.10.2015 16:00	16.10.2015 20:00	259139	6	1.5	0.4
16.10.2015 19:00	16.10.2015 23:00	259140	6	1.5	0.5
17.10.2015 08:30	15.10.2015 12:30		6	1	0.5
18.10.2015 10:00	18.10.2015 14:00	259145	6	1	0.5
18.10.2015 13:00	18.10.2015 17:00	259146	6	1	0.5
19.10.2015 22:00	20.10.2015 02:00	259165	6	1.45	0.5
20.10.2015 00.20	20.10.2015 05:00	259166	6	1.5	0.5
20.10.2015 05:00	20.10.2015 08:00	259167	6	1.5	0.5
20.10.2015 08:00	20.10.2015 11:00	259168	6	1.5	0.5
20.10.2015 11:00	20.10.2015 14:00	259169	6	1.5	0.5

Table 11.3.4. Location and depths of CTD samples obtained for heme *b* and POC analysis

Latitude °N	Longitude °W	Bedford number	Target depth (m)	Heme *b* (volume filtered, L)	POC/N (volume filtered, L)
1.00	85.50	258001	100	1.5	0.5
1.00	85.50	258007	50	1.5	0.5
1.00	85.50	258011	40	1.5	0.5
1.00	85.50	258013	35	1.5	0.5
1.00	85.50	258017	20	1.5	0.5
1.00	85.50	258020	5	1.5	0.5
0.00	85.50	258076	100	1.86	NAN
0.00	85.50	258078	50	2	NAN
0.00	85.50	258082	40	1.98	NAN
0.00	85.50	258085	35	1.95	NAN
0.00	85.50	258089	20	1.94	NAN
0.00	85.50	258092	5	2	NAN
-2.50	85.50	258118	20	1.5	NAN
-2.5	85.5	258115	45	1.5	NAN
-2.5	85.5	Moon pool	5	1.5	NAN
-10	81.55	258164	75	1.5	0.5
-10	81.55	258168	60	1.5	0.5
-10	81.55	258126	50	1.5	0.5
-10	81.55	258136	20	1.5	0.5
-10	81.55	258141	15	1.5	0.5
-10	81.55	258144	5	1.5	0.5
-9.31	80.18	258173	90	1.5	0.5
-9.31	80.18	258176	75	1.5	0.5
-9.31	80.18	258179	50	1.5	0.5
-9.31	80.18	258182	35	1.5	0.5
-9.31	80.18	258189	15	1.4	0.43
-9.31	80.18	258192	5	1.5	0.47
-9.1835	79.4638	258243	100	0.5	NAN
-9.1835	79.4638	258245	80	1.5	0.5
-9.1835	79.4638	258249	60	1.5	0.5
-9.1835	79.4638	258251	40	1.5	0.5
-9.1835	79.4638	258254	30	1.5	0.5
-9.1835	79.4638	258258	20	1.5	0.5
-9.1835	79.4638	258261	12	1.5	0.5
-9	78.9	258265	80	1.5	0.2
-9	78.9	258268	50	1.5	0.5
-9	78.9	258274	30	1.5	0.5
-9	78.9	258277	20	1.1	0.4
-9	78.9	258280	15	1.5	0.5
-9	78.9	258283	10	1	0.2
-9	78.9	258286	5	1	0.2
-10.72	78.28	258323	100	1	0.43

Latitude °N	Longitude °W	Bedford number	Target depth (m)	Heme *b* (volume filtered, L)	POC/N (volume filtered, L)
-10.72	78.28	258325	75	1	0.43
-10.72	78.28	258329	40	1	0.3
-10.72	78.28	258331	25	1	0.3
-10.72	78.28	258333	15	1	0.3
-10.72	78.28	258335	5	1	0.3
-12.25	77.078	258363	70	1	
-12.25	77.078	258370	50	1	0.3
-12.25	77.078	258374	30	1	0.4
-12.25	77.078	258377	25	1.05	0.4
-12.25	77.078	258380	15	1	0.4
-12.25	77.078	258382	10	1	0.4
-12.25	77.078	258384	5	1	NAN
-12.364	77.4375	258395	75	1	0.5
-12.364	77.4375	258397	50	1	0.5
-12.364	77.4375	258400	15	1	0.5
-12.364	77.4375	258403	10	1	0.32
-12.364	77.4375	258406	5	0.5	0.3
-12.253	77.075	258435	100	1.5	0.5
-12.253	77.075	258438	75	1.5	NAN
-12.253	77.075	258444	50	1.5	0.47
-12.253	77.075	258449	30	1.5	0.5
-12.253	77.075	258452	20	1	0.5
-12.253	77.075	258456	10	1.5	0.4
-14.628	77.281	258482	125	1.5	0.5
-14.628	77.281	258485	100	1.5	0.5
-14.628	77.281	258489	75	1.5	0.5
-14.628	77.281	258495	25	1.5	0.5
-14.628	77.281	258502	10	1.5	0.5
-14.628	77.281	258504	5	1.5	0.5
-14.4	77.282	258529	100	1.5	0.4
-14.4	77.282	258529	75	1.5	0.3
-14.4	77.282	258529	50	1.5	0.36
-14.4	77.282	258529	25	1	0.34
-14.4	77.282	258529	10	1	0.5
-14.4	77.282	258529	5	1	0.4
-14.035	76.53	258561	100	1.5	0.5
-14.035	76.53	258564	75	1.5	0.5
-14.035	76.53	258565	50	1.5	0.5
-14.035	76.53	258570	25	1	0.5
-14.035	76.53	258574	10	1	0.5
-14.035	76.53	258576	5	1	0.44
-16.075	76.579	258602	50	1.5	0.4
-16.075	76.579	258605	100	1.5	0.5

Latitude °N	Longitude °W	Bedford number	Target depth (m)	Heme *b* (volume filtered, L)	POC/N (volume filtered, L)
-16.075	76.579	258609	75	1.5	0.5
-16.075	76.579	258615	25	1	0.3
-16.075	76.579	258624	5	1	0.3
-15.67	75.895	258708	40	1.5	0.49
-15.67	75.895	258699	70	1.5	0.46
-15.67	75.895	258704	50	1.5	0.5
-15.67	75.895	258711	20	1	0.5
-15.67	75.895	258717	10	1	0.5
-15.67	75.895	258720	5	1	0.5
-15.318	75.275	258750	90	1.5	0.4
-15.318	75.275	258753	75	1.5	0.33
-15.318	75.275	258755	60	1.5	0.46
-15.318	75.275	258757	40	1.5	0.375
-15.318	75.275	258760	20	1.5	0.405
-15.318	75.275	258763	15	1.5	0.45
-15.318	75.275	258767	5	1.5	0.5

Table 11.3.5. Locations where samples for siderophores were collected.

Date and time Ship	Date and time UTC	Latitude °N	Longitude °W	Sampling method	Depth
07/10/2015 11:00	08/10/2015 17:30	0.00	85.50	cont pump	5
07/10/2015 11:00	08/10/2015 17:30	0.00	85.50	cont pump	25
07/10/2015 11:00	08/10/2015 17:30	0.00	85.50	cont pump	50
09/10/2015 02:15	09/10/2015 19:15			Fish	2
10/10/2015 10:10	11/10/2015 02:10	-9.31	80.18	cont pump	5
10/10/2015 10:10	11/10/2015 02:10	-9.31	80.18	cont pump	15
10/10/2015 10:10	11/10/2015 02:10	-9.31	80.18	cont pump	50
19/10/2015		-15.318	75.275	cont pump	5
19/10/2015		-15.318	75.275	cont pump	20
19/10/2015		-15.318	75.275	cont pump	50

Table 11.3.6. Number of transient tracer samples at the different stations of the ASTRA-OMZ cruise.

Station	**Lat / Lon**	**Number of samples**
SO243_1	1°N / 85°30'W	25
SO243_2	0°N / 85°30'W	24
SO243_3	2°30'S / 85°30'W	13
SO243_5	10°S / 81°55'W	14
SO243_6	9°30'S / 80°18'W	17
SO243_7	9°S / 84°W	17
Total		**110**

Table 11.3.7. Particle pumps depths and parameters analysed.

Station 3	8 Oct.	
Depth	25	150
Splits	failed	Failed
Incubation		
Particulate	POC, PON, POP, TAA, TCHO,	
Dissolved	Nuts, DOC, DON, DOP, DAA, DCHO, Bact enum	

Station 11	12 Oct	
Depth	30	200
Splits	4	4
Incubation	4	4
Particulate	POC, PON, POP, TAA, TCHO,	
Dissolved	Nuts, DOC, DON, DOP, DAA, DCHO, Bact enum	

Station 15	17 Oct.	
Depth	25	150
Splits	4	4
Incubation	4	4
Particulate	POC, PON, POP, TAA, TCHO,	
Dissolved	Nuts, DOC, DON, DOP, DAA, DCHO, Bact enum	

Table 11.3.8. Incubations treatments from particle pumps, dates and O_2 concentrations.

ID	Depth	O2 treat.	set up	sampling
T1 F1	30	Local	16th Oct	16th Oct
T1 F2	30	Local	16th Oct	17th Oct
T1 F3	30	Local	16th Oct	19th Oct
T1 F4	30	Local	16th Oct	21st Oct
T1 F5	200	Lowered	16th Oct	16th Oct
T1 F6	200	Lowered	16th Oct	17th Oct
T1 F7	200	Lowered	16th Oct	19th Oct
T1 F8	200	Lowered	16th Oct	21st Oct
T1 F9	25	Local	18th Oct	18th Oct
T1 F10	25	Local	18th Oct	19th Oct
T1 F11	25	Local	18th Oct	20th Oct
T1 F12	25	Local	18th Oct	21st Oct
T1 F13	150	Lowered	18th Oct	18th Oct
T1 F14	150	Lowered	18th Oct	19th Oct
T1 F15	150	Lowered	18th Oct	20th Oct
T1 F16	150	Lowered	18th Oct	21st Oct